

DEPARTAMENTO DE FÍSICA

**FACULDADE DE CIÊNCIAS E TECNOLOGIA DA
UNIVERSIDADE DE COIMBRA**

Hemodynamic Parameters Assessment

Characterization of a New Piezoelectric Probe

MASTER'S DISSERTATION IN BIOMEDICAL ENGINEERING

VÂNIA PATRÍCIA SILVA RELVAS

SEPTEMBER 2011



**FCTUC – FACULDADE DE CIÊNCIAS E TECNOLOGIA
DA UNIVERSIDADE DE COIMBRA**

Dissertation presented to the University of Coimbra
to complete the necessary requirements to obtain
the degree of Master of Biomedical Engineering.

SCIENTIFIC SUPERVISORS:

Prof. Dr. Carlos M. Correia
Dr. João Cardoso
Eng.^a. Helena Catarina B. M. Pereira



IN COLLABORATION WITH:

João Maldonado, MD



Instituto de Investigação e Formação Cardiovascular (IIFC)

Prof. Telmo Pereira, Cardiopneumology Department







Escola Superior de Tecnologia da Saúde de Coimbra (ESTeSC)

ESCOLA
SUPERIOR DE
TECNOLOGIA DA
SAÚDE DE
COIMBRA

Eng.^a. Helena Catarina B. M. Pereira



“ ...  u  ou do  amanho  ue  ejo

E  ão do  amanho da  inha  ltura... ”

 ernando  essa :  eterónimo

ABSTRACT

Over the past few years, the arterial stiffness has had an important role in the assessment and prevention of cardiovascular diseases (CVD) that according to the World Health Organization represents 30% of all the global deaths. It describes the elastic properties of the arteries and can be evaluated through different hemodynamic parameters as pulse wave velocity (PWV) and augmentation index (Aix).

The Group of Electronics and Instrumentation has been developed some apparatus in order to assess these hemodynamic parameters, in a noninvasive, robust and cheap way. The systems are based in accelerometers, piezoelectric sensors, optical sensors and also acoustic sensors. This work intends to continue the study of hemodynamic parameters assessment using new instrumentation based on piezoelectric (PZ) sensors and software required. These elements together allow analysing the PZ signal and visualizing the arterial blood pressure waveform. The new PZ probe was characterized in dedicated test bench systems and in human common carotid arteries. In order to assess the local PWV were developed and implemented some signal processing algorithms.

The test bench systems allowed simulating the clinical properties of the cardiovascular system in laboratory. These were a powerful tool to show that: the PZ sensors not suffer crosstalk effect, through the impulse response of them is able to recover the original waveform from deconvolution method and the time resolution inferred by minimum amplitude detection algorithm is 1.5 ms. Some clinical trials have been carried by our collaborators representing an important step in the validation of the probe in a large number of patients. From clinical trials made in a group of healthy volunteers, the local PWV was assessed by two algorithms. The local PWV values ranged from 2.03 to 7.22m/s and with a standard derivation from 0.74 to 6.17 m/s.

Keywords: Cardiovascular Disease, Arterial stiffness, common carotid artery, Double piezoelectric probe, local Pulse Wave Velocity (PWV), test bench system, time resolution.

RESUMO

Ao longo dos últimos anos, a rigidez arterial tem tido um papel importante na avaliação e prevenção de doenças cardiovasculares que, segundo a Organização Mundial de Saúde, representam 30% de todas as mortes globais. A rigidez arterial descreve as propriedades das artérias e pode ser avaliada através de alguns parâmetros hemodinâmicos como a velocidade de onda de pulso (VOP).

No Grupo de Electrónica e Investigação, algumas tecnologias têm sido desenvolvidas de modo a avaliar esses parâmetros hemodinâmicos de forma não invasiva, robusta e barata. Estas tecnologias são baseadas em acelerómetros, sensores piezoeléctricos (PZ), sensores ópticos e em sensores acústicos. Este trabalho pretende dar continuidade ao estudo da avaliação de parâmetros hemodinâmicos usando uma nova sonda baseada em sensores PZ e software adequado. Estes elementos permitem analisar o sinal PZ e visualizar a onda de pressão arterial. A nova sonda PZ foi caracterizada em dois modelos de bancada e a partir de sinais adquiridos na artéria carótida comum em humanos. De modo a avaliar a VOP local foram também desenvolvidos e implementados alguns algoritmos de processamento de sinal.

Os modelos de bancada permitiram simular propriedades clínicas do sistema cardiovascular em laboratório. Estes foram uma poderosa ferramenta permitindo mostrar que: os sensores PZ não sofrem efeito de crosstalk, através da resposta a impulso de ambos é possível recuperar a onda original pelo método da desconvolução e a resolução temporal determinada pelo algoritmo de detecção de amplitude mínima é de 1.5 ms. Alguns ensaios clínicos têm sido realizados pelos nossos colaboradores, representando um passo importante na validação da sonda em um grande número de pacientes. A partir do ensaio clínico realizado num pequeno grupo de voluntários saudáveis, a VOP local foi determinada usando dois algoritmos. Os valores da VOP local variaram de 2.03 – 7.22 m/s e com desvio padrão a variar de 0.74 – 6.17 m/s.

Palavras-chave: Doenças Cardiovasculares, Rigidez arterial, artéria carótida comum, Sonda dupla piezoelétrica, Velocidade de onda de pulso (VOP) local, teste de bancada, resolução temporal.

ACKNOWLEDGEMENTS

This page is dedicated to who given their contribution to the achievement of this thesis and helped me in my academic journey. I leave here my sincere thanks to everyone.

I would like to express my gratitude towards my parents, Maria and Francisco, and all my family that without them none of this would be possible.

My deepest thanks to my friends that in the last five years have also been my family. Thank you for your laughter, fellowship and friendship. A big hug to all of you.

I want also to thank Prof. Dr. Carlos Correia, Dr. João Cardoso and Eng.^ª Catarina Pereira by their support and guidance. All members at GEI I thank to help and cooperate in this work. To João Oliveira that helped us to obtain some experimental results and my partner Maria Inês who I shared all stages this project.

Thanks again to all!

Vânia Relvas

CONTENTS

ABSTRACT.....	VI
RESUMO	VII
ACKNOWLEDGEMENTS	VIII
CONTENTS	X
LIST OF FIGURES	XIII
LIST OF TABLES	XVI
ABBREVIATIONS AND ACRONYMS	XVIII

CHAPTER I

1. INTRODUCTION	1
1.1 Motivation	1
1.2 Previous Works	2
1.3 Purposes	3
1.4 Hemodynamic project team	3
1.5 Overview	4

CHAPTER II

2. THEORETICAL BACKGROUND	5
2.1 Arterial Stiffness	5
2.2 Arterial blood pressure waveform	6
2.2.1 The incisura and forward and reflected wave	8
2.3 Hemodynamic parameters	10
2.3.1 Regional PWV (RPWV)	12
2.3.1.1 Commercial devices to assess regional PWV	13
2.3.2 Local PWV (LPWV)	15
2.3.2.1 Piezoelectric sensors used in the LPWV assessment	16
2.3.2.1.1 Equivalent circuit of PZ sensor	18
2.3.2.1.2 PZ sensors used in hemodynamic studies	18
2.3.3 Limitation and pitfalls of Local and Regional PWV	19

CHAPTER III

3. PROCESS METHODOLOGY	21
3.1 Context	21
3.2 Acquisition System	21
3.2.1 Double PZ Probe	22
3.2.2 <i>CARDIOCHECK</i> Acquisition Box	22
3.3 Clinical Trials	23
3.3.1 Data Acquisition- <i>CardioCheck</i> System.....	23
3.3.2 Data Processing	24

CHAPTER IV

4 SIGNAL PROCESSING	25
4.1 Signal segmentation	25
4.1.1 Steps in algorithm	25
4.2 Algorithm to assess the PWV in the test bench II	26
4.2.1 Maximum amplitude detection algorithm	27
4.2.2 Minimum amplitude detection algorithm	27
4.2.3 Zero-crossing point identification algorithm	28
4.2.4 Pulse onset detection algorithm	29
4.2.5 Maximum of cross-correlation algorithm	29
4.3 Assessment of PWV in CCA signals	30

CHAPTER V

5 PROBE'S CHARACTERIZATION	33
5.1 TEST BENCH I	33
5.1.1 Instrumentation	33
5.1.2 Waveform Analysis	34
5.1.2.1 Gaussian Waveform	35
5.1.2.2 TYPE A Waveform	36
5.1.2.3 TYPE B Waveform	37
5.1.2.4 TYPE C Waveform	38
5.1.3 Repeatability Analysis	38

5.1.4 Crosstalk Analysis	40
5.1.5 Impulse Response (IR) and Deconvolution Method	41
5.1.5.1 Impulse Response (IR) Determination	41
5.1.5.2 Deconvolved Signals	43
5.1.6 Discussion	44
5.2 TEST BENCH II	47
5.2.1 Instrumentation	47
5.2.2 Characterization of the Test Bench II	49
5.2.2.1 Propagation of the pressure wave in the latex tube	49
5.2.2.2 Relation between DC pressure and PWV in the latex tube	51
5.2.3 Time resolution of PZ probe	56
5.2.4 Discussion	62
 CHAPTER VI	
6 PRELIMINARY CLINICAL TRIALS	66
6.1 Data acquisition Protocol	66
6.2 Recorded signals in CCA	66
6.3 Assessment of local PWV	67
6.4 Repeatability analysis in CCA signals	68
6.5 Comparison of maximum and minimum amplitude detection algorithms	70
6.6 Deconvolution method in CCA signals	72
6.7 Discussion	73
 CHAPTER VII	
7 FINAL REMARKS	75
7.1 Conclusions	75
7.2 Future work	76
 CHAPTER VIII	
8 REFERENCES	78

LIST OF FIGURES

Figure 2.1	Schematic of the important concepts of this dissertation which are related on arterial stiffness.....	5
Figure 2.2	Pressure pulse generates from ventricular systole and blood flow though arterial tree.....	7
Figure 2.3	Representation of an ABP waveform in 50 year old man and the components of arterial wave in young and elderly people waveforms.....	8
Figure 2.4	Propagation of the ABP waveform along the arterial tree.....	9
Figure 2.5	Determination of ALx, PWV and LVET from characteristic points of ABP waveform.....	10
Figure 2.6	Measurement of the distance between carotid-femoral arteries.....	12
Figure 2.7	Identification of the foot point from tree algorithms: maximum of 2nd derivate, 20% of the upslope and intersecting tangents	13
Figure 2.8	Pulse transit time (PTT) measured by Complior® and SphymoCor® systems.....	14
Figure 2.9	Molecular structure of quartz (SiO ₂) and alignment of the electric dipoles.....	17
Figure 2.10	Schematic of electronic model of a piezoelectric sensor.....	18
Figure 2.11	A MuRata® PZ sensor, the single and double headed probe.....	18
Figure 3.1	Acquisition system scheme.....	21
Figure 3.2	CardioCheck Acquisition Box and the connectors.....	22
Figure 3.3	NI-USB 6009©.....	23
Figure 3.4	Example of a <i>Cardio-Check</i> database's window.....	24
Figure 4.1	Diagram of the fundamental steps of the algorithm.....	25
Figure 4.2	A cardiac pulses waveform were segmented by an algorithm based on the idea proposed by Pan and Tompkins algorithm.....	26
Figure 4.3	Detection of the maximum amplitude peak in PZ signals by maximum amplitude detection algorithm.....	27
Figure 4.4	Detection of the minimum amplitude peak in PZ signals by minimum	

	amplitude detection algorithm.....	28
Figure 4.5	Zero-crossing point detected in PZ signals.....	28
Figure 4.6	Pulse onset detection in PZ signals.....	29
Figure 4.7	Pulse TT estimated from maximum of cross-correlation.....	30
Figure 4.8	Diagram of the process to assess the LPWV in CCA signals.....	30
Figure 4.9	Segmentation of the PZ 1 signal recorded in CCA of a volunteer.....	31
Figure 4.10	Detection of the maximum and minimum amplitude point of each PZ signal.....	31
Figure 5.1	Schematic of the test bench system I.....	33
Figure 5.2	Types of waveforms used in test bench.....	34
Figure 5.3	Gaussian waveform analysis.....	35
Figure 5.4	TYPE A waveform analysis.....	36
Figure 5.5	TYPE B waveform analysis.....	37
Figure 5.6	TYPE C waveform analysis.....	38
Figure 5.7	Repeatability test to PZ sensor 2.....	39
Figure 5.8	Results of crosstalk analysis.....	40
Figure 5.9	Schematic of IR determination method for each PZ sensor.....	42
Figure 5.10	Results of IR determination of each PZ sensors.....	42
Figure 5.11	Result of deconvolution method.....	44
Figure 5.12	The Impulse Response of a PZ1 sensor obtained by Pereira T.....	46
Figure 5.13	Schematic drawing of the test bench II.....	47
Figure 5.14	Propagation of a Gaussian waveform sensed by PZ 1 sensor at 90 cm of the tube.....	49
Figure 5.15	Representation of the data of the wave propagation in a latex tube by 3-D mesh surface.....	50
Figure 5.16	Propagation of the Gaussian waveform along the latex tube and its reflection.....	50
Figure 5.17	Recorded ACT, PS 1 and PS 2 signals at 49 mmHg of the DC pressure.....	52
Figure 5.18	Relation between the DC pressure and PWV obtained by pressure sensors.....	52

Figure 5.19	Relation between DC pressure level and diameter measured at 60, 124 and 190 cm of the tube.....	54
Figure 5.20	Exponential relationship between DC pressure and cross-section of the latex tube.....	54
Figure 5.21	Relation between the DC pressure level and PWV as a function of the distensibility of the latex tube.....	55
Figure 5.22	Representation of PWV in the three trials for lower DC pressures.....	56
Figure 5.23	Recorded signals to evaluate the time resolution of the probe.....	57
Figure 5.24	PWV assessment of five algorithms from the signals of the PZ sensors uncoupled Δx cm and pressure sensors (reference).....	59
Figure 5.25	Relative error for each distance between uncoupled PZ sensors (Δx) and each algorithm.....	59
Figure 5.26	Recorded signals of PZ and pressure sensors in response to a burst of ten Gaussian waveforms.....	60
Figure 5.27	The local PWV estimated from pressure sensors and PZ probe in 20 consecutive positions along the latex tube.....	61
Figure 5.28	Relative error between the reference PWV and determined from PZ probe for each position on the latex tube and each algorithm.....	61
Figure 5.29	Relation between DC pressure level and PWV in the silicon tube.....	64
Figure 6.1	Recorded right CCA signal recorded by a volunteer.....	67
Figure 6.2	Histogram of the mean PWV values for each volunteer during 4 weeks using two algorithms.....	71
Figure 6.3	Comparison between the deconvolved signals from PZ signals and integrated signals from PZ probe.....	72

LIST OF TABLES

Table 1	Team members of the Hemodynamic Parameters.....	3
Table 2	Gantt Diagram of duration each project task.....	4
Table 3	Features of the commercial devices that to assess the regional PWV.....	14
Table 4	The RMS error of the Gaussian waveform.....	35
Table 5	The RMS error of the TYPE A waveform.....	36
Table 6	The RMS error of the TYPE B waveform.....	37
Table 7	The RMS error of the TYPE C waveform.....	38
Table 8	Results of repeatability test.....	39
Table 9	Identification of the outliers, in gray, from the data recorded in week 4 in a volunteer.....	68
Table 10	Mean local PWV assessed by maximum amplitude detection algorithm and standard derivation for each volunteer during four weeks.....	69
Table 11	Mean local PWV assessed by minimum amplitude detection algorithm and standard derivation for each volunteer during four weeks.....	69
Table 12	Mean of local PWV \pm SD (m/s) for each volunteer and algorithm on left and right CCA.....	71

Abbreviations and Acronyms

ABP	Arterial blood pressure
ACT	Actuator
AD	Amplitude detection
AS	Arterial stiffness
<i>C</i>	Compliance
CCA	Common carotid artery
CVDs	Cardiovascular Diseases
<i>D</i>	Distensibility
DP	Double probe
IR	Impulse Response
LPWV	Local Pulse Wave Velocity
PWV	Pulse Wave Velocity
PZ	Piezoelectric
RPWV	Regional Pulse Wave Velocity
TT	Transit time
Δx	Distance between two recorded sites

CHAPTER I

INTRODUCTION

1.1 MOTIVATION

Over the past few years, the arterial stiffness (AS) has had an important role in the assessment and prevention of cardiovascular diseases (CVDs) so it has been increasingly used in clinical practice [1, 2]. Hypertension, atherosclerosis and coronary heart disease (heart attacks) are some examples of CVD which are the major causes of mortality in adults both in developing and developed countries, representing a global health problem [3, 4]. In 2008, 32% of all deaths registered in Portugal were from CVD [5]. The World Health Organization (WHO) estimates that by 2030 about 23.6 million people will die due these diseases [6]. These numbers are the mirror of the unhealthy lifestyle.

One of the key areas of work of the WHO Cardiovascular Programme is in the development of methods able to assess the pattern and trend of CVD, developing health care solutions reasonable to detect them as soon as possible [7]. Although there are some devices available in the market able to assess the AS, as Complior System[®] and SphymoCor[®] [8], its cost and the clinical level of operation are some disadvantages of these systems. In this way, the development of new noninvasive methods, cheaper, robust and feasible drives are one of the motivations behind this work.

The main aim of these technologies or devices is to quantify hemodynamic parameters as pulse wave velocity (PWV) and augmentation index (AIx). These parameters allow assessing the elastic properties of arteries, in other words the AS, that is reported as an important marker and predictor of CV risks. The PWV is related with the velocity that the arterial blood pressure (ABP) waveform propagates along the artery being inversely related to arterial wall distensibility (D). The non-invasive measurement of PWV offers a useful approach for the arterial stiffness assessment [9].

This work focuses on the principle that ABP waveform contains valuable information about the condition of the patient's cardiovascular system so that measurement is essential to assess the PWV. In this way, there is a demand for

versatile and robust clinical solutions based on development of new probes destined to measure this parameter. We developed new instrumentation which combines the Piezoelectric (PZ) technology with hardware and software required for data acquisition and data processing. From these data is able to extract accurately relevant clinical information. This new probe intends to determine the arterial wall stiffness in the carotid artery based on locally measured PWV. This new approach allows assessing the PWV in a short segment of the artery identifying local changes in arterial wall, which varies along the arterial tree and can be an indicative of atherosclerosis. Despite some researchers have development technologies to assess the local PWV acknowledging its importance in the premature diagnosis of CVD, there isn't a consensus among the scientific community of the reliability of this method in opposed to regional PWV.

1.2 PREVIOUS WORK

At the research unit, GEI, various probes have been developed for four years. They are based on different technologies but with the same purpose - to extract several hemodynamic parameters. The first studies consisted in the development of instrumental methods based on accelerometric probe for PWV hemodynamic characterization [10]. The results were promising and the studies using accelerometers continued.

The idea to explore the potential of PZ sensors to assess hemodynamic parameters came a year later. A software analysis tool was developed, called *PulScope*, which allowed to analyze the hemodynamic data and determinate the PWV and Alx. Therefore it was developed a simple and low cost hardware where the values of PWV and Alx were in agreement with reported in the literature [11]. This study encouraged us to continue to focus our attention on the development of new PZ probes (single and double headed), their characterization in test bench and new algorithms for hemodynamic parameters assessment [12, 13].

In addition, other innovative methods as optical probes and, more recently, acoustic sensors have been developed with the same purpose.

1.3 PURPOSES

The main purpose of this thesis is to develop a new double PZ probe robust, accurate, low cost and able to measure hemodynamic parameters non-invasively way. The probe was firstly characterized, in a test bench system which simulated the dynamics of arterial system and secondly, in clinical trials from human common carotid artery (CCA).

Algorithms for the signal processing were implemented in order to segment, and determine the local PWV (LPWV).

1.4 HEMODYNAMIC PROJECT TEAM

This project was developed at *Grupo de Electrónica e Instrumentação* (GEI) in the framework of a partnership with *Instituto de Investigação e Formação Cardiovascular* (IIFC), *Escola Superior de Tecnologia da Saúde de Coimbra* (ESTeSC) and *Intelligent Sensing Anywhere* (ISA).

The work team involved in this project, their contributions and the associated staff and students are summarized in the Table I.

Table 1 - Team members of the Hemodynamic Parameters.

TEAM MEMBERS	MAIN CONTRIBUTION AND MAIN AREAS OF RESEARCH		INSTITUTION
Prof Dr. Carlos Correia	Scientific and Technical Supervisors	General Software and Hardware Development	GEI
Dr. João Cardoso		Software Development	GEI
PhD Student Helena Catarina Pereira		Hemodynamic Parameters	GEI/ ISA
PhD Student Tânia Pereira	GEI		
PhD Student Vânia Almeida			
Dr. João Maldonado	Medical Supervisor	Clinical trials/Prototypes validation	IIFC
Dr. Telmo Pereira	Medical Supervisor	Clinical trials/Prototypes validation	ESTeSC

1.5 OVERVIEW

This dissertation is presented in seven chapters whose content is briefly summarized:

- Chapter 2 *Theoretical Background* - important concepts about arterial stiffness, hemodynamic parameters and devices able to assess them are described. It is writing a review paper about local and regional PWV.
- Chapter 3 *Process Methodology* – describe the general acquisition system: the probe, acquisition box and *Cardio-Check* Database.
- Chapter 4 *Signal Processing* – A segmentation algorithm based on Pan and Tompkins algorithm was implemented. The local PWV was determined either in test bench II or in human CCA using different algorithms.
- Chapter 5 *Probe Characterization* – two test benches were developed in order to simulate the properties of the cardiovascular system and characterize the new PZ probe.
- Chapter 6 *Preliminary Clinical Trials* – The PZ probe was tested on a small group of volunteers without knowledge of cardiovascular disease.
- Chapter 7 *Final Remarks* – Conclusions about this dissertation and some problems that it must be overcome to improve the results.

The table 2 shows a diagram of the tasks of the plan work carried out during the project and the duration of these tasks.

Table 2 – Gantt Diagram of duration each project task.

ID	Tasks	Beginning	End	Duration (weeks)	2010				2011									
					Set	Out	Nov	Dez	Jan	Fev	Mar	Abr	Mai	Jun	Jul	Ago	Set	
1	State of the art	01-09-2010	15-04-2011	32,6s	[Gantt bar spanning from Sep 2010 to Apr 2011]													
2	Hardware development	01-11-2010	28-02-2011	17,2s	[Gantt bar spanning from Nov 2010 to Feb 2011]													
3	Review paper	21-02-2011	08-04-2011	7s	[Gantt bar spanning from Feb 2011 to Apr 2011]													
4	Probe Characterization – Test Bench I	07-03-2011	09-05-2011	9,2s	[Gantt bar spanning from Mar 2011 to May 2011]													
5	Probe Characterization – Test Bench II	30-05-2011	29-07-2011	9s	[Gantt bar spanning from May 2011 to Jul 2011]													
6	Signal Processing	16-05-2011	29-07-2011	11s	[Gantt bar spanning from May 2011 to Jul 2011]													
7	Clinical Trials	08-06-2011	29-07-2011	7,6s	[Gantt bar spanning from Jun 2011 to Jul 2011]													
8	Project Report	01-06-2011	30-08-2011	13s	[Gantt bar spanning from Jun 2011 to Aug 2011]													

CHAPTER II

THEORETICAL BACKGROUND

2.1 ARTERIAL STIFFNESS

The blood enters at the arterial system in a series of strong bursts by the pumping action of the heart. The arterial walls are evolved to withstand the cyclical distension and contraction caused by the ejected blood from the left ventricle. But with increasing age the elastic fibers, which constituted the arterial walls, begin to fray due to mechanical stress, decreasing the elasticity of the arterial wall by the subsequent replacement of the elastin by collagen [14]. This property of the arteries in terms of elasticity or compliance is called **AS** [14]. The elastic properties of the arteries are nonlinear along the arterial tree. The ascending aorta, common carotid artery (CCA) and iliac arteries are more elastic than the brachial, radial, and femoral arteries (muscular arteries) due to the molecular and cellular structure of the arterial wall [1][14][15]. A gradual increase of the stiffness in elastic arteries causes an increase in the systolic blood pressure. It happens because the stiffer arteries aren't able to dilate or expand in order to accommodate the ejected blood by left ventricle and the increase of systolic pressure is necessary to eject the same stroke volume [18].

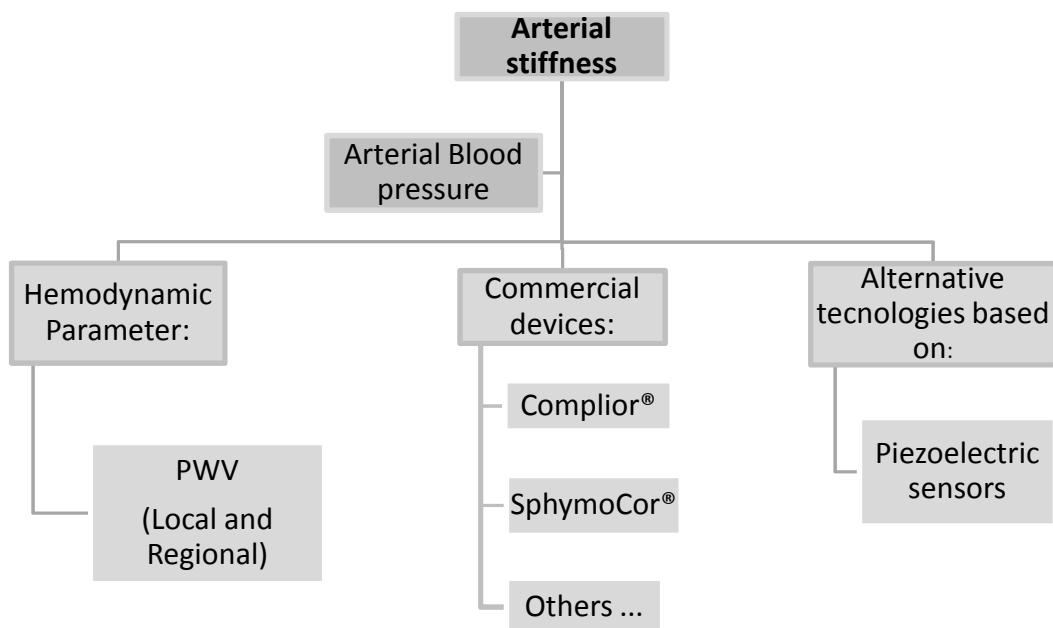


Figure 2.1 – Schematic of the important concepts of this dissertation which are related on arterial stiffness.

The increasing of AS is associated not only with the age but also to genetic factors as parental history of hypertension and diabetes; to menstrual cycle; obesity, smoking; cardiovascular diseases as coronary heart disease, among others [1].

It has been demonstrated that the AS has an important role to predict the development of **CVD**, becoming to be a started point for the early detection and prevention of these diseases [1, 9]. Some **hemodynamic parameters** have been introduced in order to assess the elastic properties of the arteries. The **Pulse Wave Velocity (PWV)** is considered the gold standard parameter that can be measured on a non-invasive way which allows the indirect estimation of the arterial stiffness [1] [2] [16]. Because the elasticity of the arterial walls varies along the arterial tree, also the velocity of the pulse wave propagation is influenced by the increasing of the arterial wall hardness. The central arteries (aorta and carotid) are more elastic and the PWV is lower in these arteries. When moving to the peripheral arteries (femoral or brachial arteries) the stiffness increased and the PWV in this sites increase too [1][17]. The measurement of the PWV can be distinguished in **local and regional PWV**. Beyond the PWV other parameters have been developed and all they extract information from the **ABP waveform** measured on arteries. The morphology of the pressure waveform measured contains key points that allow assessing the hemodynamic parameters.

Over the last years, different devices have been developed to assess PWV as the well known **commercial devices** Complior® and SphymoCor® system but due to its high cost other non invasive apparatus, based on **Piezoelectric sensors**, for example, has been developed. The figure 2.1 shows a diagram about of the important concepts which are highlighted along of the text to understand this dissertation.

2.2 ARTERIAL BLOOD PRESSURE WAVEFORM

The blood ejected from left ventricle to ascending aorta propagates throughout the arterial tree in form of waves – the arterial blood pressure (ABP) waveform. From antiquity, the arterial pulse is understood as a sign of life and its change related with the force that the blood exerts on arterial wall has been associated with the health or disease condition [19].

When the ventricular systole occurs, the ascending aorta (elastic large artery) expands and absorbs some of the transient increase in pressure generated by the ejected blood, due to the compliance of the central artery walls [14]. The compliance (C) of the arteries is defined by the ability to stretch in response to increase of the blood volume which is stored temporarily in the artery reducing blood pressure increase during ventricular ejection and to recover the original dimensions upon removal of the pressure. This relation between volume and pressure define mathematically compliance as:

$C = \frac{\Delta A}{\Delta P}$, where ΔA is changes of cross-section area of the artery ($A_{\text{systolic}} - A_{\text{diastolic}}$) and ΔP is changes in the pulse pressure [19],[20].

The distensibility (D) also is related with the elastic properties of arteries reflecting the artery diameter variability to a corresponding variability blood volume and pressure, mathematically defined as:

$D = C * \frac{1}{Ad}$, where Ad is diastolic arterial cross-section [20].

After blood ejection, there is an exchange of energy between the arterial wall of ascending aorta and the blood flow allowing the propagation of the pressure wave [14]. The figure 2.2 shows a drawing of this phenomenon that happens while the artery is compliant; otherwise the pulse pressure (difference between systolic and diastolic pressure) increases with the increased of arterial stiffness, as it was referred in previous section.

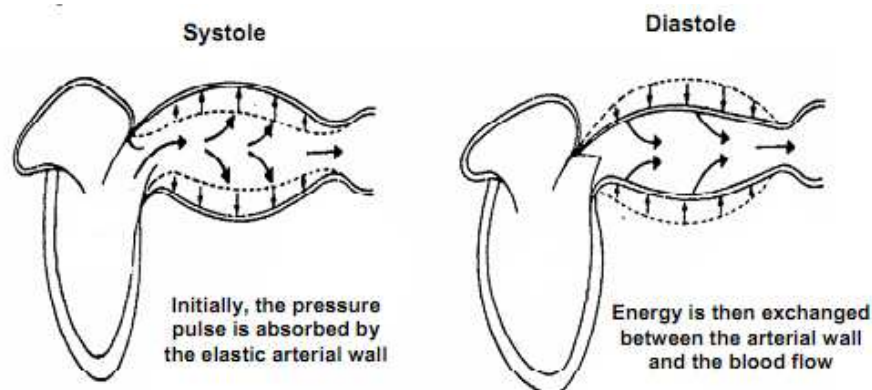


Figure 2.2 – Pressure pulse generates from ventricular systole and blood flow through arterial tree due to the change of energy between arterial wall and the blood flow during the diastole [14].

2.2.1 THE INCISURA AND FORWARD AND REFLECTED WAVE

The heterogeneity of geometric and visco-elastic properties of the arterial walls along the arterial tree have an important physiologic consequences that are reflected in changes in the morphology of ABP waveform. The morphology of the ABP wave reveals important phenomenon that occur during the cardiac cycle providing a prediction about cardiovascular risk.

Two main components characterize the ABP waveform: the propagation of incident or forward wave which results the blood ejected from left ventricle during systole (with amplitude P_s - P_d), and the reflected wave from the periphery (with amplitude P_s - P_i), figure 2.3 a) [21]. The forward wave when travels to radial artery, the mean pressure decrease slightly due to high conductive arteries and low resistance to blood flow [22]. However, the blood flows to the peripheral arteries and finds bifurcations (e.g. iliac and femoral artery), figure 2.4, that block its entry because the vascular resistance and impedance increase, causing the reflection of the pressure pulse that travel back towards the heart. In this way, the reflected wave, is called backward wave, acts to augment the pressure pulse [21- 23][32].

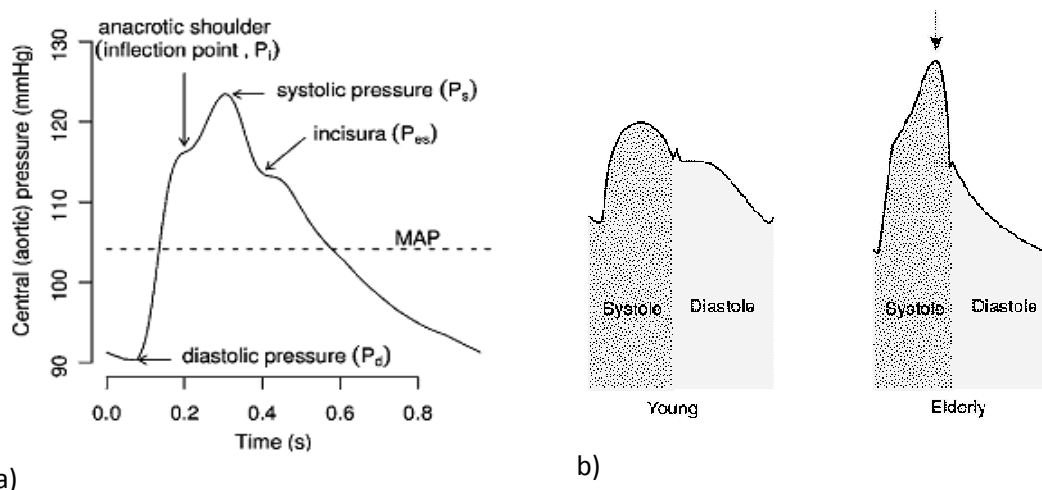


Figure 2.3 – a) Representation of an ABP waveform in 50 year old man corresponding central aortic pressure wave, the characteristic peaks (P_d , P_i , P_s , P_{es}) and the mean arterial pulse (MAP) [19]; b) two components of arterial wave in young and elderly people waveforms [21].

For young people the reflected wave coincides with the diastolic pressure wave while in elderly people the D of arteries is smaller resulting in earlier reflected wave which overlapping the systolic wave increasing the systolic pressure and consequently

the pressure pulse. The systolic peak occurs later and diastolic wave is attenuated [21,32], figure 2.3 b). The ‘interaction’ between reflected and forward wave induces a change in the ABP waveform by appearing of the inflection point P_i , figure 2.3 a). The location of inflection point in relation to systolic peak (P_s) can bring information about arterial stiffness of artery [25-26]. In figure 2.3 a) the inflection point precedes the systolic peak meaning that the reflected wave arrived in early systole and indicates that the artery is stiff. When the inflection point occurs after systolic peak represents that the artery is elastic and consequently the patient is health [12]. Murgo et al proposed a classification based on four types ABP waveforms [25]. From this classification we synthesized cardiac waves to simulate different physiological conditions, are shown in section 5.1.

Due to differences in arteries compliance and the of wave reflection the shape and amplitude of ABP wave changes with age of patient and the site of the body where is recorded, figure 2.4. At the peripheral arteries the amplitude of pressure wave is higher than central arteries because the reflection sites are closer to them, causing the ‘amplification phenomenon’ represented in figure 2.4. It means that the systolic pressure, diastolic pressure and mean arterial pressure also increase [1][24].

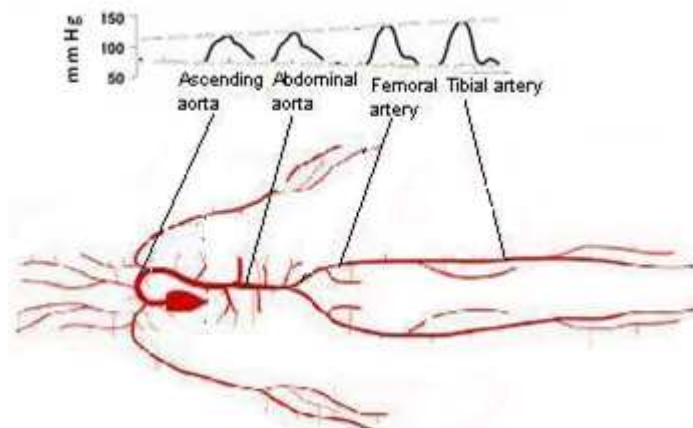


Figure 2.4 – Propagation of the ABP waveform along the arterial tree. The ‘amplification phenomenon’ is verified by of amplitude of pressure pulse. Adapted from [27, 28]

After ventricular systole the aortic valve closes causing an increase of pressure in ascending aorta which is called the incisura. The incisura point (P_{es}) marks the

beginning of ventricular diastole which is represented by dicrotic wave in ABP waveform, figure 2.3.

2.3 HEMODYNAMIC PARAMETERS

The measurement of AS is a focal point to assess the cardiovascular risk of the patients. The hemodynamic parameters allow quantify the AS through the analysis of ABP waveform, e.g. the augmentation index (Alx) measures the contribution of reflected wave in the total pressure pulse, figure 2.5 [29][31].

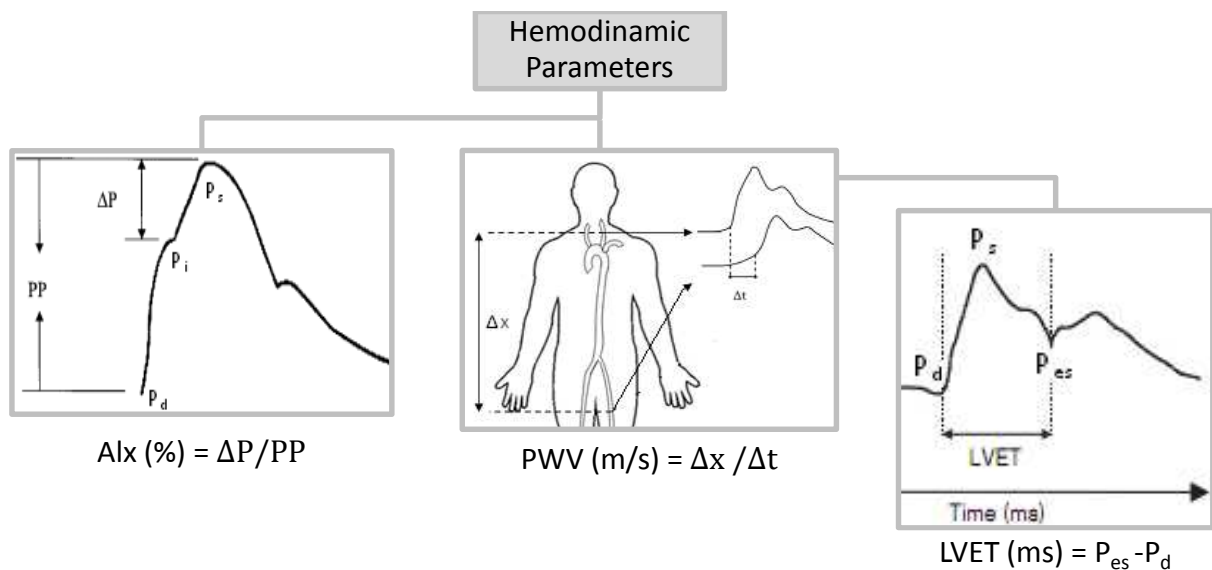


Figure 2.5 – Determination of ALx, PWV and LVET from characteristic points of ABP waveform. Adapted from [29],[31],[30] respectively.

However, the PWV is the most used marker of vascular stiffness and a predictor of CVD that measures the velocity which the ABP waveform propagates along of a segment of arterial tree, figure 2.5 [31, 34]. Elastic modulus (E) of the arterial wall, the blood density ($\rho = 1.05 \text{ g/cm}^3$), the thickness (h) and lumen radius (r) that characterize the arterial geometry are related with PWV, as Moens and Korteweg showed by the following equation:

$$PWV = \sqrt{\frac{E * h}{2 * r * \rho}} \left(\frac{m}{s} \right)$$

when described a model based on a elastic tube filled with an incompressible fluid [1][31-33]. The measurement of PWV is also inversely related to D of arterial wall by:

$$PWV = \sqrt{\frac{\Delta P * V}{\Delta V * \rho}} = \frac{1}{\sqrt{D * \rho}} \left(\frac{m}{s} \right)$$

This relation shows that the value PWV depends on geometric and elastic properties of arteries (h , r and D), which varies along arterial tree, so PWV also varies from one measurement location to another [1][26]. Thus, in humans the PWV is 4-5 m/s in the ascending aorta, increasing to 5-6 m/s in the abdominal aorta and in the iliac and femoral arteries is near 8-9 m/s [1]. PWV's value is greater than 12m/s it has been considered a predictor of CVD risk, mainly in hypertensive patients [37]. This increased of PWV along arterial tree is associated with:

- the 'amplification phenomenon';
- the increase AS in peripheral arteries that causes the increase of systolic pressure by the early arrival of reflected wave – stiff artery, high PWV;
- age and blood pressure [1].

Age and blood pressure are hemodynamic factors as well as the left ventricular ejection time (LVET) that influence the PWV. LVET measures the time interval between the opening and the closing the aortic valve which corresponds from the onset of ventricular systole to incisura point, figure 2.5 [30].

In practice, the assessment of PWV is made through the measurement of the time delay (Δt) between the pressure waves recorded in arterial system and the distance (Δx) on the body's surface between recording site(s), as is shown in figure 2.5 [31-32].

The measured in common carotid to femoral arteries is considered by the Expert Consensus document [1] the 'gold standard' method to assess aortic PWV. In fact, it's not possible to measure PWV in aorta artery by a non-invasive method and the CCA is near to the heart. Moreover, carotid and femoral are sites easily accessible representing the PWV assessment along a segment composed by elastic and muscular arteries [1, 14, 18]. A new approach to assess the PWV appeared which consists to assess PWV in a short segment of an artery.

2.3.1 REGIONAL PWV (RPWV)

The measurement of regional PWV is made from distance over a long segment of the arterial tree and the transit time (TT) between the two recorded waves in this segment. The two measurement sites are along of a segment of easy access of arterial tree like: Radial-tibial, brachial-ankle, carotid-radial, brachial-radial and femoral-tibial [26, 31, 35]. But carotid-femoral path is widely used to assess the regional PWV, as illustrated in figure 2.5 [1].

The path length between recorded sites due to the trajectory or curvature of vessels is not easy to measure. Two main hypotheses mentioned on the literature for distance determination between recorded sites:

- i) the simplest one assumes the arterial segment under study as a homogeneous and isotropic material and without any curvature, and simply takes the direct measure of the distance between the two measurement sites on the surface of the body by a tape meter;
- ii) another approach is using a corrected value resulted from the subtraction of the distance from the carotid location to the sterna notch from the total distance or by the subtraction of the distance from the carotid artery location to sterna notch from the distance between the sterna notch and femoral artery site of measurement, figure 2.6 [31].

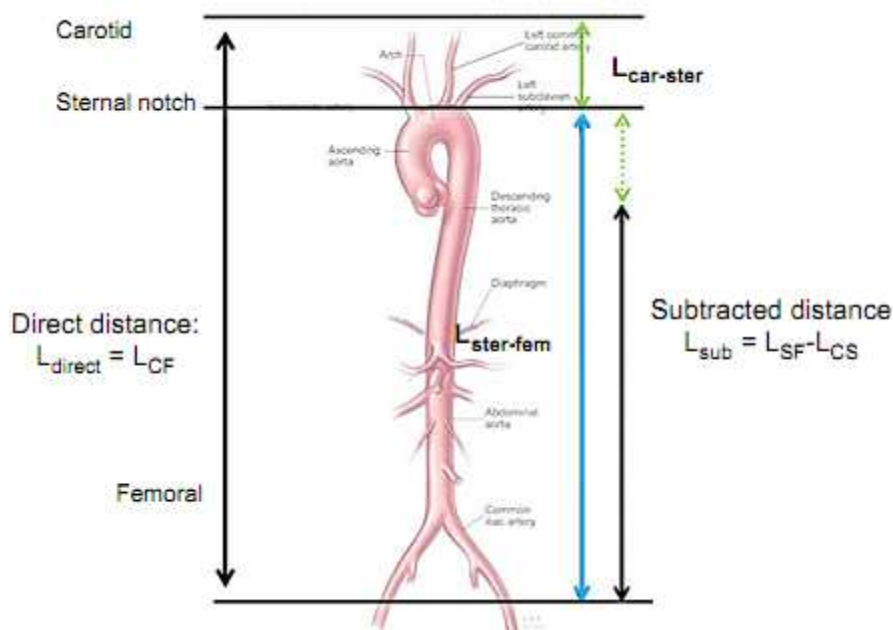


Figure 2.6 – Measurement of the distance between carotid-femoral arteries [31].

The transit time delay is determined from of a characteristic point of the pulse waves, normally by foot of wave. There are three main algorithms to identify the foot from ABP waveform, figure 2.7:

- Maximum upstroke of second derivate;
- Time-point at 20% of the upslope of ABP wave and
- Intersecting tangents – interception of minimum value of ABP wave with the steepest part of the slope, being this method the most reliable [31, 36].

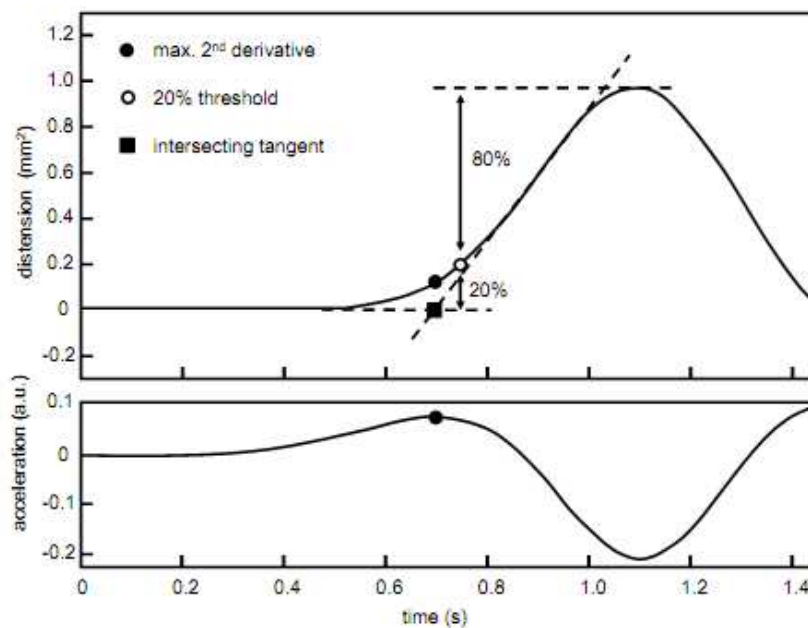


Figure 2.7 – Identification of the foot point from three algorithms: maximum of 2nd derivate, 20% of the upslope and intersecting tangents [36].

Currently, there are in the market some devices used in clinical practice which allow assess the RPWV. They estimate the TT from different algorithms and the waves are recorded by different methods.

2.3.1.1 COMMERCIAL DEVICES TO ASSESS REGIONAL PWV

Complior® and SphymoCor® Systems are the ‘gold standard’ commercial devices for the PWV assessment [31, 37]. SphymoCor® measures with a tonometer the carotid or radial wave and simultaneously is recorded the ECG signal. The foot of carotid and radial waves is estimated by intersecting tangent algorithm and the TT is estimated between the R-wave on the ECG and the foot of each wave recorded in different sites, figure 2.8. It is obtain two TT values that are combined to obtain a single TT value [14]. In relation to Complior®, it used piezoelectric sensors to record

simultaneously the signals at CCA and femoral arteries. The time delay between the foot of two recorded waves is the pulse TT, figure 2.8 [14]. The new Complior® System is able to measure three different arterial segments at the same time to study peripheral arteries, to measure the central pressure waveform and analyze the pulse wave which allows study the wave reflection by Alx.

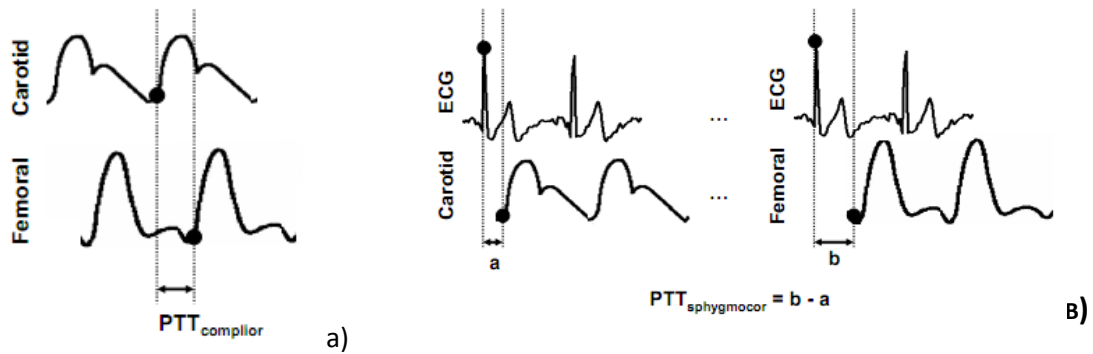






Figure 2.8 – Pulse transit time (PTT) measured by: a) Complior® and b) SphymoCor® systems. Adapted from [14].

Other devices commercialized more recently are: Arteriograph® and PulsePen®, where the first uses an upper arm cuff to occlude the brachial artery and the second uses the same method that SphymoCor® but it analyses directly the pulse wave without a transfer function [37]. The main characterizes of commercial devices are summarized in the table 3.

Table 3 - The features of some commercial devices that assess the regional PWV.

Devices	Company	Pulse waves detected on	Measurement technique	Principles and Features	Algorithm transit time	Other Parameters
 <p>Complior System®</p>	Artech Medical, Pantin, France	Carotid-femoral; carotid-radial; carotid – distal	Piezoelectric sensor	TT between foot of two recorded waves	Correlation algorithm	Heart rate; Central pulse pressure; LVET; Alx
 <p>Sphymocor® system</p>	AtCor Medical, Inc., Sydney, Australia	Carotid and femoral	Applanation tonometry +ECG	Use a transfer function to measure Alx and aortic pulse wave	R-wave + foot (Intersecting tangent algorithm)	Heart rate; Alx
 <p>TensioClinic™ Arteriograph</p>	TensioMed Ltd., Budapest, Hungary	Brachial	Oscillometric method	PWV estimated by oscillations detected on the upper-arm cuff.	occluded brachial artery	Blood pressure; Alx; Pulse Pressure
 <p>PulsePen® device</p>	Diatecne, Milano, Italy	Carotid, brachial, radial, femoral	Applanation tonometer + ECG	Determine Δt delay between pressure waves	Foot + R-wave	Heart rate; Blood pressure; Alx; LVET

Some studies were done in order to compare the PWV measured by Arteriograph®, Complior® and SphygmoCor® and that reported: a) there are a poor agreement between the PWV values determined by these devices and b) it still hasn't been enough studies that show Arteriograph how a 'gold standard' technique [38]. With these available devices are calculated different PWV because each device overestimate the distance between recorded sites and use different algorithms to assess the transit time based on different characteristic time-point of the waveform. This not allows comparing perfectly the devices hence one solution could be all manufactories to establish the same principles for measuring the travel distance [37][18].

2.3.2 LOCAL PWV (LPWV)

Another approach to assess PWV consists in measurement of pulse wave in a short segment of an artery, usually on CCA. ABP waves are recorded simultaneously by two sensors at close positions which allow know exactly the distance that were recorded [18, 41]. As mentioned previously, the elastic and geometric properties of arteries vary significantly along arterial tree as well as the pressure and blood flow due to the branches [39]. CCA has an elastic behaviour and femoral is a muscular artery, these properties change with age. While the RPWV measure the average PWV along a segment with different proprieties, the LPWV measures the PWV and pressure in the same artery so it's an advantage to the regional assessment [39].

The pulse TT is also measured the time delay between two recorded waves. The foot of waves are the reference point to estimate the TT but the systolic foot isn't free from reflected waves [26, 40]. In this case, the artery's segment to assess PWV locally without reflections sites, is only considered the backward and forward propagations waves [39, 40].

PWV is inversely related to the D of the artery. It means that to measure locally the PWV from D of artery, the local pulse pressure and diameter of artery need to be estimated [40]. Khir et al. measured the change in pressure and volume at the end of a latex tube to assess the LPWV. However, isn't easy to estimate the local pulse pressure therefore new methods based on ultrasound appeared without local pulse pressure measurements and lower coefficient of variation (CV).

Two ultrasound probes spaced at 9 mm were used by Brands et al. to calculate the ratio between temporal and spatial gradient with B-mode image [42]. A more recent approach to assess and use the diameter waveform for LPWV determination was proposed by Meinders et al, suggesting a multiple M-line system with 16 lines that allows the simultaneous recording of the diameter waveform on 16 positions [43].

Later, Hermeling et al. developed a method to measure the local PWV using an M-mode ultrasound. They identified the foot of distension waveforms, from time delay algorithms in figure 2.7, the purpose is to measure the change of diameter over time. This method exhibited good results with CV of 1% [18].

Also the MRI technology has been mentioned as an alternative to measure LPWV. Tarnawski M. et al (1994) applied the comb-excited Fourier velocity-encoded MRI technique to measure simultaneously wavespeed at two stations, 14 cm apart, on the femoral artery. In order to allow the selection of a straight artery segment and localize the tow stations, 2-D MR phase contrast (sagittal and coronal) angiograms of the femoral artery were acquired [44].

Our research group has been devoted to the development and characterization of new sensors for LPWV assessment. The aim of this thesis is to characterize a new probe to assess LPWV based on piezoelectric sensors.

2.3.2.1 PIEZOELECTRIC SENSORS USED IN THE LPWV ASSESSMENT

The electric measuring of mechanical quantities has been increasingly used in research and industry (process control) since the middle of the 20th century. Velocity, acceleration, force and pressure are some mechanical quantities that can be measured [45].

Piezoelectric (PZ) sensors are able to measure pressure, acceleration, strain and force. [46] They are characterized to have a transduction element and are called active sensors because they don't need an external power source to yield an electric charge (output signal) in response to a mechanical load due to behaviour of the PZ material which is made the transduction element, namely crystals and ceramics. [45]

The quartz (SiO_2) crystal is an example of the PZ material which changes its dimension when transform energy of a mechanical input into an electric output. The PZ crystals have a molecular structure of the ionic bonded crystal (figure 2.9 a)) and a permanent electrical polarization (figure 2.9 b)). As a consequence of the symmetry of the crystal structure the electric dipoles are aligned and the respective positive and negative ions cancel each other. As a result, the electric field is not observed. [47]

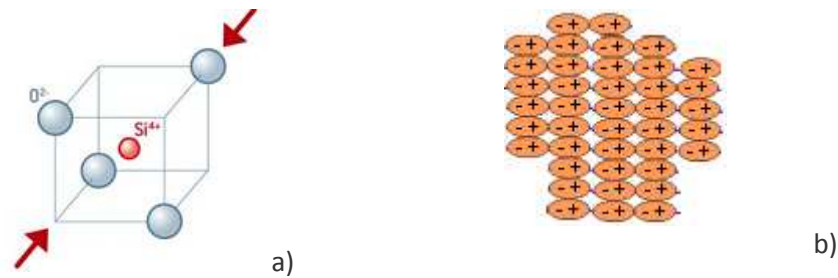


Figure 2.9 – a) Molecular structure of quartz (SiO_2) [48], b) alignment of the electric dipoles, adapted [46]

When a force is applied on PZ material there is the separation of the charges with the loss of the symmetry of the crystal structure, the orientation of the dipoles change and the crystal became electrically polarized creating an electrostatic output voltage - this phenomenon was labelled the piezoelectric effect. The polarity of the voltage generated depends on the atomic structure of the material and the direction in which the force is applied. This voltage (V) caused by the new charge distribution (Q) is mathematically expressed by:

$$V = \frac{Q}{C}$$

where C is the capacitance of the material.

Some advantages are recognized of PZ sensors as:

- High rigidity, able to measure deflection in the μm range;
- Reproducibility;
- High natural frequency (up to over 500 kHz);
- Wide operating temperature range [45].

2.3.2.1.1 EQUIVALENT CIRCUIT OF PZ SENSOR

A PZ sensor can be modelled by an RC circuit, it means by a capacitor with capacitance C in parallel with a current source and a resistor, in turn, is in parallel with the other two, as show in figure. The PZ actuates as a differentiator, the current flow is equal to the derivate of the charge then the current source is $\frac{dq}{dt}$ [49]. The capacitance is determined by the area, the width, and the dielectric constant of the material.

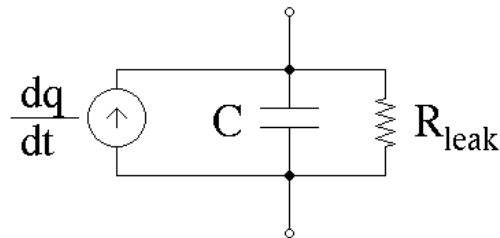


Figure 2.10 - Schematic of electronic model of a piezoelectric sensor. [49]

The voltage, V , at the source is proportional to the applied pressure on PZ sensor and is measured across the PZ terminals. The resistor, R , results in a high-pass filter which explains why the PZ can sound high-passed. One possibility to decrease this effect is to use a voltage follower circuit between the PZ and the input to the ADC [49].

2.3.2.1.2 PZ SENSORS USED IN HEMODYNAMIC STUDIES

As mentioned in chapter I, new probes have been developed at GEI in order to assess hemodynamic parameters. These probes based on PZ sensors (MuRata®), consist in a single and a double headed probes, as shows in figure 2.11 b) and c). Both probes have shaped pieces of ‘mushrooms’ as an interface between PZ sensor and the CCA. The studies with both probes involved besides the characterization in test bench system, the determination of the local PWV and AI_x , showing encouraging results.



Figure 2.11 – a) A MuRata® PZ sensor, b) single and c) double headed probe.

Other studies have been carried out using a thin film piezoelectric sensor system (McLaughlin J et al 2003) in order to assess regional PWV between radial and brachial arteries, non-invasively using different methods [50].

More recently, *Clemente F. et al 2010*, proposed a non-invasively method based on piezo-film sensor too. This allowed to measure the blood pressure waveform at radial artery and to reconstruct it online [51].

2.3.3 LIMITATIONS AND PITFALLS OF LOCAL AND REGIONAL PWV

The first limitation that can be referred about RPWV determination is the fact that it represents only an average value due to its variation of the properties of the arterial segment under study [52]. In fact, elastic properties of vessel walls are site dependent, which causes an increase of PWV from a measurement point near the heart (usually CCA) to a peripheral artery (usually femoral).

The path length carotid-femoral to assess RPWV is difficult to measure and there are two approaches referred in section 2.3.1. However, both methods have the disadvantage because the measurement is made on body surface inducing errors on the absolute value of PWV. On the other hand, distance measurements can also be hindered in patients with abdominal obesity or in women with large bust size. Magnetic resonance imaging has as its major advantage the possibility of measuring with great accuracy the path length, but its temporal resolution is low when comparing with other techniques [26].

The lack of standardization of the measurement method of TT makes the commercial devices use different algorithms that can influence the final value of PWV. This problem is caused by the inherent difficulty on the definition of the foot of the wave mostly because, during its propagation along the arterial tree there are wave reflections, which in turn causes the time-point used in the identification of the onset of the wave is shifted to a different position within the waveform [18]. Despite these problems about measurement of distance and TT estimated the Complior® System continues to be the gold standard technology.

If the difficulty to measure a distance between recorded sites is the tender spot of RPWV, the LPWV resolves it easily because the distance between recorded sensors is well known. But one problem can emerge: to know the minimum space along a short arterial segment to allow assessing simultaneously two arterial waveforms with higher temporal resolution [42, 53].

The foot's identification of recorded waves is used as time reference point to estimate pulse TT, and consequently to assess LPWV, because isn't affected by reflections. However, the backward propagation waves change the shape of ABP waveforms and can interfere with the foot's identification affecting the pulse TT estimation [40].

The precision of measured methods to assess LPWV is poor yet but promising techniques have been developed suggesting the dicrotic notch as an alternative time-reference point [54].

CHAPTER III

PROCESS METHODOLOGY

In this chapter the hardware development by the hemodynamic team is described – the conception of the new PZ probe, the *CardioCheck* acquisition box and the *Cardio-Check* system v1.0.

3.1 CONTEXT

As previously stated in chapter 1, this project aims to continue the study of pulse wave assessment using PZ sensors. The previous development studies at GEI demonstrated the feasibility of PZ sensors in extracting relevant information of pulse wave signal at CCA [12, 13].

The developed acquisition system allows visualize the ABP waveform. It is a new feature of the system that intends to reproduce the ABP waveform. This system was used to characterize the PZ probe in the test bench and in clinical trials.

3.2 ACQUISITION SYSTEM

The main elements which constituted the acquisition system are: the double PZ probe, the acquisition box and a PC as the schematic in figure 3.1 shows. A description of the elements follows.



Figure 3.1- Acquisition system scheme. 1- Common carotid artery, 2- Measurement probe (Double PZ probe), 3- Data acquisition system (*CardioCheck* Acquisition Box), 4- Data logging processing and storage (PC), 5- NI software (*Measurement & Automation*) or *Cardio-Check* database.

The ABP waveform is recorded on common carotid artery by PZ probe. The *CardioCheck* Acquisition Box, with data acquisition (DAQ) module, sends the data to PC by USB cable. The data are recorded using the *National Instruments* software, in the

test bench systems, or the *Cardio-Check* system, in the clinical trials, and after processed in Matlab® software.

3.2.1 DOUBLE PZ PROBE

The new instrument proposed is a double headed probe based on PZ sensors (MURATA® 7BB-12-9 Sounder, 12mm of diameter) that are placed apart. It allows the assessment two signals: the PZ signal (the derivate of the pressure waveform, dP/dt , – piezo-electric effect) and the integrated PZ signal (the ABP waveform, – obtained by the electronic circuit of the probe). For more information's about DP see the appendix.

A RJ45 connector allows connecting the double probe to *CardioCheck* acquisition box.

3.2.2 CARDIOCHECK ACQUISITION BOX

The *CardioCheck* acquisition box, represented in figure 3.2, supports the double PZ probe and has additional inputs for PZ probe characterization in the test benches which are: one entry for the arbitrary waveform generator, *Agilent*, and two entries for pressure sensors. Into this unit there are a data acquisition (DAQ) module and a power supply +5V/-5V.

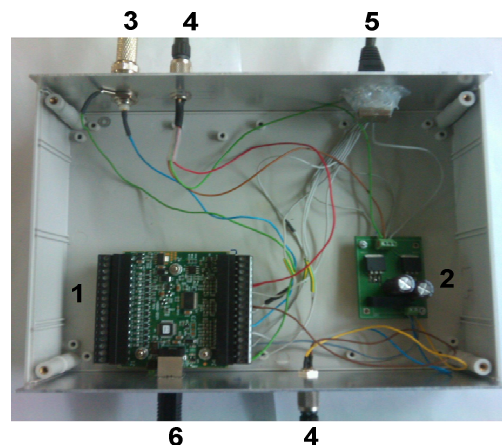


Figure 3.2 – CardioCheck Acquisition Box and the connectors. 1 – NI-USB 6009, 2 – Power supply, 3 - waveform generator connector , 4 – Pressure sensors connectors , 5 – PZ probe connector, 6- USB.

In Figure 3.3 shows the DAQ module used is in this measurement system. It's the NI-USB 6009©, it has 8 analog inputs, 14-bit resolution and it can sample up to

48kS/s [55]. Driver software is necessary to configure the NI-DAQmx© in order to acquire, analyze and log the measurement data. If the data are logged in NI software they will be saved in a .txt format and after will be processed in Matlab®.

The power supply is based on a layer printed circuit board (PCB) that used as input the ground and +5 volt from NI-USB 6009 and as output +5 volt, -5 volt and ground that power the PZ probe.



Figure 3.3 – NI-USB 6009© [55].

3.3 CLINICAL TRIALS

Two more prototypes of PZ probe and CardioCheck acquisition box were developed in order to record data in human carotid in IIFC by João Maldonado and in ESTeSC by Telmo Pereira. The clinical data were also recorded in a small group of volunteers at GEI.

3.3.1 DATA ACQUISITION – *CARDIOCHECK* SYSTEM

There was developed a graphic interface in Microsoft Access® database- *Cardio-Check Database* v1.0 - useful to store and record clinical data of a large number of patient. The data base allows:

- i) To select which probe are recording the data (PZ probe, Acoustic probe or accelerometric probe);
- ii) To save the cardiac signals recorded;
- iii) To register the operators;
- iv) To save patient's information (personal information, personal history, family history, clinical parameters (age, sex, weight, height), biochemical analysis and notes) ;

- v) To register the PWV with reference device (Complior[®]), the diastolic and systolic pressure.

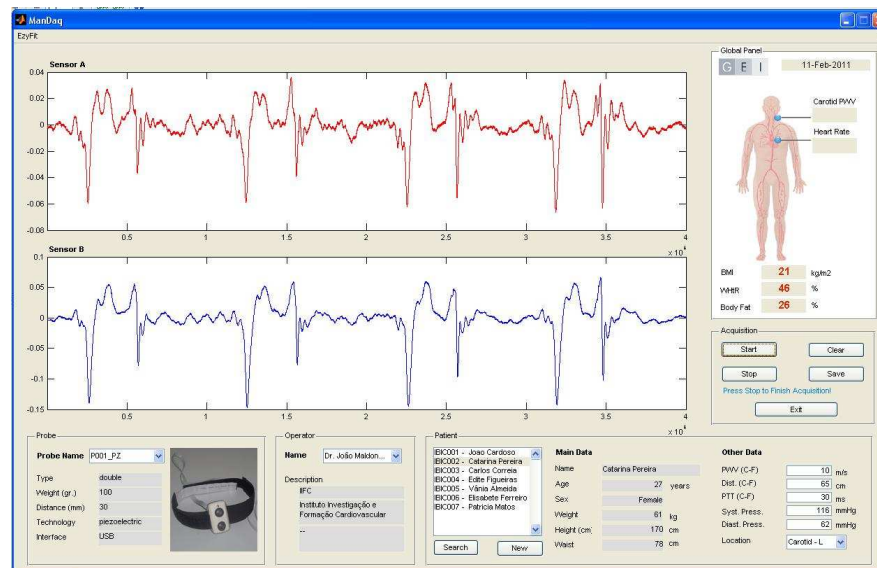


Figure 3.4 – Example of a window of the data acquisition software in real-time.

The software to acquire signals in human CCA in real-time is connected to the database. The figure 3.4 shows an example a window of the acquisition software. The signals were acquired by another double PZ probe.

3.3.2 DATA PROCESSING

The data acquired are processed in Matlab[®] where the signals are filtered, segmented and was assessed the local PWV. The algorithms used to assess the local PWV are described next chapter.

CHAPTER IV

SIGNAL PROCESSING

This chapter describes the algorithms used to segment the pulse waves and to determine the LPWV either in the test bench II or in the human CCA signals.

4.1 SIGNAL SEGMENTATION

One of the important steps of the cardiac signals processing is the signal segmentation. There are some algorithms to detect the onset of ABP, as *Zong W. et al* (2003) concerning the importance of ABP onset detection to study the PWV [56].

In this work was implemented an algorithm based on the idea proposed by Pan and Tompkins [57], which is able to detect the onset and the end of the each pressure waveforms segmenting a signal into periods. The basic idea of the original algorithm is to determine the energy of the signal and detect the higher-energy peaks.

Before applying any algorithm, the signals are normalized after being removed the DC component.

4.1.1 STEPS IN ALGORITHM

The algorithm consists in four fundamental steps, as shown in figure 4.1: i) the signal passes through a moving average filter, ii) differentiation, iii) squaring, iv) setting the threshold by the mean of the squaring signal.

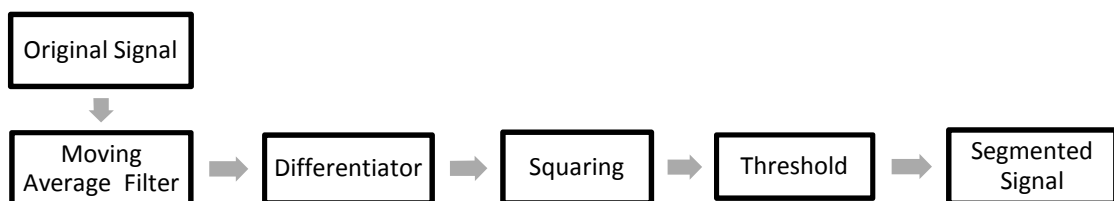


Figure 4.1 –Diagram of the fundamental steps of the algorithm.

The moving average filter allows smoothing the signal and decreasing the high frequency noise. The operation of differentiation is like a high pass filter, the differential signal notes the peaks with the greatest variation of the signal. In order to not obtain the negative data, the next step of the algorithm is to square the signal.

The most important step in this algorithm is the calculation of the threshold which tries to be independent of the signal and ideally allows its adjustment to changes in the signal to analyzing. The threshold is defined as 20% of the mean of the square signal and the points of the original signal that are above the threshold are stored in a matrix of zeros where the onset and the end of pulses are identified, as shows the example in figure 4.2.

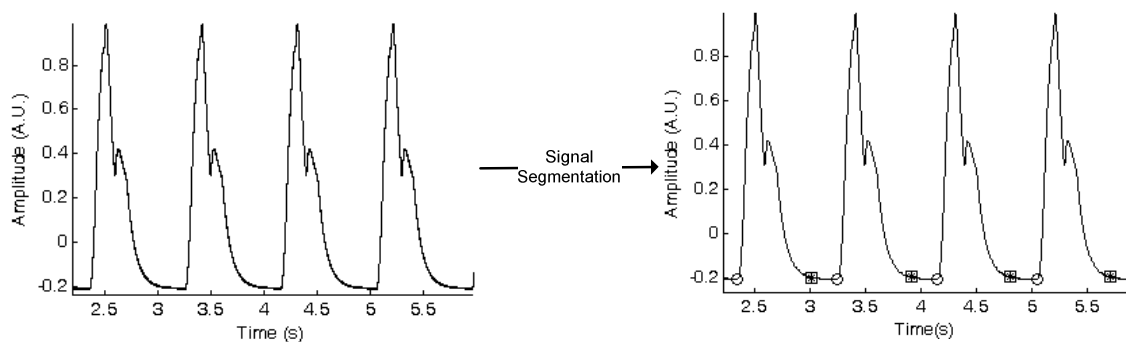


Figure 4.2 – A cardiac pulses waveform (on the left) were segmented by an algorithm based on the idea proposed by Pan and Tompkins. In the segmented signals (on the left) are represented with circles the onset of each cardiac pressure waveform and with the squares the end of it.

4.2 ALGORITHMS TO ASSESS THE LOCAL PWV IN THE TEST BENCH II

The main purpose of this work is to assess the LPWV by a new double PZ probe. The test bench II was developed to simulate the arterial system able to assess the PWV. It is calculated from the measurement of the distance travelled by the wave pressure between two recorded sites divided by the pulse TT. In this case, the distance between the recorded sites by pressures sensors or PZ sensors is well known and the pulse TT was estimated using five algorithms described below, some of them were implemented by *Pereira et al* and *McLaughlin et al* [50, 58]. All signals were filtered by Moving Average filter of 70 points.

4.2.1 MAXIMUM AMPLITUDE DETECTION ALGORITHM

The TT is calculated between the peaks with maximum amplitude of the recorded signals. After the detection of the maximum peak, a sixth degree polynomial fit is made between a set of points that includes this maximum peak initially detected. This fit pretends to re-calculate the maximum value in order to ensure the proper identification of the maximum amplitude peak. An example of application this algorithm is shown in figure 4.3, where on the left is calculated the maximum of recorded two signals and on the right the maximum is re-calculated by the polynomial fit.

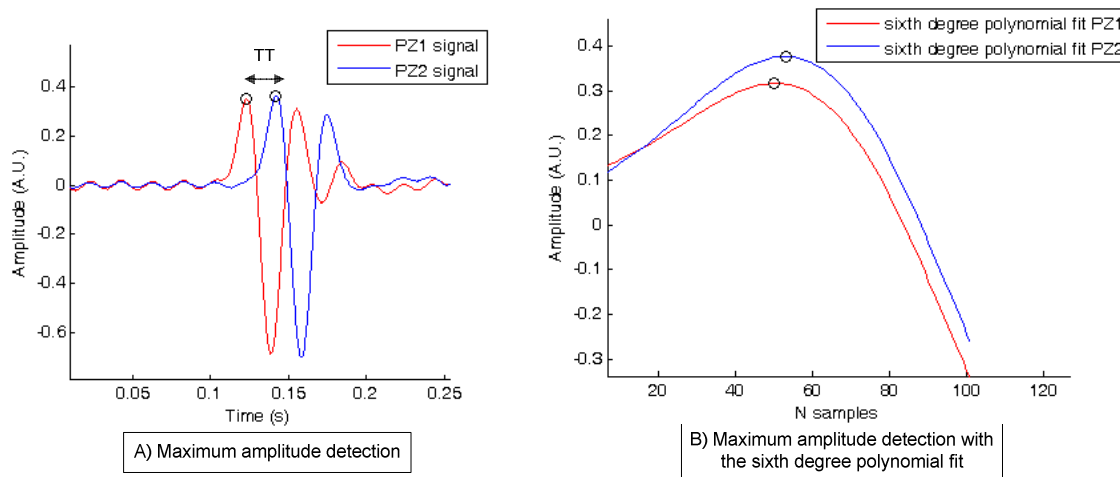


Figure 4.3 – Example of detection of the maximum amplitude peak (represented by black circles) in recorded PZ signals in the test bench II by maximum amplitude detection algorithm. The sixth degree polynomial fit (in B) is made at the region around of the maximum detected initially in A). The TT is determined between two maximum peaks re-calculated by polynomial fit.

4.2.2 MINIMUM AMPLITUDE DETECTION ALGORITHM

This algorithm allows detecting the minimum amplitude peak of recorded signals using the same methodology as maximum amplitude detection algorithm. The TT is determined from the time difference of two peaks detected by a sixth degree polynomial fit with minimum amplitude, as shows the figure 4.4.

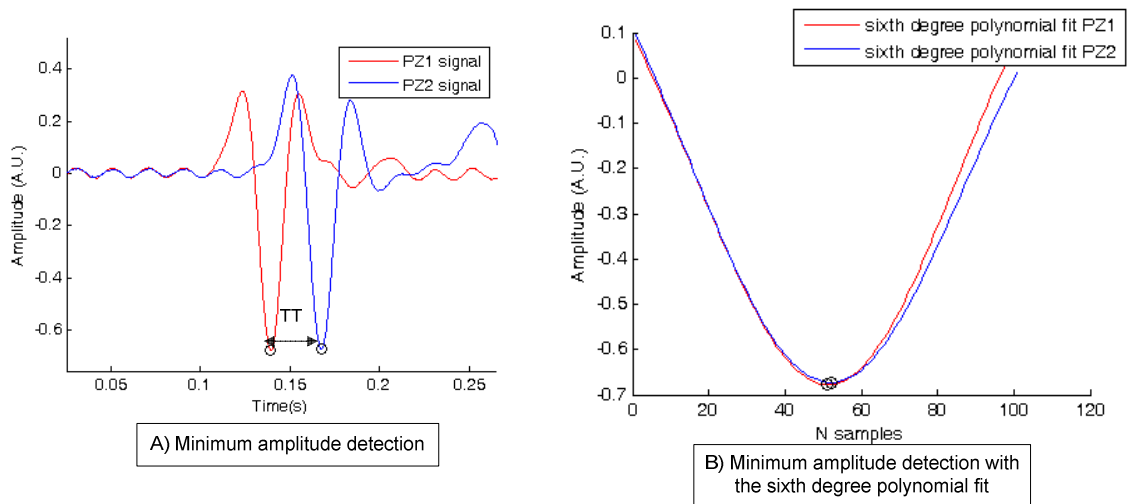


Figure 4.4 – Example of detection of the minimum amplitude peak (represented by black circles) in PZ signals recorded in the test bench II by minimum amplitude detection algorithm. The TT is determined between two minimum peaks re-calculated by polynomial fit.

4.2.3 ZERO-CROSSING POINT IDENTIFICATION ALGORITHM

The zero crossing point is estimated through a linear fit between the maximum and minimum peak of the signal. The *crossingcorr* function finds the location where the signal crosses the zero. The figure 4.5 shows the zero-crossing detected by this algorithm from recorded PZ signals in two sites in the test bench II. The TT is estimated between both zero-crossing points detected.

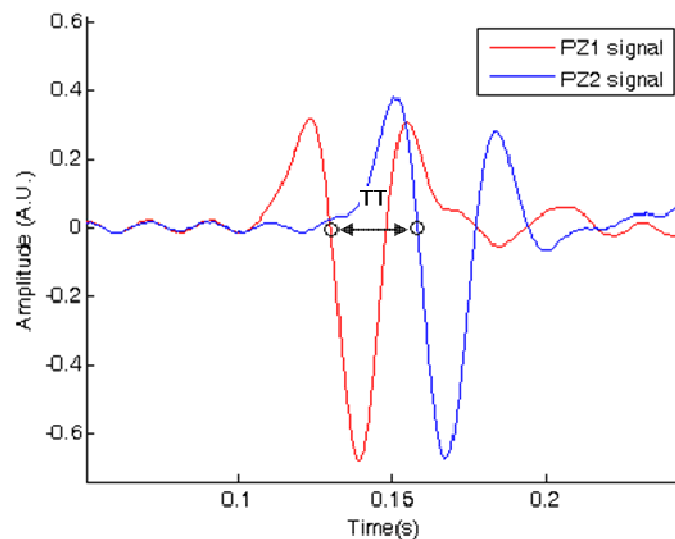


Figure 4.5 – Example of zero-crossing point detected, represented by black circles, in recorded PZ signals in the test bench II. The TT estimated between both zero-crossing detected.

4.2.4 PULSE ONSET DETECTION ALGORITHM

The segmentation algorithm described in section 4.1 was used to detect the pulse onset.

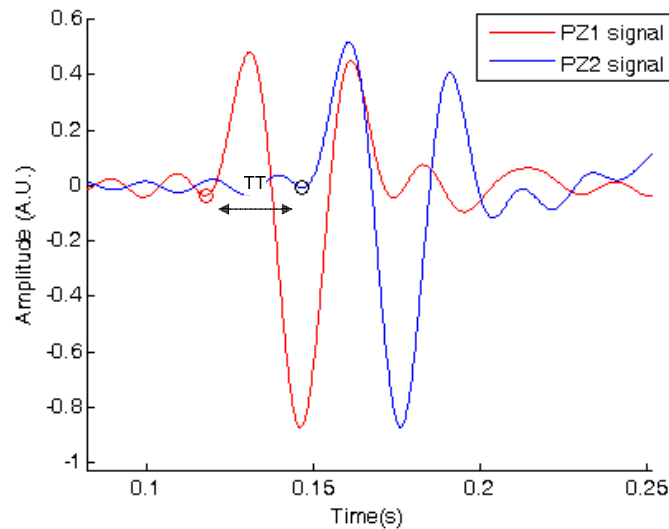


Figure 4.6 – Example of pulse onset detection represented by a red circle for PZ1 signal and by a black circle for PZ2 signal. The TT is estimated between two onset points detected. The PZ signals were recorded in the test bench II.

The signal is filtered by a band pass filter due to signal noise. The threshold is defined as the maximum amplitude of the first 300 samples of the signal. The rising time of two signals is estimated because the threshold is high to detect the true pulse onset point. The rising time allows knowing how many samples are necessary to subtract the onset detected initially by defined threshold, with this setting is obtained the pulse onset point closed expected for all signals, as shows the result in figure 4.6.

4.2.5 MAXIMUM OF CROSS-CORRELATION ALGORITHM

With the cross-correlation algorithm, it is intended to measure the degree to which a reference signal and a measurement signal are correlated. In test bench II, the 700 μm Actuator, Physik Instrumente GmbH P-287, produced a Gaussian waveform that is used as the reference signal. To compare the two signals, the reference signal was differentiated once to compare with pressure sensors signals and twice to compare with PZ signals. From the time difference between the maximum values of the cross-correlation between reference signal and pressure signals or PZ signals the TT is estimated. An example is shown in figure 4.7.

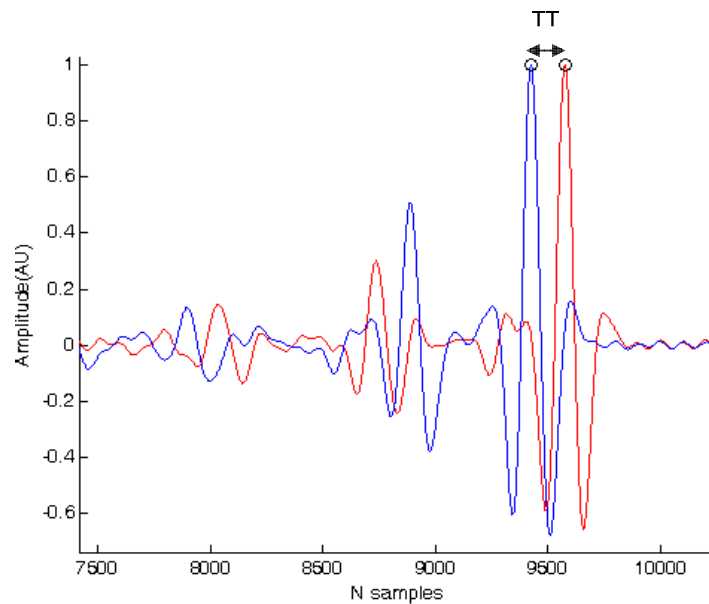


Figure 4.7 – Example of pulse TT estimated from maximum values of correlation between reference signal and PZ 1 sensor (red) and reference signal and PZ 2 sensor (blue).

4.3 ASSESSMENT OF LOCAL PWV IN CCA SIGNALS

The PWV was also determined from the recorded signals in CCA. The pulse TT was determined by maximum and minimum amplitude detection (AD) algorithms (section 4.2.1 and 4.2.2).

It was recorded four signals of the probe – the PZ signals and the integrated signals of both sensors but only the PZ signals were used to determine the pulse TT because they were acquired directly from CCA. Each recorded signal had seven pulse waves, as shows figure 4.9, these were segmented and the PWV was assessed.

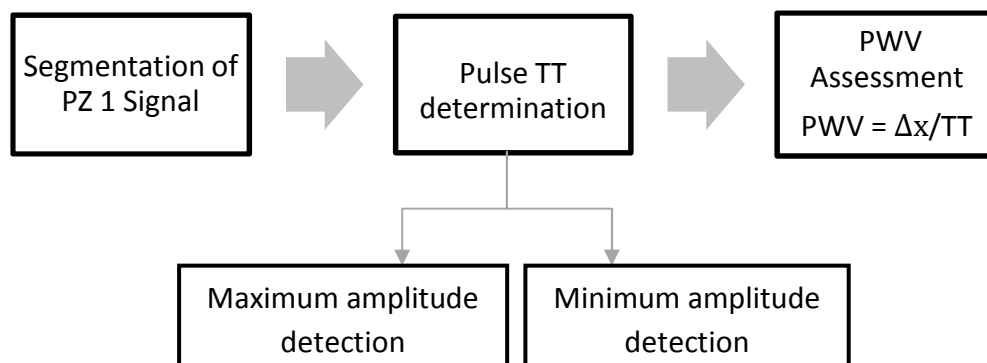


Figure 4.8 – Diagram of the process to assess the LPWV in CCA signals.

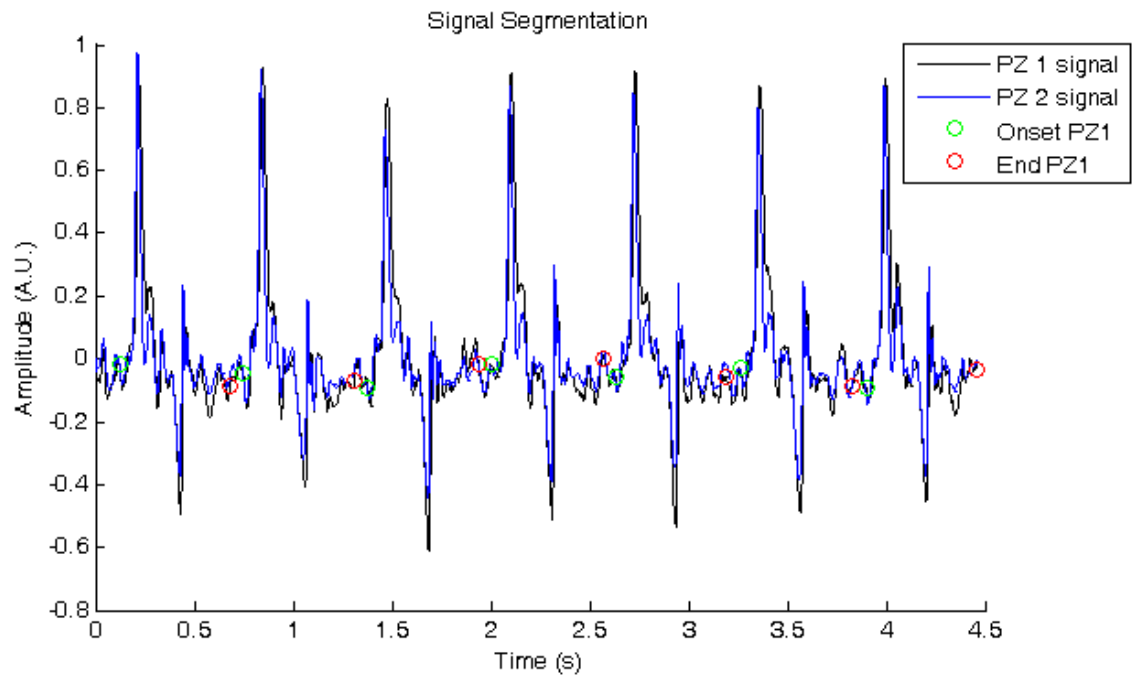


Figure 4.9 – Segmentation of the PZ 1 signal recorded in CCA of a volunteer. The onset and the end of the seven pulse waves are identified in green and red circles, respectively.

The segmentation algorithm (section 4.1) is applied to PZ signal acquired by PZ 1 sensor where the onset and the end of the seven pulse waves are identified, as is shown in figure 4.9. The PZ 2 signal is segmented with the same onset and end points identified in the PZ 1 signal.

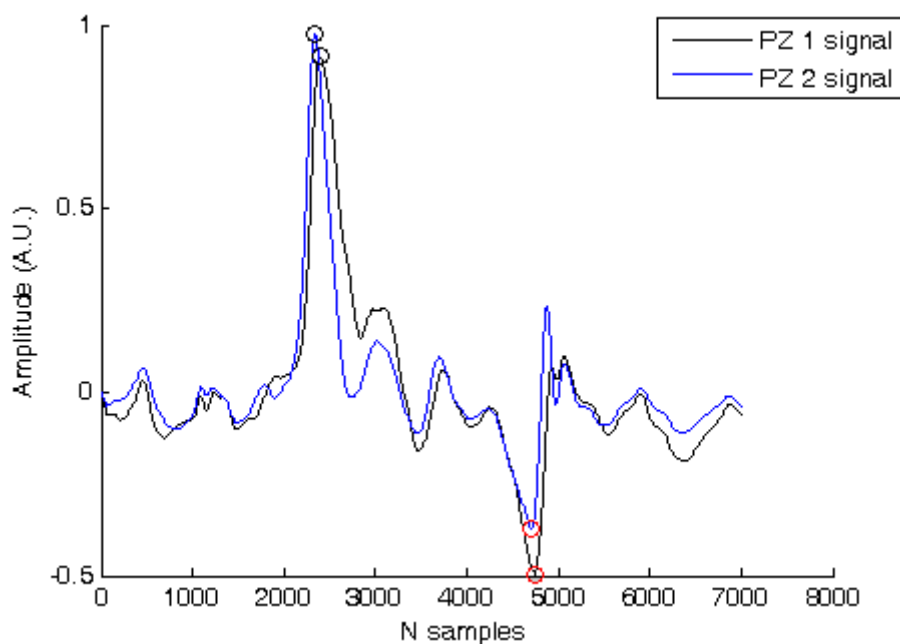


Figure 4.10 – Example of the detection of the maximum and minimum amplitude point of each PZ signal of the first pulse wave. The temporal difference between two detected maximum (black circle) and minimum (red circle) correspond to pulse TT.

For each segment or pulse wave is determined the pulse TT from maximum and minimum AD algorithms between two recorded PZ signals, as is described in sections 4.2.1 and 4.2.2. In figure 4.10, it is shown an example of a pulse wave recorded with two PZ sensors where the algorithms were implemented. The temporal difference between two maximum and minimum is calculated from the sample rate which signal was recorded and the pulse TT is determined.

The local PWV was assessed for each pulse wave from pulse TT determined with both algorithms and the distance between two recorded sites (Δx), as it shows the following equation:

$$PWV = \frac{\Delta x (m)}{TT (s)}.$$

The mean PWV of the all seven pulse waves correspond to the local PWV in each recorded signal.

CHAPTER V

PROBE'S CHARACTERIZATION

The two bench tests developed were powerful tools to characterize the DP in laboratory. These were able to reproduce the hemodynamic properties of the cardiovascular system using programmable arbitrary pressure waveforms, including cardiac waveforms.

The test bench I allowed to study the probe's response to different types of waveforms, the crosstalk effect between both PZ sensors, the repeatability and the determination of the impulse response (IR) of each PZ sensor.

With the test bench II, the time resolution was studied through the propagation of Gaussian waveform in a latex tube.

5.1 TEST BENCH I

5.1.1 INSTRUMENTATION

The first test bench was carried out with four main studies. The synthesized Gaussian and cardiac waveforms were delivered by an arbitrary waveform generator (WG), Agilent 33220A, driven by a high-voltage linear amplifier and after generated by a 700 μ m actuator (ACT), Physik Instrumente GmbH P-287, which transmits it to the PZ sensor through a PVC 'mushroom'. The signal generated by the ACT is synchronizing with DAQ (NI-USB 6009©), being this one and the output of the probe to this stimulus acquired simultaneously. The data are sent to PC as is illustrated in the schematic in figure 5.1.

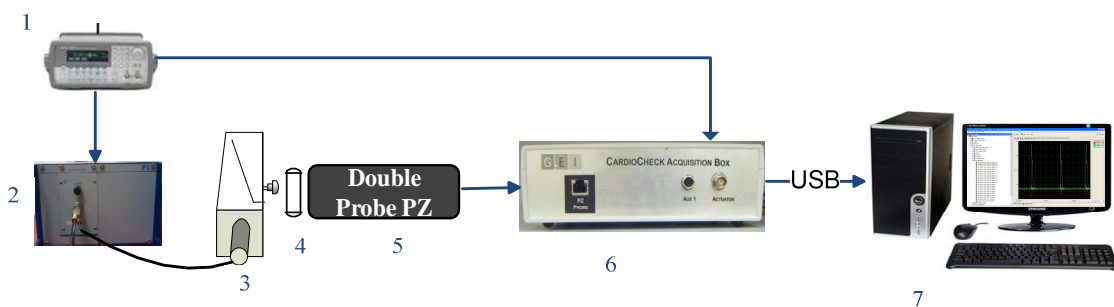


Figure 5.1 - Schematic of the test bench system. 1-Agilent 33220A arbitrary waveform generator, 2- high-voltage linear amplifier (HV) (Physik Instrumente GmbH, E-508), 3- 700 μ m Actuator (ACT) (Physik Instrumente GmbH, P-287), 4 – Tube with air; 5 – Double Probe PZ, 6 – Data Acquisition (National Instruments©- USB 6009), 7- signals are logged by *Measurement & Automation* software and processed using *MATLAB*®.

The synthesized arbitrary pressure waveforms reproduce three types of cardiac waveforms morphologically different in order to simulate different physiological conditions. Figure 5.2 shows the synthesized waveforms used in test bench (Gaussian and cardiac). The period of waveforms were chosen in order to characterize the behaviour of the probe in a range of periods that included the period of a cardiac cycle (near 800ms) [59].

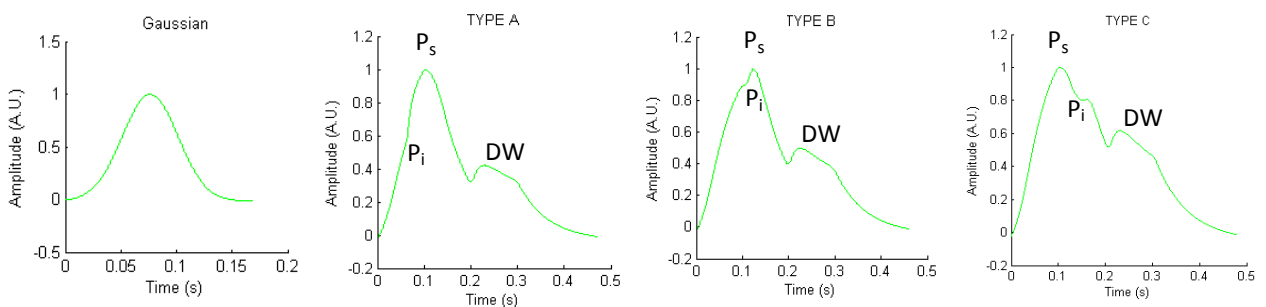


Figure 5.2 – Types of waveforms used in test bench and the characteristic points Ps – systolic pressure, Pi – inflection point and DW – dicrotic wave.

The first stage of probe's characterization in test bench was to study an appropriate interface between ACT and PZ sensor. It was very important to do this study in order to simulate the carotid artery, the existing tissue and skin on it, otherwise the probe's signals saturated. The best interface that reproduced the best results was when was put a bit of glue pads (UHU patafix) on PZ sensor and a silicon tube with air between ACT and probe. This allowed us to perform the tests presented below.

5.1.2 WAVEFORMS ANALYSIS

The main aim of this study is to assess the probe's response for the different types of waveforms shown in figure 5.2. For each type of wave was also studied the effect the period and amplitude variation in the probe's response by Root Mean Squared error (RMSE).

Beyond the ACT signal and the response of one PZ sensor (the PZ signal and its integrated signal), it is also represented the signal obtained by integration method. This signal is obtained through the Matlab® function, *cumsum*, from the PZ signal.

The RMS of the error was calculated between: the integrated PZ signal (PZ Int) and the signal obtained by integration method (Int method); the integrated PZ signal and the ACT signal; and the ACT signal and the signal obtained by integration method. All signals were already filtered by a moving average filter and were sampled to 12.5 kSamples/s.

5.1.2.1 GAUSSIAN WAVEFORM

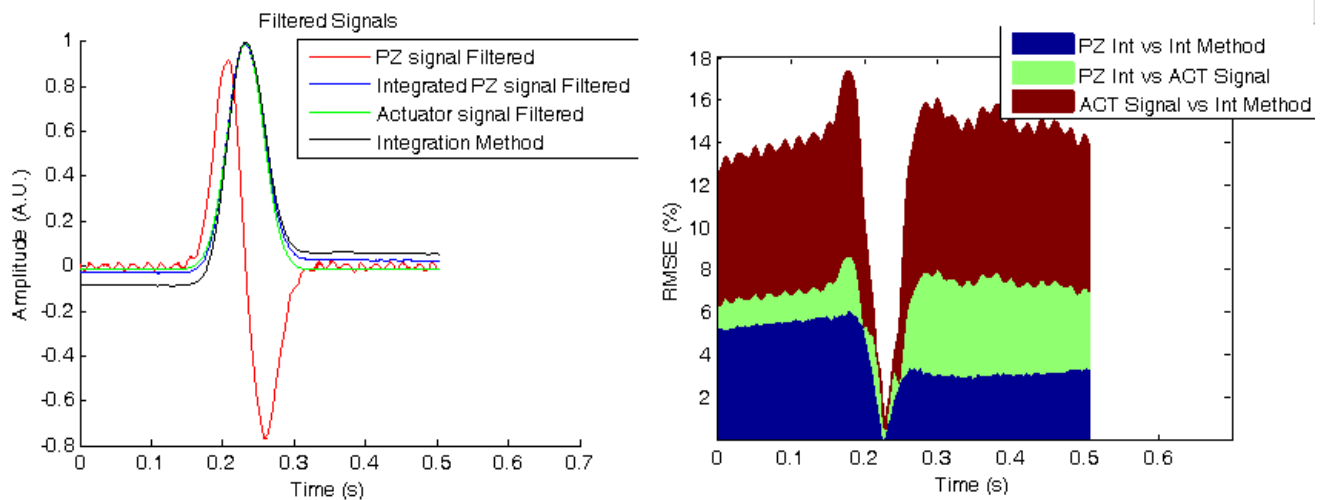


Figure 5.3 – The generated ACT signal is a Gaussian with amplitude 2 volts and period 500ms. The PZ signal and integrated signal of one PZ sensor and the signal by integration method are represented (on the left). The three distributions of the RMS of the error for Gaussian with amplitude 2 volts and period 500ms (on the right).

Table 4 – The RMS of the error was calculated for different amplitudes and periods of the Gaussian waveform.

Actuator Signal	RMSE (%)		
	PZ Int vs Int Method	PZ Int vs ACT signal	ACT signal vs Int Method
Amplitude (volt)/ Period (ms)			
2 / 500	3.375	6.604	6.979
2 / 600	2.897	3.397	6.294
2 / 800	6.470	3.309	3.161
2 / 900	6.250	0.107	6.357
3 / 500	3.267	0.815	4.082
3 / 800	6.171	2.670	3.500
3 / 900	6.951	2.031	4.920

5.1.2.2 TYPE A WAVEFORM

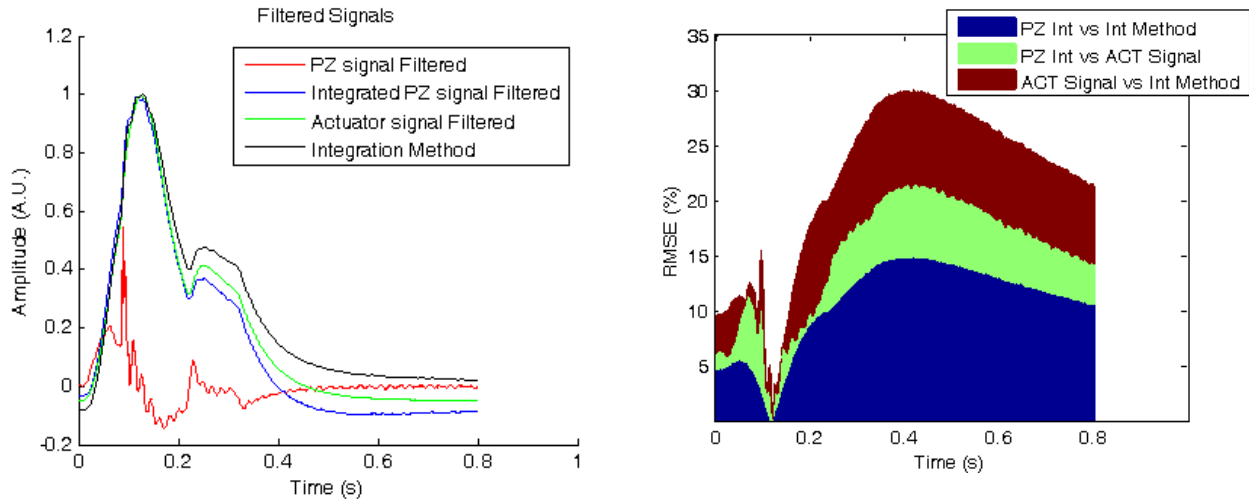


Figure 5.4 – The generated ACT signal is a TYPE A waveform with amplitude 3 volts and period 800ms. The PZ signal and integrated signal of one PZ sensor and the signal by integration method are represented (on the left). The three distributions of the RMS of the error for TYPE A waveform with amplitude 3v and period 800ms (on the right).

Table 5 – The RMS of the error was calculated for different amplitudes and periods of the TYPE A waveform.

Actuator Signal	RMSE error (%)		
	PZ Int vs Int Method	PZ Int vs ACT signal	ACT signal vs Int Method
Amplitude (volt)/Period (ms)			
2 / 500	6.273	1.899	4.374
2 / 600	8.987	2.998	5.989
2 / 800	9.462	2.602	6.860
2 / 900	11.246	5.461	5.785
3 / 500	11.024	6.781	4.243
3 / 600	13.099	5.140	7.960
3 / 800	10.724	3.787	6.937

5.1.2.3 TYPE B WAVEFORM

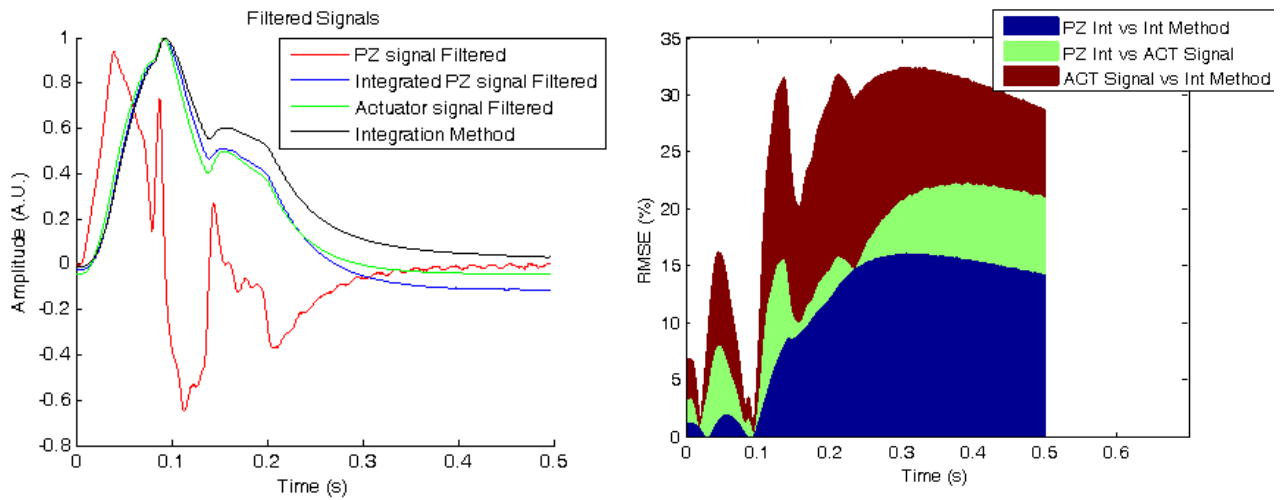


Figure 5.5 – The generated ACT signal is a TYPE B waveform with amplitude 3 volts and period 500ms. The PZ signal and integrated signal of one PZ sensor and the signal by integration method are represented (on the left). The three distributions of the RMS of the error for TYPE B waveform (amplitude 3v and period 800ms) on the right.

Table 6 – The RMS of the error was calculated for different amplitudes and periods of the TYPE B waveform.

Actuator Signal Amplitude (volt)/Period (ms)	RMSE error (%)		
	PZ Int vs Int Method	PZ Int vs ACT signal	ACT signal vs Int Method
2 / 700	7.870	3.268	4.602
2 / 800	12.726	3.322	9.403
2 / 900	9.652	7.408	17.060
3 / 500	14.366	6.745	7.621
3 / 700	4.480	0.478	4.957
3 / 800	13.913	6.389	7.524
3 / 900	16.774	8.166	8.608

5.1.2.4 TYPE C WAVEFORM

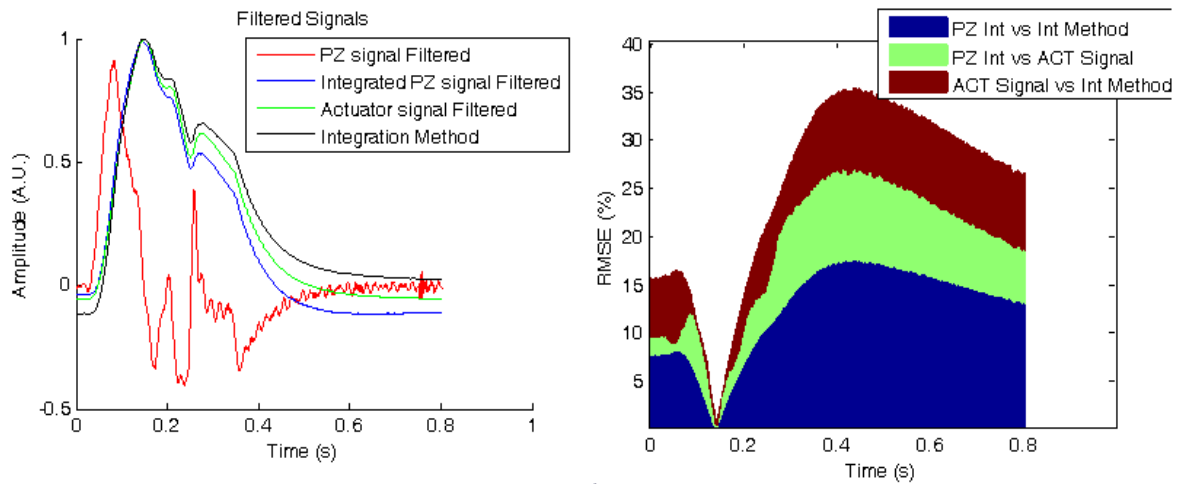


Figure 5.6 – The generated ACT signal is a TYPE C waveform with amplitude 2 volts and period 800ms. The PZ signal and integrated signal of one PZ sensor and signal by integration method are represented (on the left). The three distributions RMS of the error for TYPE C waveform (amplitude 2v and period 800ms) on the right.

Table 7– The RMS of the error was calculated for different amplitudes and periods of the TYPE C waveform.

Actuator Signal	RMSE error (%)		
	PZ Int vs Int Method	PZ Int vs ACT signal	ACT signal vs Int Method
Amplitude (volt)/Period (ms)			
2 / 500	12.591	9.231	3.361
2 / 800	12.560	5.038	7.522
2 / 900	14.903	5.387	9.516
3 / 500	13.058	7.806	5.252
3 / 700	14.510	8.187	6.322
3 / 800	14.002	6.043	7.960
3 / 900	14.911	6.645	8.266

The next issue will be if the output of PZ probe is the same under the same conditions. In order to answer this question the test of repeatability was done.

5.1.3 REPEATABILITY ANALYSIS

With the repeatability test it is intended to measure the same item repeatedly by the same person and PZ probe, under the same conditions. The main aim is to know the variability of the measurements or precision of the measurement equipment [60].

Twenty five pulses of type B and C synthesized cardiac waveforms, spaced by five seconds, were reproduced by actuator and sensed by each PZ sensor, as is shown in figure 5.7. The measurements were repeated, in the same conditions, a few days after. The signals were sampled 5 kSamples/s.

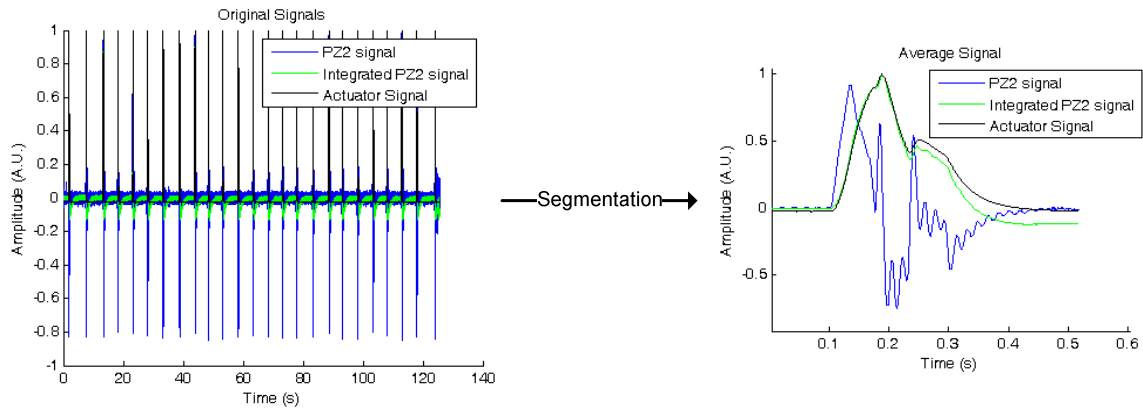


Figure 5.7 - Repeatability test to PZ sensor 2, the actuator wave was: TYPE B with 3 volts amplitude and period 500 ms. The original signal was segmented and the average signal was calculated.

The synthesized cardiac waveforms were segmented by a method based on the algorithm proposed by Pan and Tompkins (see section 4.1) in order to segment the signal into periods and calculate the average signal, figure 5.7. The RMSE was calculated between the actuator signal and the integrated PZ signal. The results are presented in the table 8.

Table 8– Results of repeatability test. The data, measurement 1 and measurement 2, were done on different days.

Actuated PZ	TYPE/ Amplitude (volt)/ Period (ms)	Measurement 1 RMSE 1(%)	Measurement 2 RMSE 2(%)	RMSE 1 – RMSE2 (%)
1	B / 3/ 500	8.295	8.301	0.006
	B /3/ 800	8.540	8.390	0.150
	B /3 / 900	9.312	8.061	1.251
	C / 3/ 500	5.223	5.353	0.130
	C / 3/ 800	8.466	7.931	0.535
	C / 3/ 900	10.938	8.925	2.013
2	B /3/ 800	8.913	8.086	0.827
	B /3/ 900	8.989	8.100	0.889
	C /3/ 800	9.370	9.949	0.579
	C /3/ 900	10.194	9.645	0.549

5.14 CROSSTALK ANALYSIS

The repeatability and crosstalk tests were done simultaneously for all measurements of the table 8. While a PZ sensor was being actuated, the other one wasn't being actuated but the signal was being recorded. During the acquisition the PZ 1 sensor wasn't responding when the PZ 2 sensor was being actuated and vice versa, as show in figure 5.8 a) and b). After signal segmentation, the average signal was calculated and the output of PZ sensor not actuated is a straight line whose amplitude is near zero, see figure 5.8 c) and d). It shows that for all types of waves, amplitude and period shown in the table 8 it didn't occur the crosstalk effect.

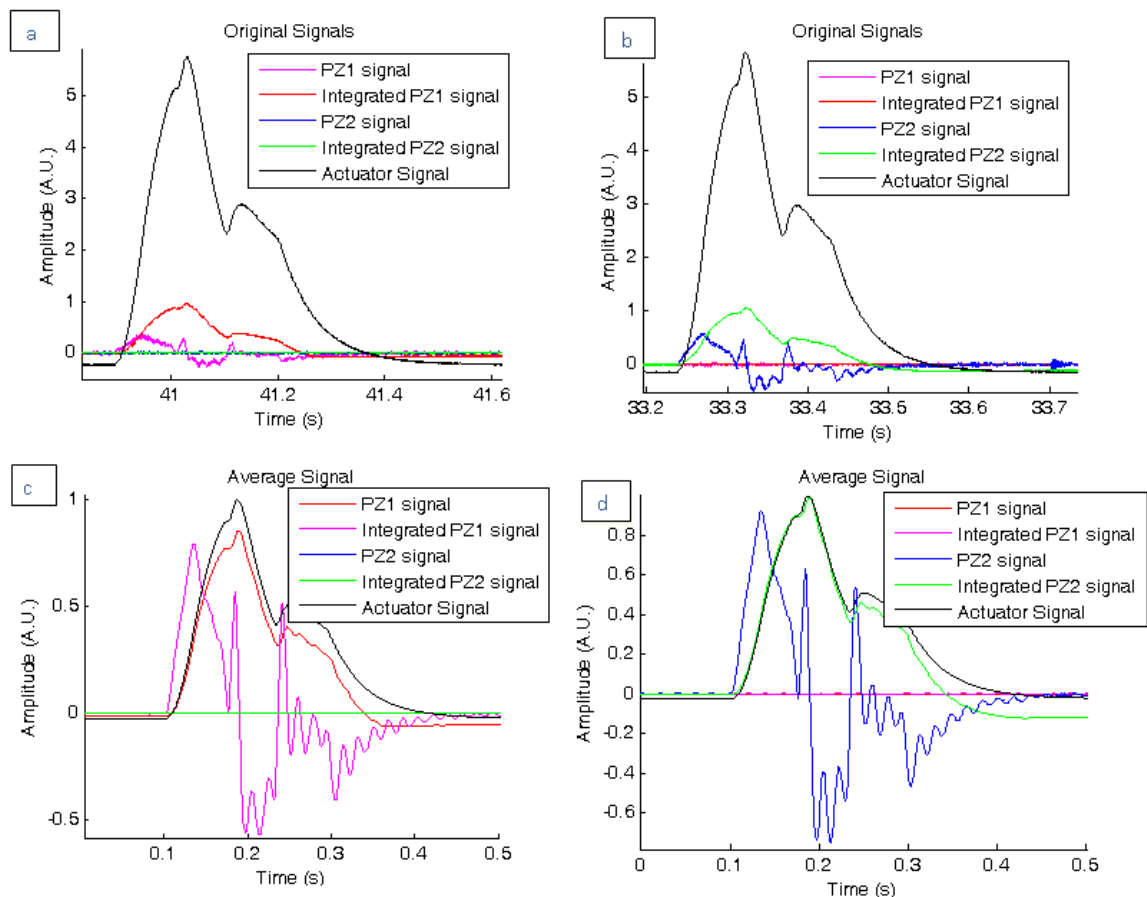


Figure 5.8 - Results of crosstalk analysis during data acquisition where: the PZ1 was being actuated a) and PZ2 was being actuated b). The average signals of PZ 1 c) and PZ2 d). The waveform is TYPE B with amplitude 3volts and period 500ms.

5.1.5 IMPULSE RESPONSE (IR) AND DECONVOLUTION METHOD

The determination of impulse response (IR) of each PZ sensor is another important study to be done to characterize the PZ probe. The determined IR, in turn, is used to obtain the original signal (the cardiac waveform) by deconvolution method in order to show that it is able to recover it.

The deconvolution method was studied and discussed in other works [11, 13] proving to be an accurate method. It allows to get the original signal or input signal ($x(t)$) from the differentiated signal of PZ probe ($y(t)$) and its IR ($h(t)$), as it can be mathematically expressed by convolution theorem:

$$y(t) = x(t) * h(t) \quad (5.1)$$

In the frequency domain is easier to solve the equation (5.1), in other words the convolution of two functions in time domain is equivalent to a product of their Fourier transform:

$$y(t) = x(t) * h(t) \Leftrightarrow Y(j\omega) = X(j\omega) \cdot H(j\omega) \Leftrightarrow X(j\omega) = \frac{Y(j\omega)}{H(j\omega)} \quad (5.2)$$

Where $H(j\omega)$ is the system's transfer function, the Fourier transform of IR.

5.1.5.1 IMPULSE RESPONSE (IR) DETERMINATION

The method used to determine the IR for each PZ sensor is similar to the one used by *Pereira H. et al* [58]. A linear sweep is generated by the WG (Agilent 33220A) and reproduced by ACT 700 μm (Physik Instrumente GmbH P-287) which actuate on each PZ sensor. The relation between Fast Fourier Transform of PZ output and the linear sweep results the transfer function, $H(j\omega) = \frac{Y(j\omega)}{X(j\omega)}$. Through Inverse Fast Fourier Transform the $H(j\omega)$ is transformed to the time domain resulting the IR. Figure 5.9 illustrated this method. The interface used between ACT and PZ probe was the same as in previous tests, air tube and glue pads.

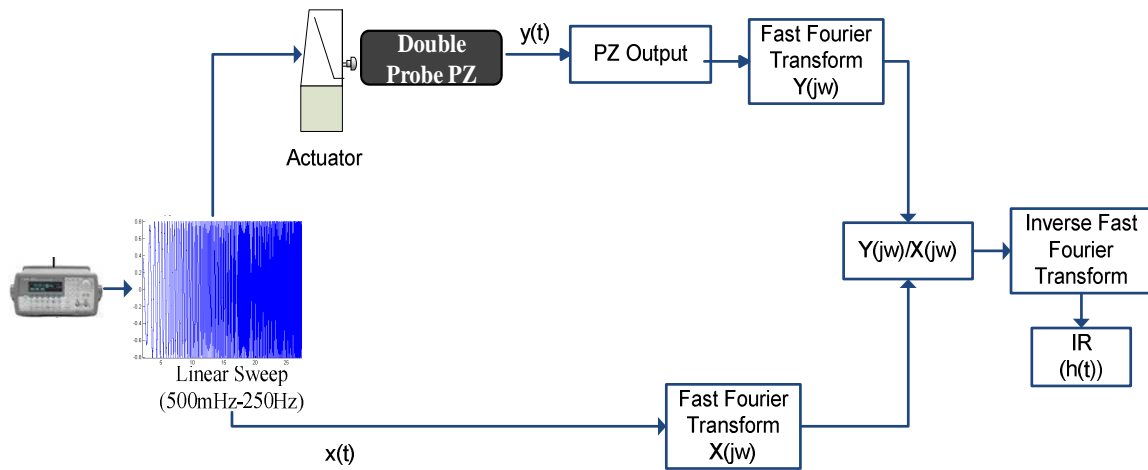


Figure 5.9 – Schematic of IR determination method for each PZ sensor.

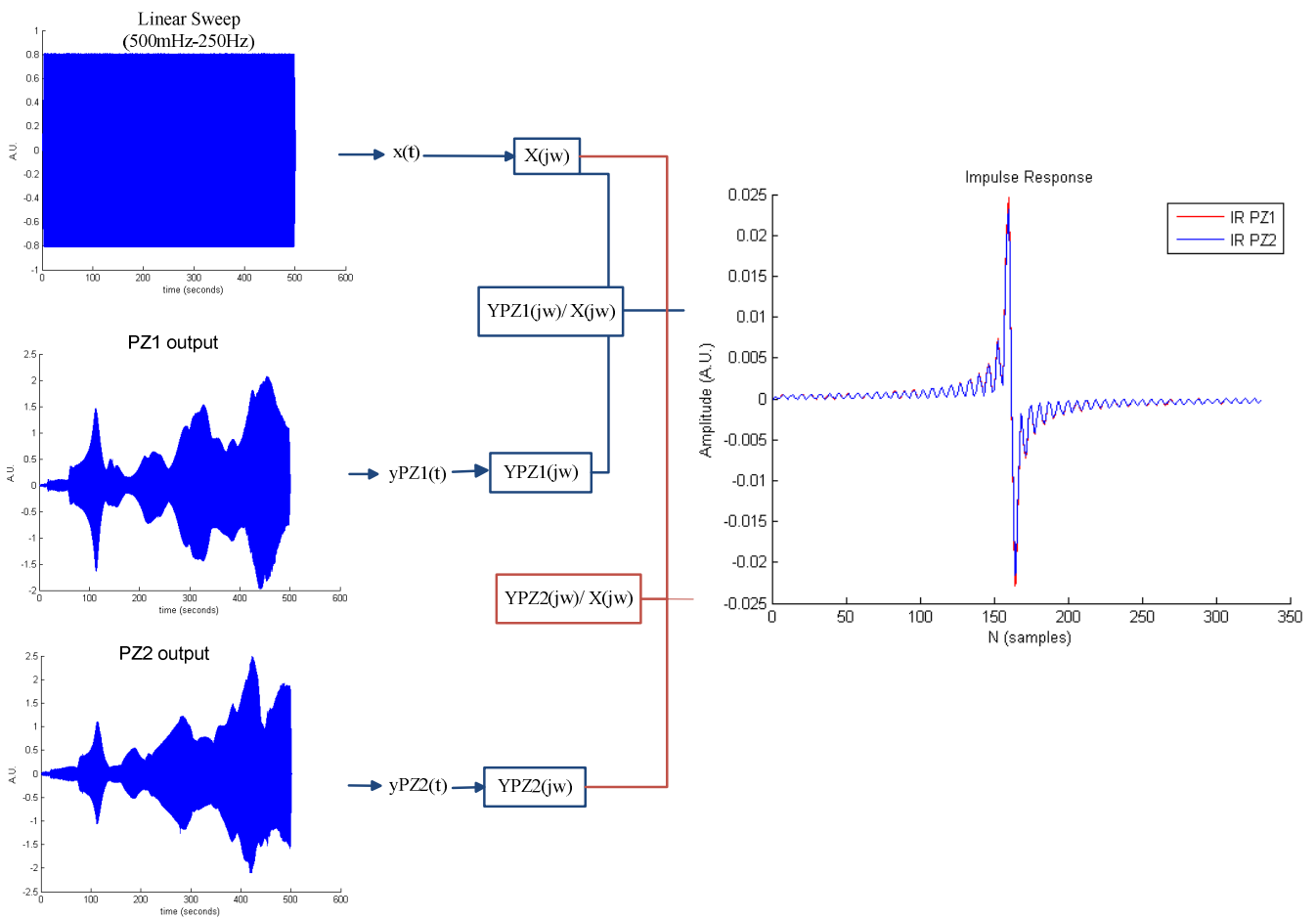


Figure 5.10– Results of IR determination of each PZ sensors.

The frequencies' range used to make the linear sweep was 500 MHz to 250 Hz because for frequencies above 250 Hz both PZ sensors saturated due to power supply (± 5 v). The linear sweep characteristics are:

Sine amplitude:	1.600 Vpp
Frequency start:	500 mHz
Frequency Stop:	250Hz
Sweep time:	500 seconds
Sample rate:	NI-USB 6009 5 kSamples/s

The figure 5.10 illustrates the output and the IR for each PZ sensor. Both IRs are similar whether in amplitude or shape. This method to obtain the IRs was repeated and the same results were obtained as long as the interface was well positioned. But we were able to reproduce the results showing the IRs are repeatable.

When a PZ sensor was being actuated by linear sweep, the output of the other one was being recorded too. It was noticed that the integrated signal from the PZ actuated responded to some frequencies but with very low amplitude. The integrated signal from another PZ sensor didn't respond unlike PZ signal which responded to higher frequencies but this output didn't result any IR.

5.1.5.2 DECONVOLVED SIGNALS

From IR to each PZ sensor we are able to apply deconvolution method in order to obtain the original signal transmitted by ACT and that was actuated on PZ sensors, proving the accuracy of the IR determined. Both PZ sensors were actuated simultaneously by ACT and sampled by 5 kSamples/s. The differentiated PZ 1 and PZ 2 signals were deconvolved with their respective IR. It was selected a segment of IR to be deconvolved with PZ signal taking in account the frequency spectrum of both. The DC components of the IR and PZ signal were recovered. The result is presented in figure 5.11 where the original pressure waveform (type C waveform with amplitude 3 volts and period 900 ms) was recovered.

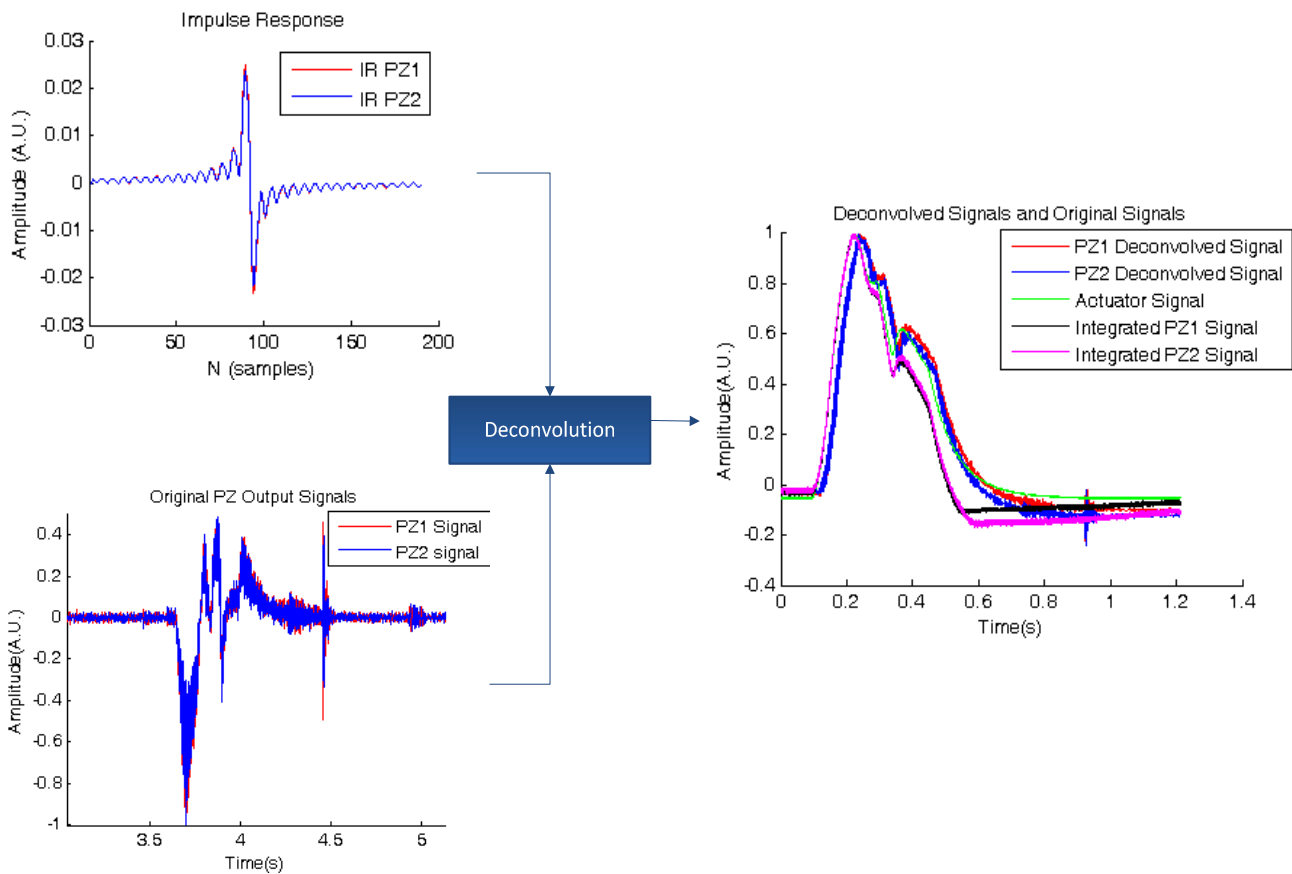


Figure 5.11 – Result of deconvolution using IR of and PZ output each PZ sensor. The original signal (type C with amplitude 3 volts and period 900ms) (green) is recovered (red and blue). The integrated PZ1 and PZ2 signal are also represented (black and purple).

5.1.6 DISCUSSION

WAVEFORMS ANALYSIS

This test shows that the PZ probe can reproduce the synthesized cardiac and Gaussian waveforms. The integrated PZ signal has exactly the same shape of synthesized waveforms and the PZ signal identify the inflection points of waves, see figures 5.3, 5.4, 5.5 and 5.6 (on the left). Regarding waveforms, the new PZ probe is able to reproduce the original wave. The signal obtained by the integration method, in some of the acquired signals, doesn't have the same amplitude as the integrated PZ signal (obtained by electronic probe) or ACT signal but their shape is the same.

In the majority of the signals acquired it appears that the RMSE values between the integrated PZ signal and the ACT signal were smaller than the signal obtained by

integration method and ACT signal, see tables 4, 5, 6 e 7. This means that the integrated PZ signal can reproduce more faithfully the original wave. For cardiac waveforms, the RMSE values between integrated PZ signal and signal obtained by integration method were the biggest, comparing to the other ones. It shows a large discrepancy between two paths that intended reproduce the same ACT signal. The integrated PZ signal is able to reproduce the main characteristic points of the waves with low error, showing to be a good approximation to the original wave. From the results in table 4 for the Gaussian waveform, table 4, is difficult to draw general conclusions.

In order to know how the RMSE varies along the waveform the figure 5.3, 5.4, 5.5 and 5.6 on the right show the RMSE distribution. The error is increased after the systolic upstroke of waves and systolic peak, it means after near 0.2 seconds in Gaussian waveform, 0.1 seconds in TYPA, TYPEB and TYPEC waveforms. When the waveforms back to the baseline the RMSE is decreased. This can be explained by the electronic circuit of the probe, specifically by the effect of a capacitor.

In this test bench, the interface between actuator and PZ probe is the most important factor. If the air tube is in a slightly different position or doing more or less pressure on actuator's mushroom, it influences the shape of the probe signal (PZ signal and integrated PZ signal) and consequently the RMSE. However, an operator working regularly with this test bench system can adjust the interface and identify whether the signal is saturated or the interface is to interfere with PZ signal.

REPEATABILITY ANALYSIS

The repeatability analysis consisted to know the precision of PZ probe when this measures the same input signal, produced by ACT, several times. In other words, if the PZ probe always responds in the same way at the same input signal. In order to quantify this study, for each measurement was calculated the RMSE between the integrated PZ signal and the ACT signal of the average signal, see table 8.

The RMSE values weren't consistent in both measurements, as we can see in table 8. For three data, shaded in gray, the discrepancy between RMSE of both measurements ($|RMSE_1 - RMSE_2|$) wasn't significant compared to others. The number of cardiac waveforms analysed (the twenty five pulses) may not be enough to get good

results and show the repeatability of the probe as well as the different way the probe and interface were coupled. However more measurements should be made to obtain conclusive results and to draw more conclusions.

CROSSTALK ANALYSIS

The test showed there isn't crosstalk effect between both PZ sensors. The transmission of a synthesized waveform to one PZ sensor doesn't affect the response of the other PZ sensor.

IR DETERMINATION AND DECONVOLUTION METHOD

The IR was determined, see figure 5.10, for each PZ sensor using appropriated range of frequencies and interface in order to not saturate of the PZ signals during the linear sweep. The profile of both IRs is similar, there is only difference a little difference regarding the amplitude. The determined IR in dissertation *Methodologies for Hemodynamic Parameters Assessment* is represented in figure 5.12 [13]. It was used the same methodology but with another PZ double probe and it was obtained different IRs. The electronic associated with each probe was different, justifying this results.

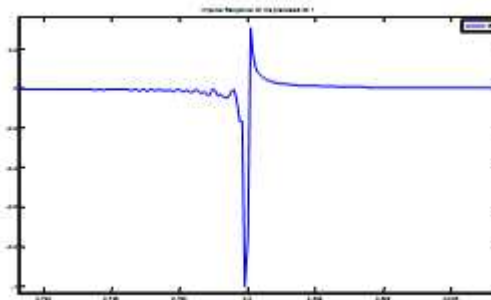


Figure 5.12 – The Impulse Response of a PZ1 sensor obtained by [13].

Figure 5.11 shows that the determined IRs were capable to recover accurately the original waveform by deconvolution method. In fact, both deconvolved signals are similar to each other and with the original signal too. The deconvolved signals aren't filtered and the RMS value between both is 3.01%. The integrated signals are very close to each other and the shape is equal to deconvolved signals and original signal. In general, we can say that the waveforms given by probe are a good approximation to original signal and deconvoluted signals.

5.2 TEST BENCH II

The test bench II was thought to simulate some hemodynamic properties of the cardiovascular system namely the propagation of the arterial pressure wave (APW) in arteries and the components: the incident and reflected waves.

The first system developed at GEI for this purpose showed to be an important tool in the study of the forward and backward propagation pressure waves, in the recovery of the APW by deconvolution as well as in the validation of the algorithms [61]. The encouraging results led to the development of another test bench system whose length of the tube was greater allowing the execution of the previous studies and estimate the time resolution of the probe [58]. This system is used now to characterize the new PZ probe too.

5.2.1 INSTRUMENTATION

The experimental setup was adapted from *Pereira et al* 2010 and it is illustrated in figure 5.13. Regarding this system, the silicon tube was replaced by a latex tube that in literature is considered the best material to simulate the compliance of the human carotid artery [62, 63].

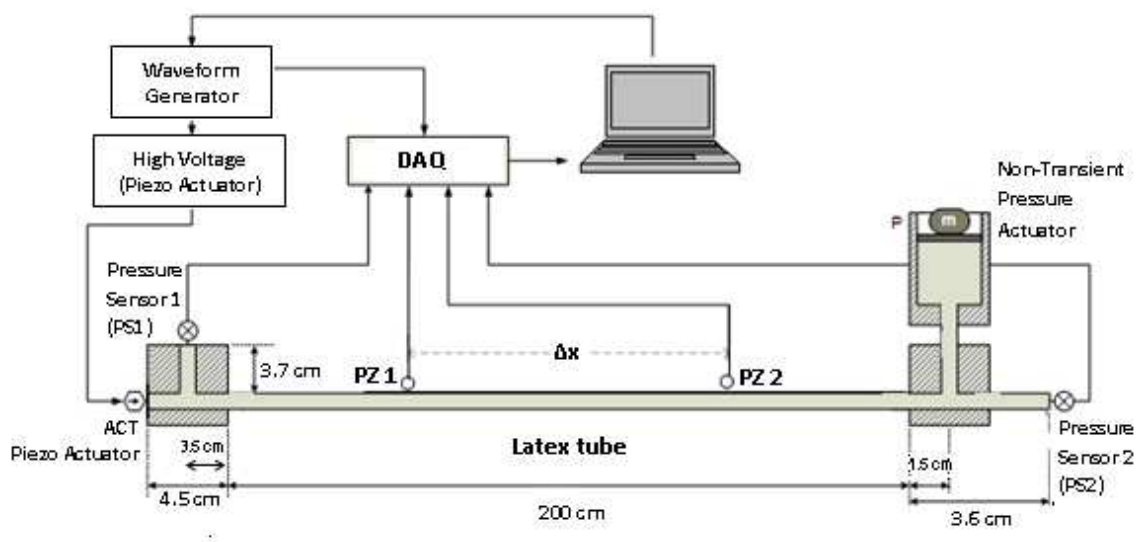


Figure 5.13 – Schematic drawing of the test bench II. Two PZ sensors are placed on latex rubber tube that sense the Gaussian waveform generated by ACT. The pressure sensors (PS1 and PS2) monitored the DC pressure, controlled by the piston (P) and mass (m), and are used as reference to assess the PWV. Adapted from *Pereira et al* [58].

In fact, the latex tube is more distensible than silicon tube being able to expand and constrict due to the pressure's action replicating the blood flow of the arterial system. It's expected that the elastic characteristics of the tube are similar to normal arteries under physiologic pressures (80-150 mmHg).

Like in the test bench I, a waveform is delivered from WG, Agilent 33220A, driven by a high-voltage linear amplifier (Physik Instrumente GmbH, E-508) and delivered by a 700 μm ACT (Physik Instrumente GmbH, P-287). The test bench II tries to characterize the new PZ probe under similar physical conditions. The ACT generates a synthesized Gaussian pressure waveform, to simulate the propagation of the pulse wave from ascending aorta to arteries of the system arterial. This phenomenon is simulated by a natural rubber latex tube (length 200 cm, inner diameter of 7.937 mm and wall thickness of 0.7937 mm) filled with water. A latex membrane is used as an interface between the ACT and the water into the tube at the left extremity of latex tube.

The arterial pressure is controlled by a piston (P) and a mass (m) allowing to change the DC pressure level which is monitored by two pressure sensors (Honeywell S&C-40PC015G1A) coupled to a digital voltmeter (Digital panel meter 3-1/2D LCD) placed transversely and longitudinally to the tube, PS1 and PS2 respectively. The pressure sensors are used as reference to assess the PWV in the tube, and both are connected to the data acquisition system (NI- USB 6009). Their responses to the wave delivered by the ACT is recorded by the NI software.

The PZ sensors are placed on the latex tube doing some pressure on it through of the an acrylic structure with a hole to fixed the PZ sensor. The PZ sensors are connected to the electronic of the probe through an electric wire.

Four main studies were done with this experimental setup that consisted in: studying the wave propagation along the tube; characterizing the behaviour of latex tube with different DC pressure levels; to determining the time resolution of the PZ probe and assessing the dispersion of the PWV measure with the probe along twenty positions along the tube.

5.2.2 CHARACTERIZATION OF THE TEST BENCH II

5.2.2.1 PROPAGATION OF THE PRESSURE WAVE IN THE LATEX TUBE

In this study, only the PZ 1 sensor is placed on the latex tube detecting a Gaussian waveform (period: 100 ms and amplitude: 3 volts), generated by the ACT, at 2 to 2 cm along the tube. The PZ sensor is able to sense this Gaussian waveform that propagates along of the tube, and that is composed by an incident Gaussian waveform and a reflected Gaussian waveform, figure 5.14. The study was done at the pressure 40.86 mmHg and all acquired signals were sampled at 11 kSamples/s and with 10 kSamples to read.

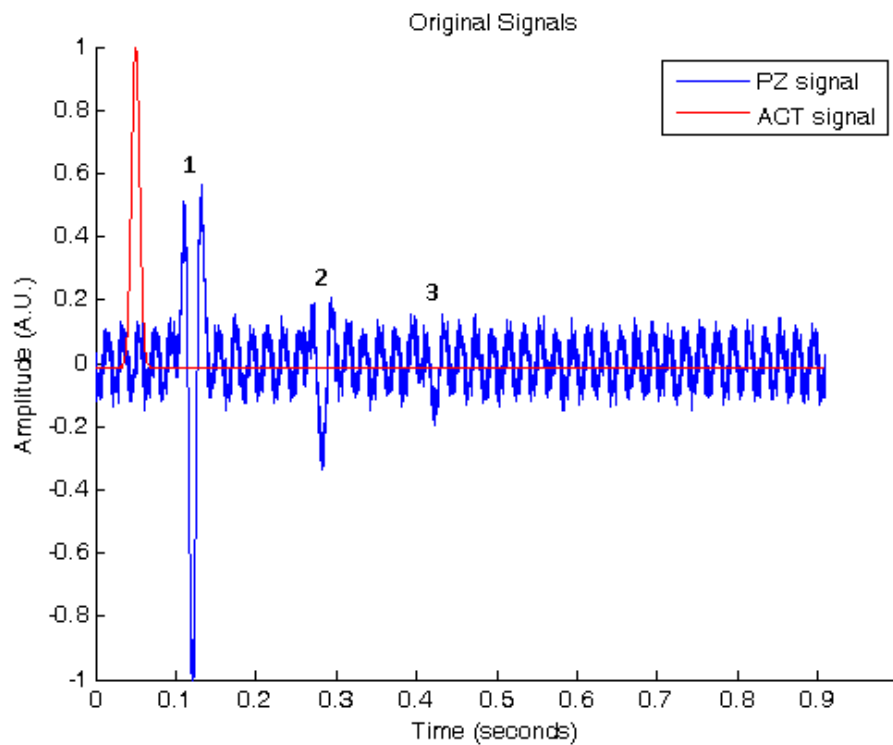


Figure 5.14 – Propagation of a Gaussian waveform (amplitude 3 volts and period 100 ms) sensed by PZ 1 sensor at 90 cm of the tube. The PZ and ACT signals were recorded. 1- Forward wave sensed by PZ1 sensor, 2- Reflected wave at the end of the tube, 3- Reflected wave at the beginning of the tube.

The *imagesc* and *mesh* functions of Matlab® allowed representing the wave propagation along of the tube length in function of time. The figure 5.15 represents the data in a 3-D mesh surface and the figure 5.16 shows the propagation of the wave along the tube where is represented the incident wave generated by the ACT – the forward wave (represented by line 1)- that is reflected at the end of the tube – the backward wave (represented by line 2) - and this last one was reflected again at the tube

beginning (represented by line 3). It's also possible to see more reflections along the tube (lines 4, 5 and 6) although weaker, as expected, due to wave dissipation.

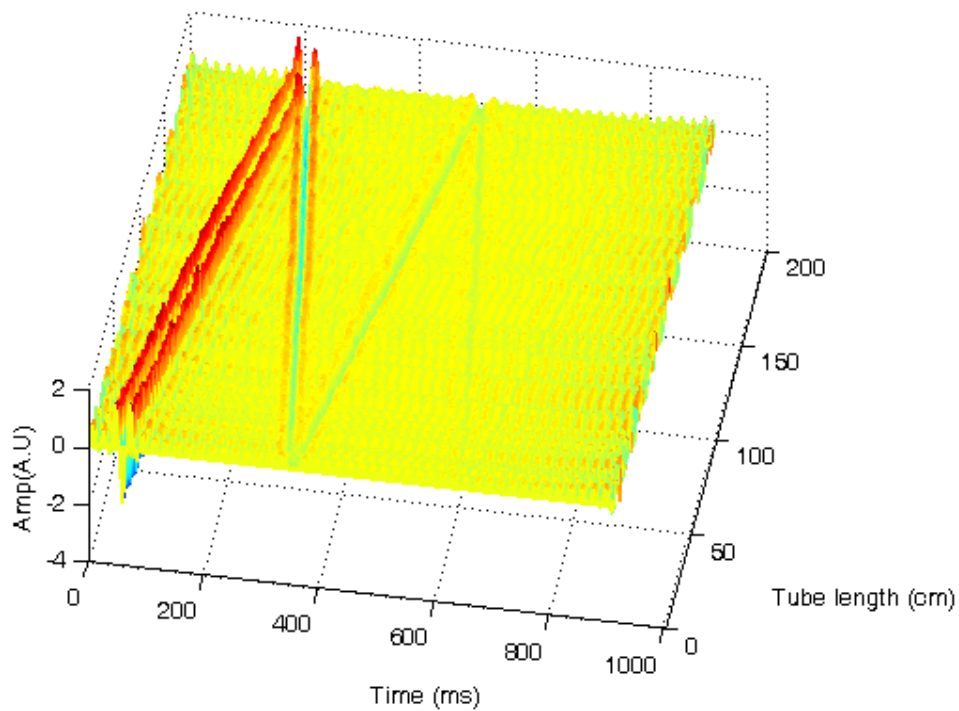


Figure 5.15 – Representation of the data of the wave propagation in a latex tube by 3-D mesh surface.

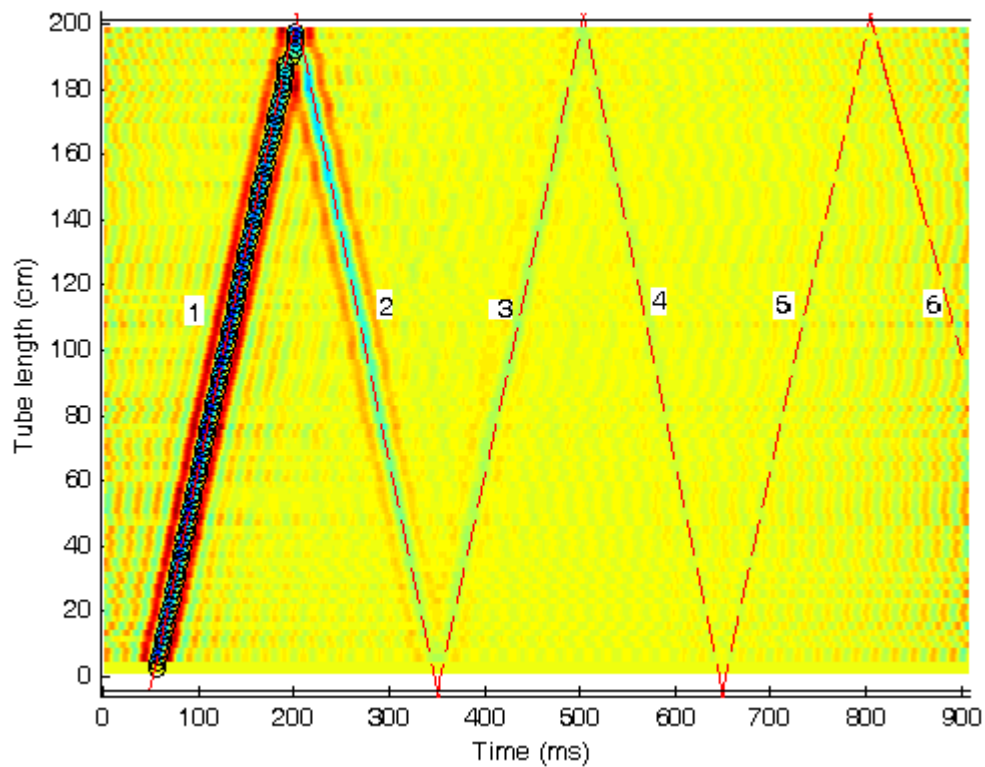


Figure 5.16 – Propagation of the Gaussian waveform along the latex tube and its reflection. Line 1 represents the propagation of forward wave and Line 2, 3, 4 and 5 represent the backward waves reflected at the end of the tube. The black horizontal lines corresponds the sites where wave was reflected, at -4.5cm and +1.5cm.

In the acquisitions made at the tube's beginning, the multiple reflections of the wave at the ends of the tube were more difficult to see.

The black circles along the line 1, in figure 5.16, represent the minimum value of the forward wave sensed by the PZ sensor along the tube. The lines were drawn from the amplitude of absolute minimum of the PZ signal and the interceptions of these also represent the physical sites where the Gaussian wave is reflected. The horizontal black lines in figure 5.16 show that the reflection occurred: at 4.5 cm before the beginning of the tube, where is located the latex membrane through which the ACT releases the pressure wave, and at 1.5 cm after the end of the tube where is located the piston. These components of the test bench close the latex tube.

The velocity of the Gaussian waveform propagation is determined by the slope of the line 1 which in this case is near 13.4 m/s.

5.2.2.2 RELATION BETWEEN DC PRESSURE AND PWV IN THE LATEX TUBE

This second study allowed characterizing the behaviour of the latex tube for different DC pressure levels. The PWV in the tube for different DC pressures was determined from the response of the pressure sensors (PS 1 and PS 2) to a Gaussian waveform, with amplitude 3 V and 150 ms of period, released by the ACT. The ACT, PS 1 and PS 2 signals are recorded at 5 kSamples/s for each and every one of the 33 levels of DC pressure acted on latex tube by the piston - an example of the signals recorded are presented in figure 5.17. The distance between the two pressure sensors (Δx) is 2.108 m and the pulse TT was determined from maximum amplitude detection, zero-crossing point identification and maximum of cross-correlation algorithms described in section 4.2. The signals were filtered by moving average filter with 70 points.

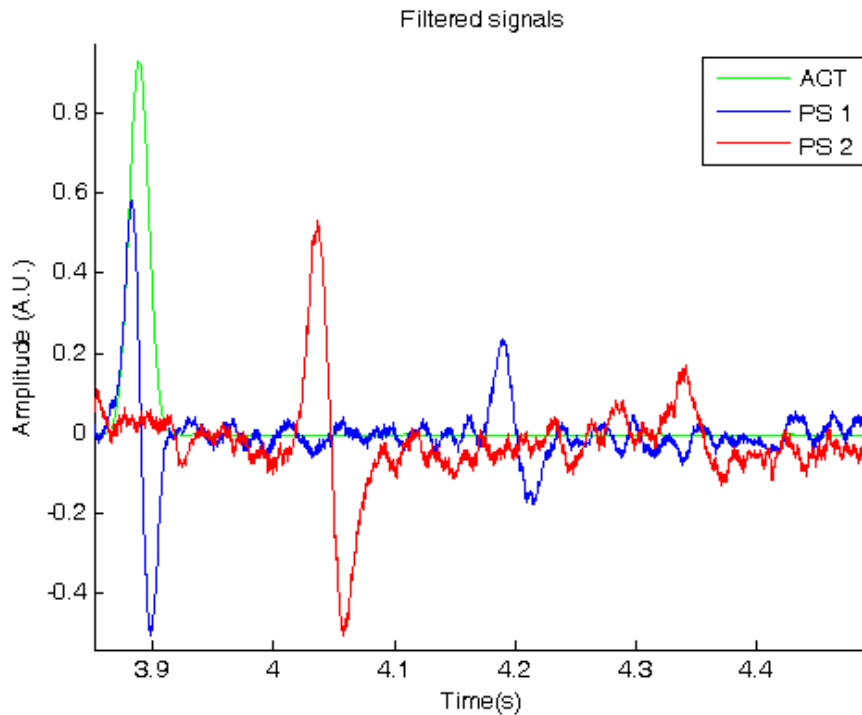


Figure 5.17 – Recorded ACT, PS 1 and PS 2 signals at 49 mmHg of the DC pressure.

Three trials were made in order to prove the repeatability of the measurements. The figure 5.18 shows the results where each point represents the mean PWV obtained in the three trials in each algorithm.

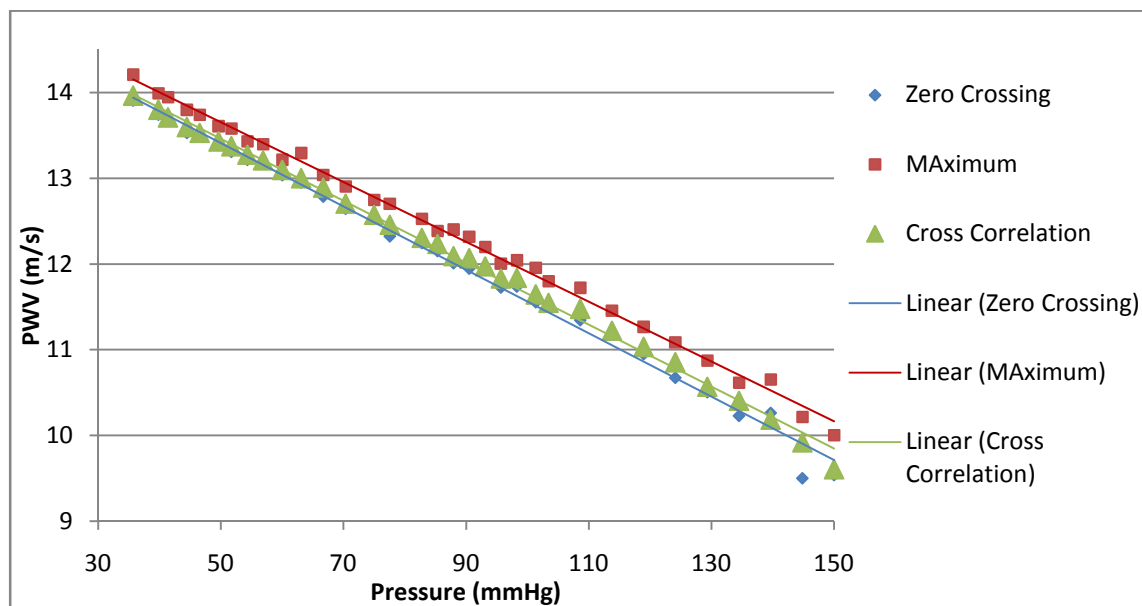


Figure 5.18 – Relation between the DC pressure and PWV obtained by pressure sensors from three algorithms in the latex tube. The linear fit was made for each algorithm: maximum: $y = -0.034x + 15.39$, $R^2 = 0.996$; zero-crossing: $y = -0.037x + 15.25$, $R^2 = 0.993$ and cross-correlation: $y = 0.036x + 15.26$, $R^2 = 0.996$.

These results showed that the PWV decrease linearly with the pressure increase. A linear fit was done for the determined PWV with each algorithm where the Pearson's coefficient varies 0.993 to 0.996, very close to 1. The results are consistent and the PWV assessed by the three algorithms is similar.

According to the Bramwell-Hill expression which related the local wave speed with the D :

$$PWV = \sqrt{\frac{1}{\rho D}}, \text{ where } D = \frac{dA}{A_d \cdot dP}, \quad (5.3) [20]$$

the increase of the pressure causes an increase of PWV, assuming that the cross section of the tube doesn't vary.

During the experiments the increasing pressure seemed to cause an increase of tube's diameter and length. In the last of the three experiments, with 144 mmHg DC pressure, the tube besides swelling also extended 'jumping' of the structure where it was on it. Given the results in figure 5.18 and the observations during the experience, it was concluded that the diameter or D of the tube should be measured. Using ultrasound would be an accurate way to obtain the cross sectional area of the tube for each pressure but in this case the diameter was measured at 60, 124 and 190 cm of the tube three times for each DC pressure level with a calibre. The experience was repeated three times so each point of the figure 5.19, 5.20 is the result of the mean of the three trials.

The figure 5.19 shows that in fact the diameter of the tube increases with the increasing of the DC pressure and increase equally along the three measured positions. The area of the cross-section of the tube was determined from the mean value of the diameter in the three measured positions for each DC pressure as is shown in figure 5.20.

It was verified that there is an exponential relationship between the pressure (p) and the area (A), as is described in *Meinders et al* [20]:

$$p = p_0 * e^{\gamma A}, \text{ where } p_0 \text{ and } \gamma \text{ are constants.} \quad (5.4)$$

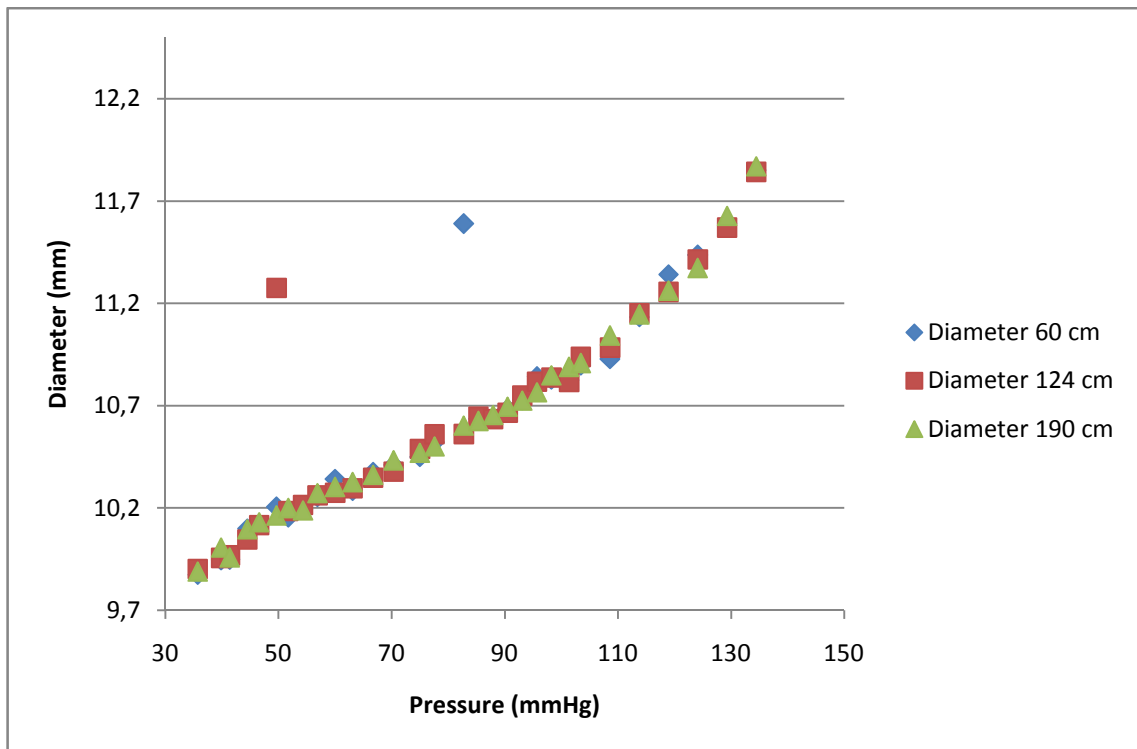


Figure 5.19 – Relation between DC pressure level and diameter measured at 60, 124 and 190 cm of the tube.

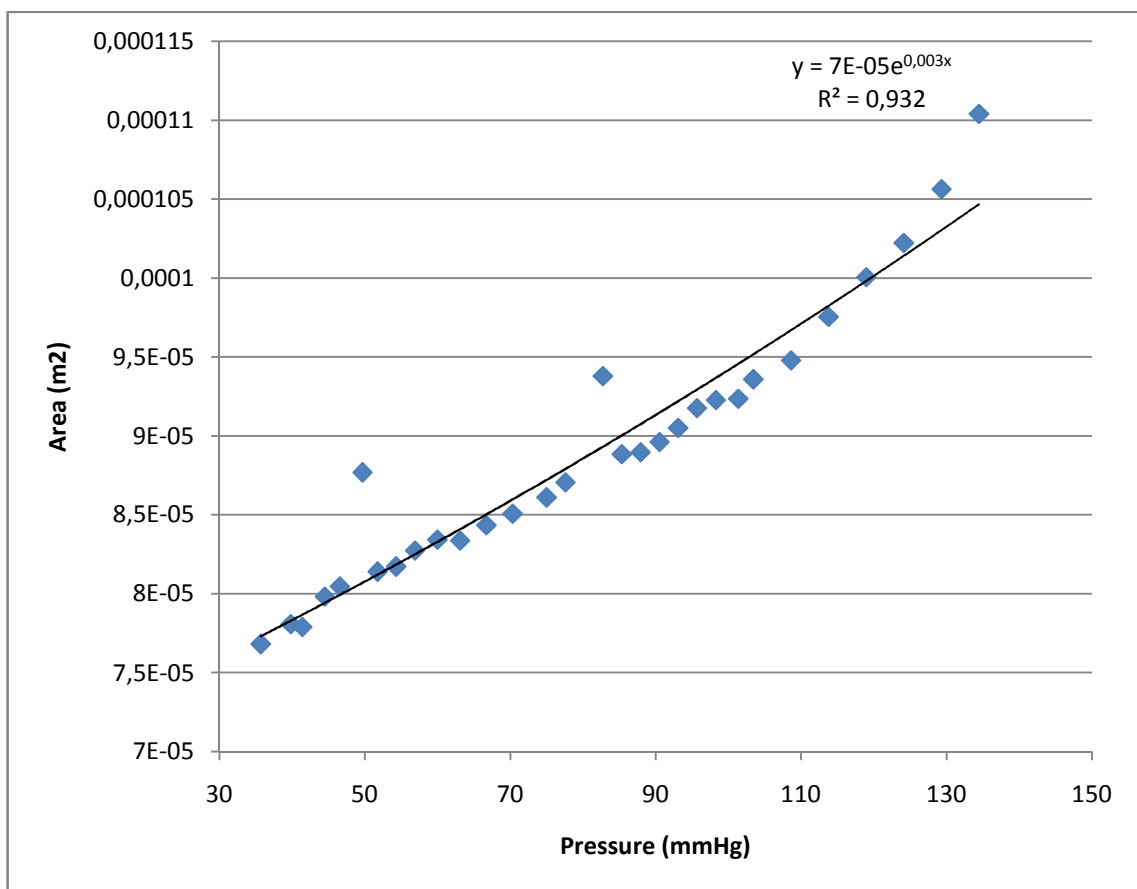


Figure 5.20 – Exponential relationship between DC pressure and cross-section of the latex tube. An exponential fit was made to the data with equation: $y=7 \cdot 10^{-5} e^{0,003x}$ and $R^2=0.932$.

The two data points, in figures 5.19 and 5.20, are far from the other points which it was due to a lack of precision in the measure with the calibre, which it will be reflected in the assessment of PWV.

From diameter measured in the tube we determine the D , as 5.3 equation, where: $dA = A_s - A_d$ and $dP = P_s - P_d$, A_s and P_s is systolic arterial cross-section and systolic pressure and A_d and P_d is diastolic cross-section and diastolic pressure. Assuming that: the diastolic pressure corresponds to the initial DC pressure (35.68 mmHg); the diastolic area corresponds to the initial area of the tube at 35.68 mmHg; the systolic pressure corresponds to each DC pressure level and the systolic area corresponds to area of the tube for each DC pressure level. The density of the water is 1 Kg/m³.

The PWV as a function of D of the tube was assessed for different DC pressure levels, as is shown in figure 5.21. Each point corresponds to the mean PWV of the last two experiments.

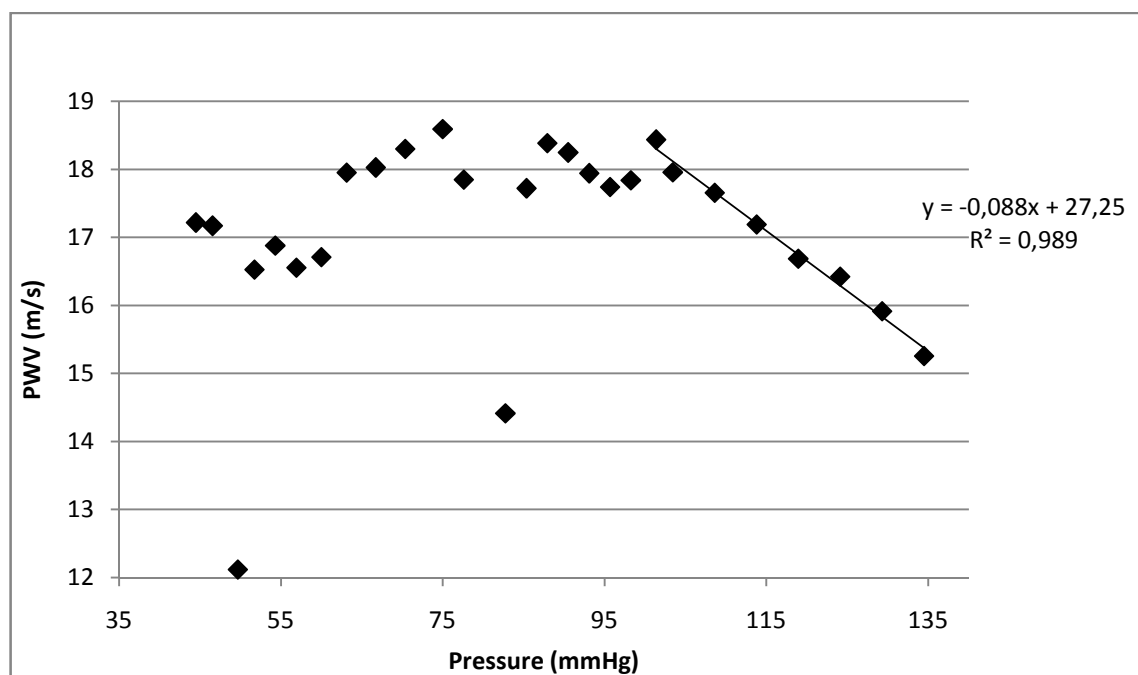


Figure 5.21 – Relation between the DC pressure level and PWV as a function of the distensibility of the latex tube. A linear fit was made to the last points with equation $y = -0.088x + 27.25$ and $R^2 = 0.989$.

Considering the D of the tube to assess PWV we verified that PWV varies to 16.5-18.5 m/s for range pressures 44-100 mmHg, thereafter the PWV seems to decrease linearly as shows the linear fit in the last points.

The first trial was excluded to determine the PWV in the latex tube because the ACT was removed from the experimental setup, and consequently, with the increasing DC pressure the latex membrane (whose is the interface between ACT and water into the tube) stretched and this influenced the PWV obtained for lower pressures, as shows figure 5.22. It means that not exerting force on the latex membrane, leaving it 'free', it dilates to compensate the pressure it is exerting on the tube decreasing the PWV.

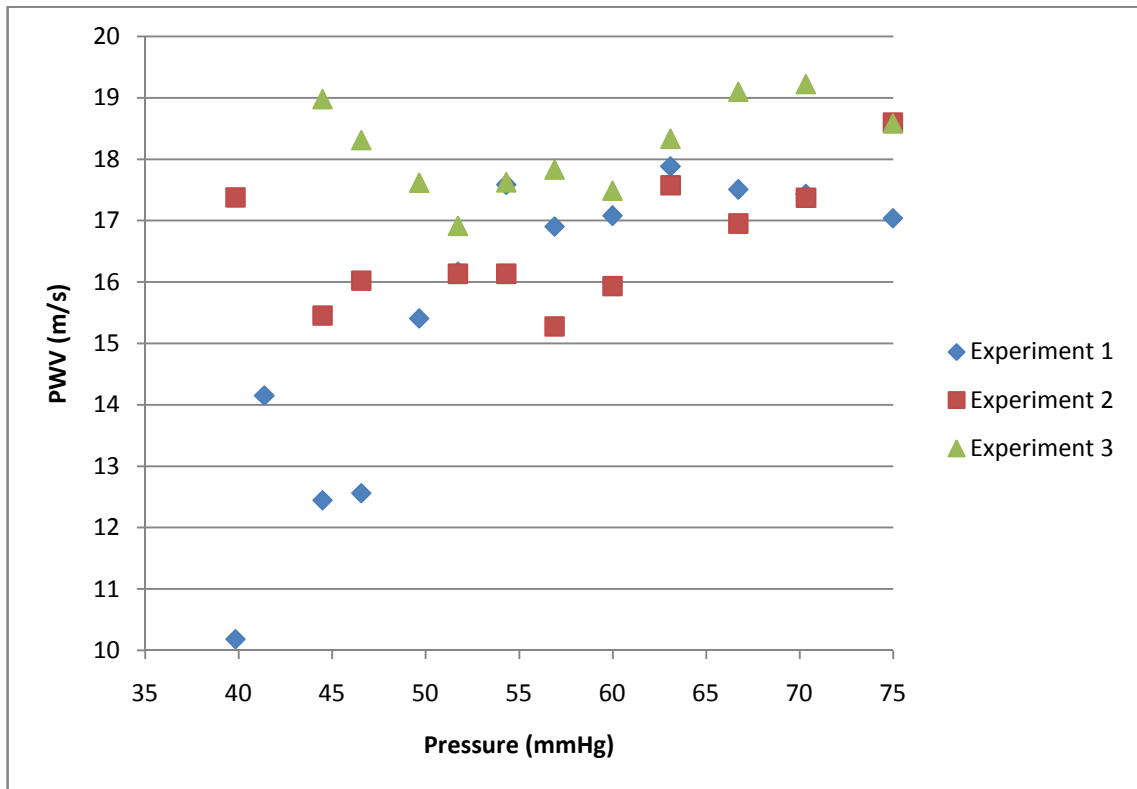


Figure 5.22 – Representation of PWV in the three trials for lower DC pressures.

5.2.3 TIME RESOLUTION OF PZ PROBE

The time resolution of the probe was showed through the LPWV assessment. The pulse TT between two recorded PZ signals was determined from several algorithms. They allowed assessing the smallest changes that the TT value can be measured.

Two experimental studies were done in order to evaluate the time resolution of the PZ probe. In the first one, two uncoupled PZ sensors on the latex tube were separated initially of 40 cm (Δx), as illustrates the figure 5.13. The PZ 1 was fixed in the same position on the tube while the PZ2 was approaching it every 2 to 2 cm. It was determined the LPWV for each separate distance (Δx) when a Gaussian waveform, with 3 volts amplitude and 150 ms of period, was sensed by both sensors. The section 4.2 describes the algorithms used to assess the pulse TT.

The signals of pressure sensors, PZ sensors and ACT were sampled to 5 kSamples/s at DC pressure of 39 mmHg. The PWV determined from the signals of the pressure sensors was used as the reference value. The figure 5.23 shows the signals recorded when Δx was 14 cm.

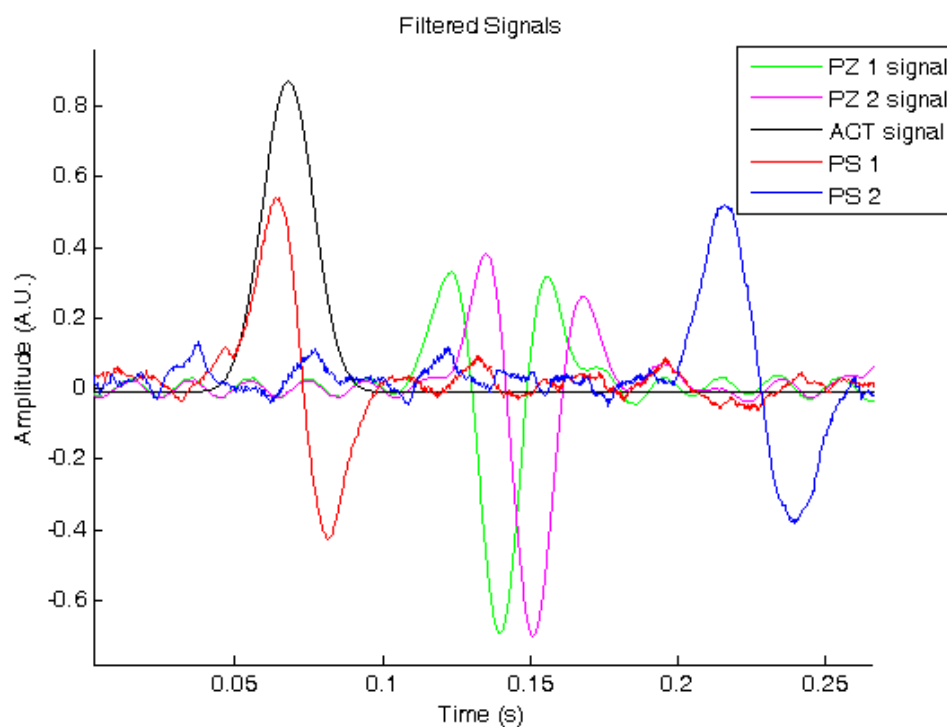


Figure 5.23 – Recorded signals to evaluate the time resolution of the probe. The Δx between PZ sensors was 14cm. The signals were filtered by a moving average filter.

Three trials were made and in each one was determined the PWV between the signals of the PZ sensors and pressure sensors with five algorithms. Each point of the figure 5.24 represents the mean PWV of the three trials. The distance between pressure sensors was 2.108 m and between uncoupled PZ sensors varied (Δx) but it's well known.

The relative error for each distance between uncoupled PZ sensors for each algorithm, figure 5.25, was determined as:

$$\text{Relative error (\%)} = \frac{PWV_{ref} - PWV_i}{PWV_{ref}} * 100,$$

where PWV_{ref} is the PWV value determined with pressure sensors and PWV_i is the PWV value determined with the PZ sensors.

Figure 5.24 shows the PWV values estimated from pressure sensors remained constant with increasing distance between uncoupled PZ sensors. With the pulse onset detection algorithm, the PWV values obtained are more widely dispersed than other algorithms. For $\Delta x=2\text{cm}$, the PWV estimated with PZ sensors is greater than the reference and the relative error is near 8% for maximum AD, minimum AD and zero-crossing algorithm. In opposite the PWV estimated with onset algorithm is lower than the reference and the relative error is near 6%. When Δx increases the PWV values deviate from the reference values but for Δx greater than 22 cm the PWV values again approach the reference values with a relative error for all algorithms near to 8%.

The mean of all relative errors was 7.9% for maximum AD algorithm, 10.45% for minimum AD algorithm, 9.847% for pulse onset detection algorithm, 9.08% for zero-crossing point algorithm and 8.89% for maximum of cross-correlation algorithm. Although there isn't a large discrepancy between the mean relative errors for each algorithm the maximum amplitude algorithm showed a lower error for the most Δx . However, the pulse onset algorithm showed lower error for Δx of 2 and 4 cm.

When the PZ sensors are placed 2 cm apart, the pulse TT estimated them by all algorithms was 1.3 ms except the onset algorithm that was 1.4 ms.

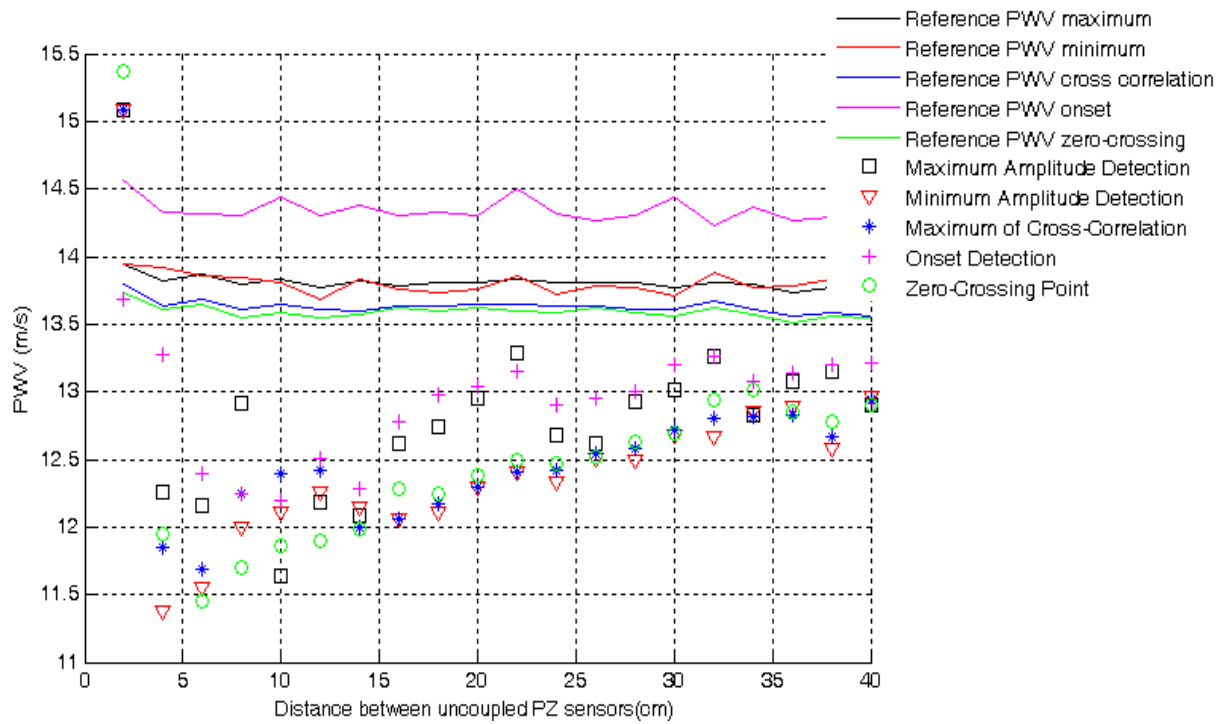


Figure 5.24 – PWV assessment of five algorithms from the signals of the PZ sensors uncoupled Δx cm and pressure sensors (reference).

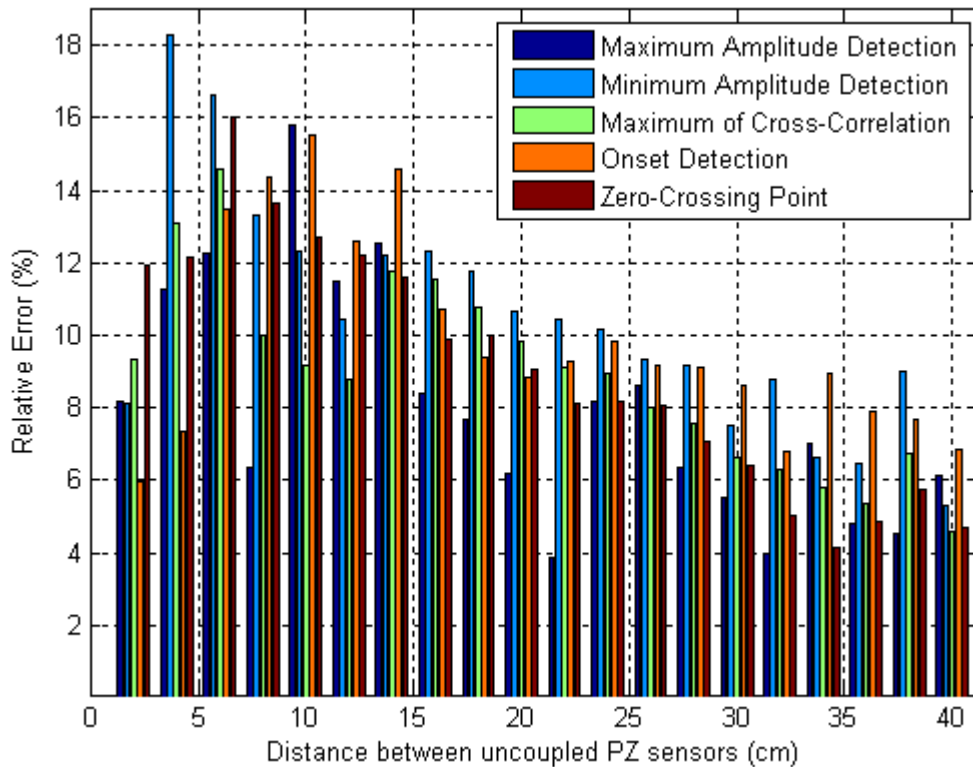


Figure 5.25 – Relative error for each distance between uncoupled PZ sensors (Δx) and each algorithm.

The second study consisted in generating a burst of ten Gaussian waveforms, with amplitude of 3 volts and 150 ms of period, it was sensed by PZ probe and pressure sensors. The two PZ sensors were placed near 16.8 mm apart on the tube where they were placed in twenty consecutive positions along it (90 - 130 cm of the tube in 2 to 2 cm). As in the first study, the PWV was estimated from pressure sensors, (reference value), and from PZ signals, using three different algorithms – maximum and minimum AD and pulse onset detection. Figure 5.26 shows an example of recorded signals in this study in response to a burst generated by the ACT. The first two pulses and the last one of all recorded signals weren't analysed.

It was also made three trials and in each one was estimated the reference PWV and the PWV from PZ signals. The ACT signal was segmented (segmentation algorithm in section 4.1) and found the onset of each Gaussian waveform, dividing the signal into periods. For each period was determined the pulse TT between two PZ or pressure signals and from the mean of the TT estimated in all periods was determined the PWV for each position on the tube. In the figure 5.27, each point represents the mean PWV of the three trials and in the figure 5.28 the relative error between the reference PWV and determined from PZ probe associated to each algorithm for each position.

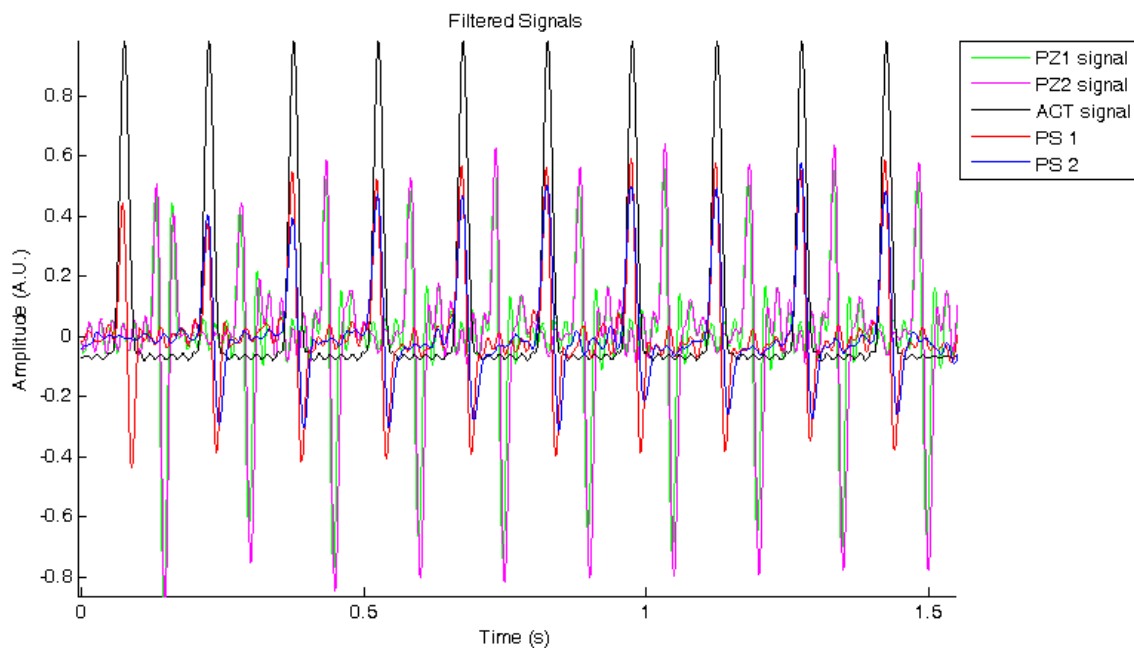


Figure 5.26 – Recorded signals of PZ and pressure sensors in response to a burst of ten Gaussian waveforms (in black). The PZ probe is at 90 cm of the tube.

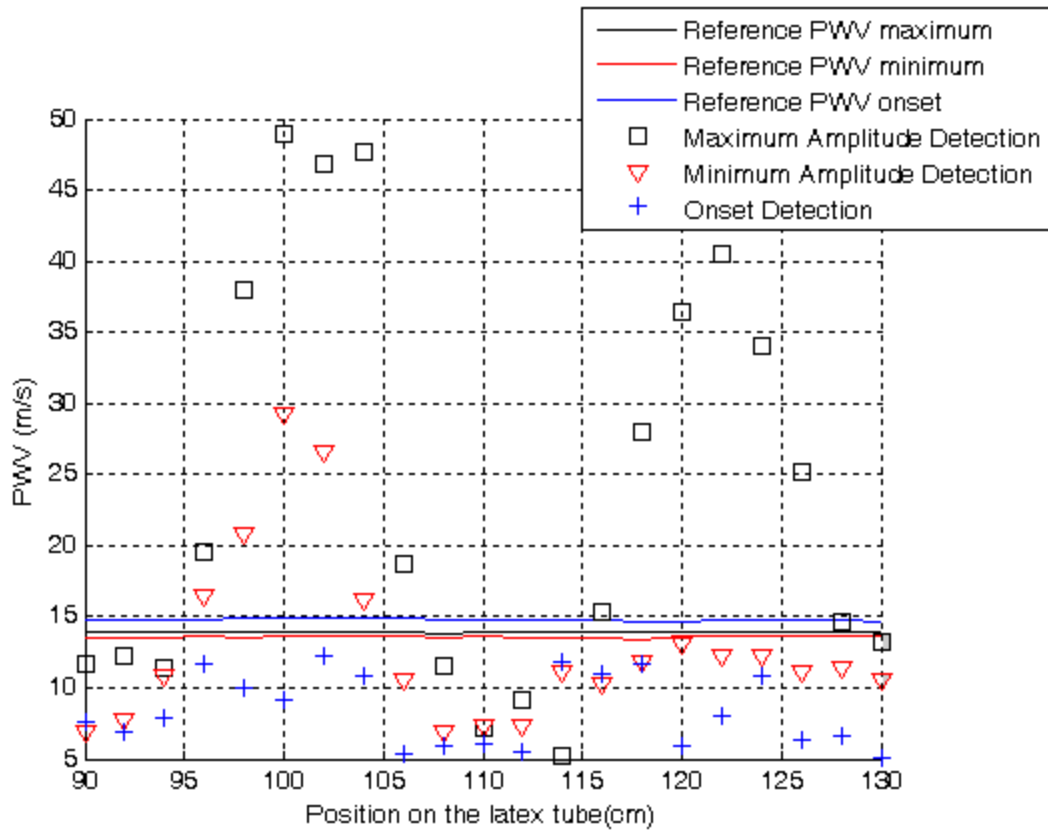


Figure 5.27 – The local PWV estimated from pressure sensors and PZ probe in 20 consecutive positions along the latex tube.

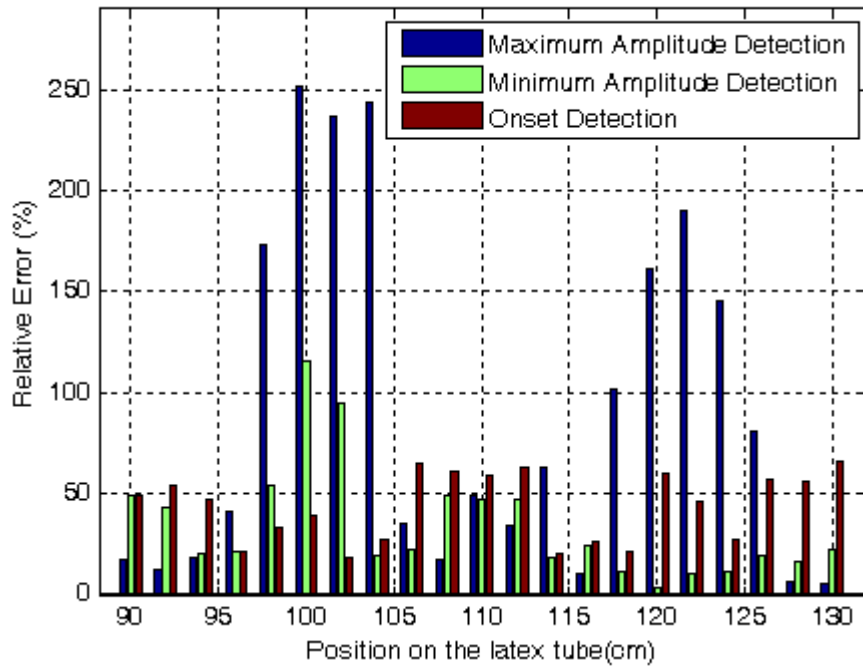


Figure 5.28 – Relative error between the reference PWV and determined from PZ probe for each position on the latex tube and each algorithm.

The LPWV assessed by maximum AD algorithm showed a greater dispersion of the measurements in relation to the reference PWV, as we can see in figure 5.27 and 5.28. The dispersion is greater in positions 98-104 cm and 118-126 cm on the latex tube where the PWV ranged from 20 to 50 m/s. Physiologically, these PWV values don't make sense.

The mean of the all relative errors with minimum AD was 33.87%, with onset detection was 43.19% and maximum AD was 89.9%. Although the dispersion of PWV measurements by PZ probe in relation to the reference are large, the PWV values obtained with minimum AD, whose mean PWV of the distribution was 12.89 ± 6.07 m/s, tended to approach to the correspondent reference values that was near 13.56 ± 0.03 m/s. The mean of reference PWV obtained with onset detection was 14.78 ± 0.07 m/s and the mean PWV obtained with PZ probe was 8.39 ± 2.47 m/s. The algorithm with worst performance in this study was the maximum AD, where the mean of the reference PWV was 13.906 ± 0.03 m/s and the mean of PWV obtained with the PZ probe was 23.59 m/s and high standard derivation was 14.55 m/s. In order to compare the deviation of the two PWV distributions (reference and PZ probe) determined with minimum AD, the coefficients of variation were calculated. The CV of the reference PWV was 0.53% and for PWV determined from PZ signals was 47.07%.

In this study the PZ probe could discriminate two points where the mean of TT estimated, with minimum AD along the all positions on the latex tube, was 1.5 ms.

5.2.4 DISCUSSION

CHARACTERIZATION OF THE TEST BENCH II

The characterization of the latex tube constituted the first part of the tests in the test bench II. The propagation of a Gaussian waveform along the tube was studied with a PZ sensor of the new PZ DP which was able to sense the incident wave and their reflections at the ends of the tube. The figures 5.15 and 5.16 show the incident wave is more visible because it was detected with great amplitude. Over the time, with the multiple reflections, the wave was dissipated. The study of the phenomena of wave

propagation allowed verifying the physical location in the test bench where the wave is reflected, in other words, the components at the ends of the tube – the latex membrane and piston. The Gaussian wave propagated into the latex tube 13.4 m/s at 40.86 mmHg.

The latex tube showed to be a distensible tube because it was able to stretch and dilate under the increasing of DC pressure. In this tube, the PWV estimated through the pressure sensors as the reference value, didn't reflect the actual behaviour of the tube because it swelled and the caused a difference in diameter with the DC pressure. It was shown that there is an exponential relationship between the DC pressure and area cross-section of the tube. The results of the PWV assessed by measuring the diameter or D , see figure 5.21, showed a different profile from the first in figure 5.18 and the silicone tube in figure 5.29, where the PWV varied to 16.5-18.5 m/s for range pressures 44-100 mmHg. For DC pressures above 100 mmHg the PWV decreased and a possible explanation is that the tube increased in diameter but also in length compensating the difference in pressure, as it was seen in early trials. The method to measure the diameter wasn't the most precise and it would be necessary more trials to obtain better results but this can show that the PWV in a latex tube is approximately constant for a range of DC pressures.

During the trials with DC pressure variation it's necessary to be careful with the latex membrane because for high pressures (near 140 mmHg) which can break it. However, it was possible to vary DC pressure simulating the biological pressures in the human adult (80 mmHg diastolic and 120 mmHg systolic) in opposite with the silicone tube (10 mmHg to 70 mmHg, see figure 5.29) [64].

The initial diameter of the tube, according to the product description, was 9.5244 mm and the initial diameter measure with the calibre varied to 9.79-9.92 mm. Another interesting study would be to prove, with another method of measuring the diameter, if the tube beyond distensible is compliant, which means is able to come back to its original dimensions. The ultrasound was used to measure the diameter in the carotid artery and it seems to be the best alternative to measure the diameter in the tube [20]. Another alternative would be to measure it optically.

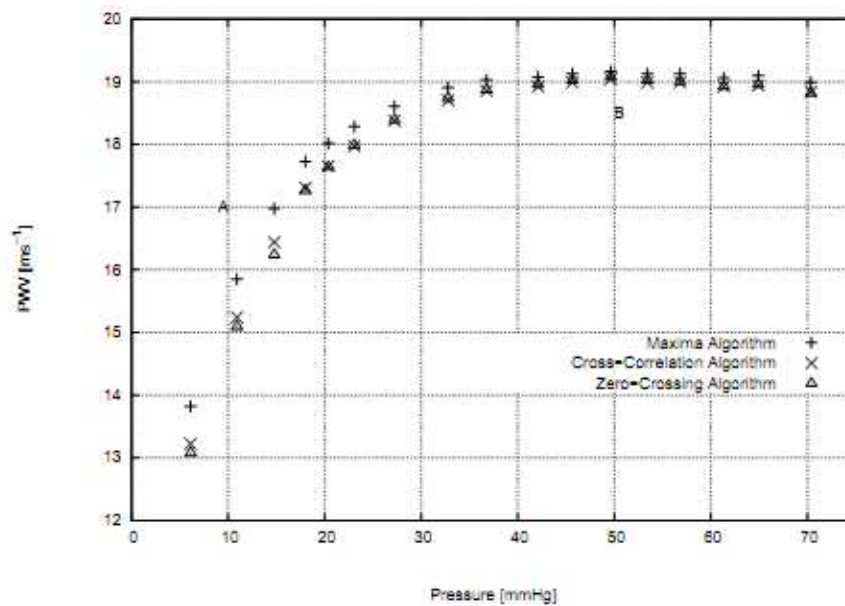


Figure 5.29 – Relation between DC pressure level and PWV in the silicon tube [58].

TIME RESOLUTION

To evaluate the time resolution of the new PZ probe, several algorithms were implemented in order to calculate the pulse TT and find the best way to assess the LPWV, from PZ signals, and also the most accurate way in relation to reference PWV. In both studies the dispersion between reference PWV and PWV estimated from PZ signals was high for all algorithms but in each study was found the best algorithm, the algorithm with the lowest relative error. The maximum and minimum AD algorithms showed best performance for the first and second study, respectively.

In the first study, it was possible to determine the pulse TT with all algorithms when the distance between uncoupled PZ sensors was decreasing.

In the second study, the dispersion of the PWV measured along the tube was quantified by CV. Although the mean of PWV (12.89 ± 6.07 m/s) determined by minimum AD and obtained by PZ probe along the twenty positions, being near the reference PWV (13.56 ± 0.03 m/s) the standard deviation isn't enough to compare the two distributions of PWV. The CV revealed a large discrepancy between the distributions, 0.53% for reference PWV and 47.07% for PWV determined from PZ probe. The CV was greater

than the CV obtained with the previous double probe (10.32%) and the local PWV assessed with this new PZ probe was near 13 m/s while the previous was near 19 m/s.

The position along of the tube where were acquired the PZ signals also could have contributed for these results due to the influence of the backward waves. The reflected waves at the ends of the tube changed the morphology of the acquired signals by PZ probe and the algorithms to assess LPWV weren't the most appropriated for these signals. On the other hand, as mentioned in chapter 2, the PWV increases in arteries near the reflection sites. Similarly, along these positions in the latex tube this phenomenon could have happened.

The average of the time resolution estimated along the 20 positions on the tube when both PZ sensors were placed near 16.8 mm apart was 1.5 ms.

In order to improve the results, the algorithms to assess pulse TT should be optimized because the relative errors and LPWV values were large. An appropriate interface between PZ sensor and the measurement site should also be studied so that there is only one point of contact between them both. To choose a region along the tube where the PZ signals there aren't affected by reflected waves could be another solution to improve the results. More trials should be done to have more measurements and increased the statistic of the data because three trials aren't enough.

CHAPTER VI

PRELIMINARY CLINICAL TRIALS

The clinical trials are another important step in the PZ probe's characterization. The clinical validation of the probe is a long process which will be carried out by our collaborators and for this reason the clinical trials shown in this thesis were collected in a small group of volunteers at GEI.

6.1 DATA ACQUISITION PROTOCOL

The clinical trials involved eight healthy volunteers, two male and six female, in the age range from 22 to 28 years old and without history of cardiovascular disease, hypertension and diabetes. For a month, once a week, were collected signals on CCA on each patient using the following protocol:

- 1) The volunteers were sat on a chair and at rest before the acquisitions started;
- 2) The operator of all acquired signals with the PZ probe was the volunteer himself;
- 3) The signal was acquired at right CCA and recorded seven consecutive pulse waves. The procedure was repeated for left CCA.
- 4) The step 3) was repeat a second time. It means each week two signals were recorded at right CCA and left CCA.

6.2 RECORDED SIGNALS IN CCA

The CCA signals were recorded at 11 KSamples/s in Measurement & Automation software and processed in MATLAB®.

Although the volunteers used to deal with similar probes the data acquisition process wasn't easy. Anyway, the integrated PZ signal as a approximation to the real ABP waveform is a new trend to help to the operator to recognize more easily its ABP and identify if it's a normal or abnormal signal. Figure 6.1 shows an example of a recorded signal in a volunteer where the DC component was removed, the signals were normalized and filtered by a moving average in 50 samples.

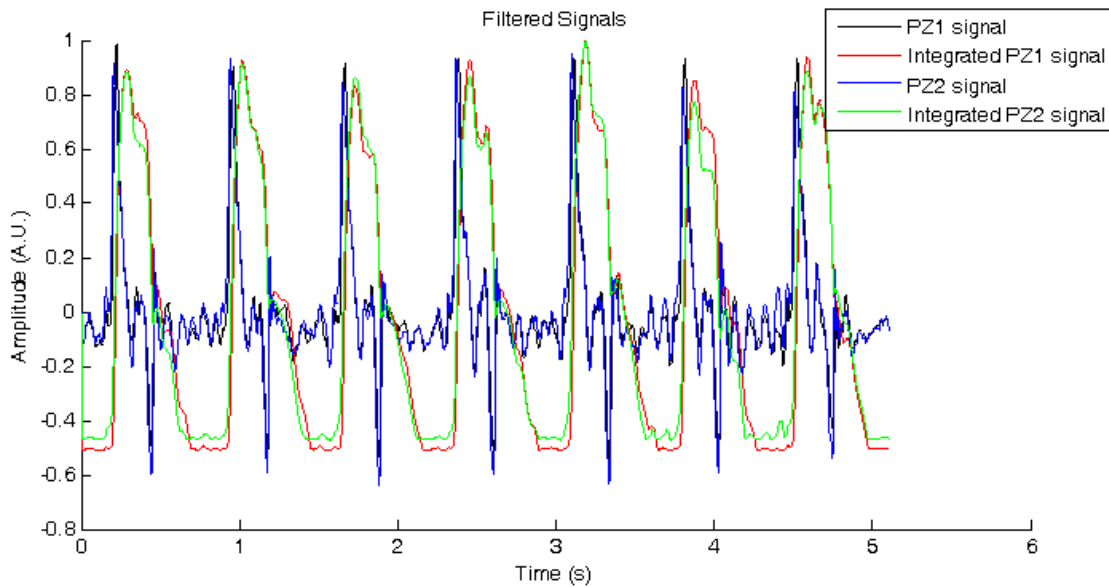


Figure 6.1 – Example of a recorded right CCA signal recorded by a volunteer. It is represented the PZ signal and the integrated signal of both PZ sensors.

6.3 ASSESSMENT OF LOCAL PWV

In section 4.3 of this thesis, the method used to determine the local PWV was explained taking into account the distance between two recorded sites (Δx). The PWV was calculated in each segmented pulse wave of each recorded signal at left CCA and right CCA by two methods: maximum and minimum AD algorithms.

Some of the PWV values obtained from a pulse wave were distant from the PWV values of the other pulse wave in the same recorded signal or the other PWV values obtained in other recorded signals in the same week. Statistically, the values that appear to differ dramatically from the rest of the data are defined as outliers. In order to improve the results the outliers were identified and removed by the assumption that an outlier is a value (y_i) that is more than two standard derivations away from the mean of the PWV, mathematically expressed by $(y_i - \text{mean}(PWV)) > 2 * SD$ [65]. The table 9 shows an example of identified outliers, in gray. Although it was identified the outliers, there are PWV values far from physiological values, 4-10 m/s [1]. So a second criterion was used to removal outliers which consisted to removal PWV values > 15 m/s, represented with * in table 9.

Table 9 – Identification of the outliers, in gray, from the data recorded in week 2 in a volunteer.

Week 2 – PWV assessment (m/s)				
Maximum Amplitude Detection Algorithm				
Pulse waveform	Left CCA		Right CCA	
	Signal 1	Signal 2	Signal 1	Signal 2
1	4.06	44.68*	2.71	1.71
2	3.50	13.75	2.93	0.02
3	5.96	25.53*	3.19	1.70
4	5.26	22.34*	2.79	1.82
5	3.72	70	2.93	1.67
6	5.11	44.68*	2.66	1.49
7	5.96	44.68*	2.66	1.58
Mean PWV±SD	17.63±16.96 m/s		2.14±0.86 m/s	

The two recorded signals in the same location at the CCA (left and right) allow having more samples to determinate the PWV, initially the number of samples was 14 pulse waves (N=14). With the outliers identification the number of samples decreased, for example in table decreased to N=8 at left CCA, table 9.

6.4 REPEATABILITY ANALYSIS IN CCA SIGNALS

Repeatability and reproducibility studies are essential to probe the precision of the new PZ probe. The repeatability analysis was discussed on section 5.1.3 when the probe was characterized in test bench I, not showing conclusive results. In CCA signals recorded, the repeatability study can be carry out from the local PWV assessment in the in the same volunteer and with the same operator in four measurements recorded once a week. With the reproducibility test, it is intended to reproduce the same measurements by different operators but this test wasn't made yet.

Tables 10 and 11 show the mean local PWV values and standard derivation (SD) of the N pulse wave for each volunteer during four weeks at right and left CCA. The local PWV was determined by maximum AD algorithm, table 10, and minimum AD, table 11.

Table 10 – Mean local PWV and standard derivation for each volunteer during four weeks. The local PWV was assessed by maximum amplitude detection algorithm. The indexes correspond to the number of samples: ¹N=14; ²N=13; ³N=12; ⁴N=8, ⁵N=11, ⁶N=10.

PWV assessment±SD (m/s) – Maximum amplitude detection algorithm								
Volunteer	Week 1		Week 2		Week 3		Week 4	
	Left CCA	Right CCA	Left CCA	Right CCA	Left CCA	Right CCA	Left CCA	Right CCA
1	1.88±0.98 ¹	2.35±0.74 ¹	5.91±3.31 ⁴	2.14±0.86 ¹	1.75±0.39 ¹	5.27±4.24 ¹	5.29±3.3 ²	3.58±1.43 ¹
2	8.07±3.15 ²	4.80±2.26 ¹	1.84±0.59 ¹	5.47±5.04 ⁵	1.52±0.20 ¹	2.72±0.99 ¹	4.05±2.39 ¹	2.28±0.25 ¹
3	6.09±3.05 ³	8.105±3.48 ⁵	3.18±1.15 ⁴	3.86±1.71 ²	2.07±0.24 ¹	1.83±0.15 ¹	3.04±0.59 ¹	1.51±0.40 ¹
4	4.24±1.82 ²	1.86±0.52 ¹	6.52±3.73 ⁶	3.38±1.80 ²	3.99±3.12 ¹	4.96±2.38 ⁵	2.14±0.68 ¹	2.78±1.20 ¹
5	4.57±2.37 ⁶	2.57±1.55 ¹	3.07±1.01 ¹	3.92±2.97 ³	2.37±0.36 ¹	6.75±3.37 ⁴	2.67±0.44 ¹	3.08±2.50 ³
6	2.06±0.49 ¹	3.38±0.55 ¹	3.33±1.67 ¹	2.51±0.93 ¹	5.04±3.71 ¹	3.53±0.75 ¹	1.96±0.27 ¹	6.17±4.74 ²
7	4.61±4.05 ¹	1,66±0,88 ¹	5.20±5.18 ⁵	1.93±0.25 ¹	5.87±2.61 ¹	2.53±0.84 ¹	3.32±1.80 ¹	1.98±0.56 ²
8	5,27±2,51 ³	5.21±2.42 ³	1.85±0.52 ¹	3.59±4.99 ³	5.83±1.32 ¹	1.65±1.42 ²	1.35±0.13 ¹	6.68±3.83 ⁶

Table 11– Mean local PWV and standard derivation for each volunteer during four weeks. The local PWV was assessed by minimum amplitude detection algorithm. The indexes correspond to the number of samples: ¹N=14; ²N=13; ³N=12; ⁴N=8, ⁵N=11, ⁶N=10, ⁷N=9.

PWV assessment±SD (m/s) – Minimum amplitude detection algorithm								
Volunteer	Week 1		Week 2		Week 3		Week 4	
	Left CCA	Right CCA	Left CCA	Right CCA	Left CCA	Right CCA	Left CCA	Right CCA
1	2,93±0,93 ¹	4,05±1,42 ¹	4,35±2,06 ³	5,27±3,47 ¹	2,11±0,72 ¹	7,17±4,65 ¹	4,22±1,81 ¹	6,40±2,66 ¹
2	2.54±2.58 ¹	4,90±3,69 ¹	2.66±2.17 ⁵	11,38±8,64 ⁵	4,81±3,46 ¹	8.30±5.20 ⁶	2,62±1,87 ¹	4.54±3,98 ⁶
3	2,22±1,79 ¹	2,61±2,21 ²	3,06±1,77 ¹	1,35±0,48 ¹	3,85±2,81 ¹	1,39±3,02 ¹	3,07±1,47 ¹	3,89±2,19 ²
4	1,75±0,36 ¹	7,52±4,73 ²	1,20±0,47 ¹	2,20±0,93 ¹	3,58±3,65 ²	1,65±1,08 ¹	4,06±2,05 ¹	2,97±3,85 ¹
5	6,69±0,70 ¹	5,83±1,19 ¹	4,05±0,21 ¹	5,17±1,94 ²	4,45±1,62 ²	8.77±4.19 ⁵	4,05±1,05 ¹	5,71±2,52 ¹
6	1,57±0,88 ¹	3,81±2,26 ³	3,14±1,78 ¹	1,96±1,18 ¹	1,64±0,75 ¹	2,62±1,95 ¹	2,19±1,12 ¹	3,18±0,94 ¹
7	5.53±2.05 ⁶	8.58±3.35 ³	5.19±3.56 ⁴	6.73±10.62 ³	1,95±1,80 ¹	5.58±4.54 ⁷	5.85±13.65 ⁶	4,94±1,92 ¹
8	6,25±2,78 ²	4,46±1,84 ²	3,40±2,56 ¹	5.62±4.95 ⁵	1,04±1,06 ²	5.33±2.79 ⁶	2.10±1,19 ¹	6,44±4,93 ²

The mean local PWV values with maximum AD algorithm has a range from 1.35 m/s to 8.105 m/s while with minimum AD algorithm has a range from 1.20 m/s to 11.38 m/s. In literature, the typical PWV values in carotid artery range from 3-5 m/s in health young people, in this 'clinical data' it was obtained PWV values close from the

reference values of the literature and by other methods as ultrasound or Doppler[1, 66-67].

Although the removal outliers helped to improve the results these aren't still good enough to prove the repeatability of the probe in some volunteers. There is an evident discrepancy between PWV values determined during four weeks with both algorithms and the SD showed the variation of the PWV values from the PWV mean, table 10 and 11. The high SD indicates that despite the removal outliers the data is still far from the mean PWV value. If the outliers weren't removed the discrepancy would be greater. In fact, the quality of the recorded signals can be questioned because the signals weren't acquired with a qualified operator (a doctor for example), so it would be the first reason given as the cause of these results. In some recorded signals in the same week, the PWV assessed in the first signal on one location of CCA was substantially different from the second signal recorded in same location of CCA, which can mean that it didn't record a good signal. Anyway, once again it's hard to prove the repeatability of the probe in these preliminary clinical trials. However, we can compare the two algorithm used to assess the LPWV.

6.5 COMPARISON OF MAXIMUM AND MINIMUM AMPLITUDE DETECTION ALGORITHMS

The mean of PWV and SD for the four weeks was calculated for each volunteers and each algorithm, as shown table 12. Figure 6.2 shows a histogram that represents graphically the mean PWV of the table 12 for each volunteer and algorithm. Though the number of samples used to assess PWV isn't equal in each algorithm, as previously mentioned, it allows improving the results.

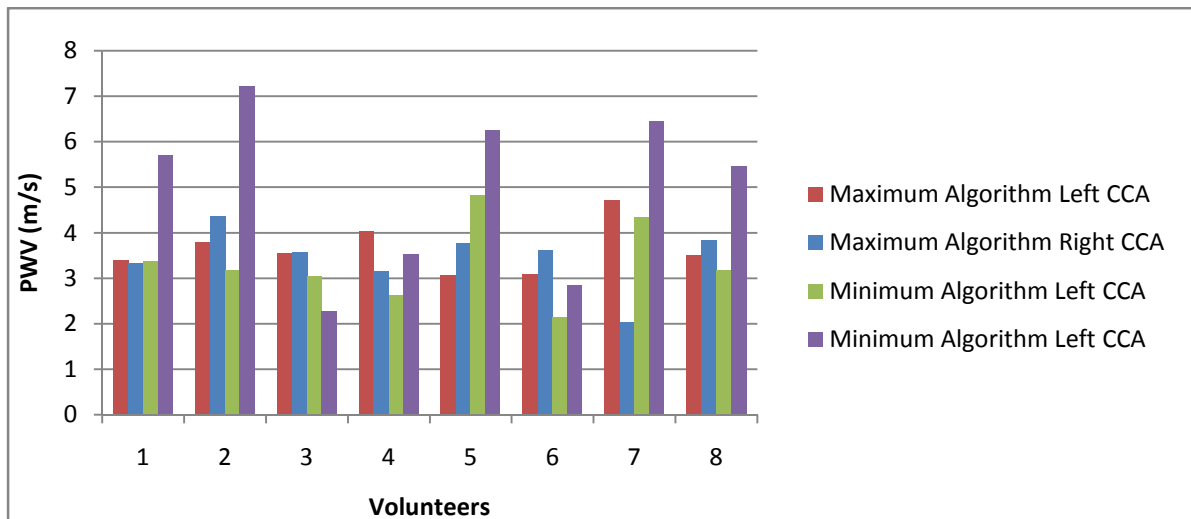


Figure 6.2 – Histogram of the mean PWV values for each volunteer during 4 weeks using two algorithms.

Table 12 – Mean of local PWV±SD (m/s) for each volunteer and algorithm on left and right CCA.

Volunteer	Maximum Algorithm (N=834)		Minimum Algorithm (N=835)	
	Left CCA	Right CCA	Left CCA	Right CCA
1	3.40±2.85	3.33±2.57	3.37±1.70	5.70±3.44
2	3.80±3.14	4.37±4.47	3.18±2.72	7.22±6.17
3	3.54±2.21	3.58±3.09	3.05±2.05	2.27±2.36
4	4.04±2.87	3.15±1.87	2.63±2.35	3.53±3.78
5	3.06±1.39	3.78±2.88	4.82±1.50	6.26±2.85
6	3.10±2.36	3.61±1.72	2.14±1.33	2.86±1.73
7	4.71±3.53	2.03±0.74	4.35±6.93	6.45±6.03
8	3.51±2.42	3.84±3.13	3.18±2.78	5.47±3.83
Overall mean PWV±SD for the 8 volunteers (m/s)	3.65±0.65	3.46±1.12	3.34±1.80	4.97±1.60

The mean PWV with both algorithms varies between near 2-7 m/s, being the overall mean PWV for this group of volunteers in left CCA of 3.65 m/s and 3.34 m/s for maximum and minimum algorithm, respectively. Concerning the right CCA the overall mean PWV is 3.46 m/s and 4.97 m/s for maximum and minimum algorithm, respectively.

Although the SD is high in both algorithms, the maximum AD algorithm has the lowest overall mean SD for the eight volunteers (0.65 m/s in left CCA and 1.12 m/s in right CCA) comparing with the minimum AD algorithm. The mean PWV during the four weeks was obtained with both algorithms, inside the expected values of PWV in CCA, which means between 3-5 m/s. In respect to assessment of PWV in two recorded sites (left and right CCA), the difference of the mean PWV in two location is less when the PWV is determined with the maximum AD algorithm.

6.6 DECONVOLUTION METHOD IN CCA SIGNALS

Deconvolution method was described in section 5.1.5. The same method was applied in recorded signals in volunteers, using the IR obtained in test bench I (see figure 5.10). An example of deconvolved signals in a CCA signal is shown in figure 6.3. The deconvolved and integrated signals of both PZ sensors are represented in order to compare them.

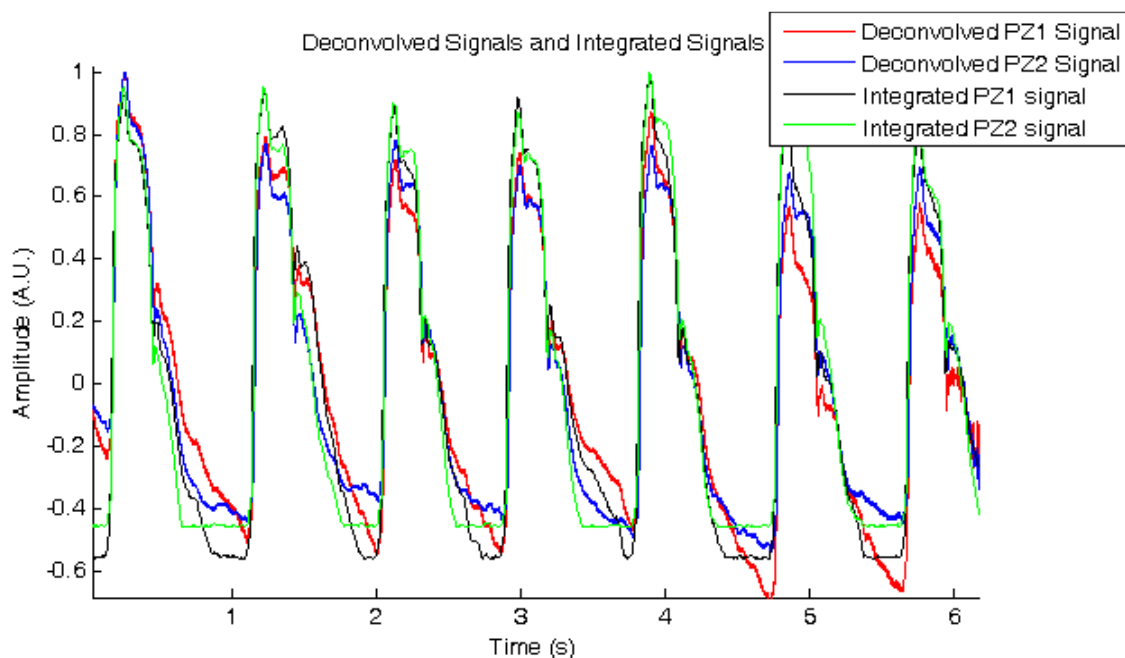


Figure 6.3 – Comparison between the deconvolved signals from PZ signals and integrated signals from PZ probe. The RMSE between deconvolved and integrated signals to PZ1 is 14.76% and to PZ2 is 13.48%.

The comparison between deconvolved signals and integrated signals was quantified by calculating the RMSE for all recorded 'clinical data'. The RMSE ranged from 5 to 21%, the mean RMSE between deconvolved and integrated signals for each PZ sensor was near 13.05%.

With the deconvolution method was obtained the ABP waveform, proving the effectiveness of IR determined in CCA signals. In comparison to integrated signal, the shape of both is similar but having a little difference in amplitude. In general, there is a good similarity between the two signals obtained by different ways.

6.7 DISCUSSION

Despite initial difficulties in acquiring signals with PZ probe, these preliminary clinical trials revealed the ability to record signals in CCA and visualize the ABP waveform given by the probe. The ABP waveform obtained by the probe proved to be much closer to the expected waveform by deconvolution method, the minimum RMSE between the two waves in the all recorded signals was 5%.

By decreasing the distance between two PZ sensors, we can facilitate the acquisition signals but this study will be made with the data collected with the other prototypes.

Not all the recorded pulse waves were considered good signals to assess local PWV. Although the removal of outliers has improved results, it's not enough to prove the repeatability of the probe. It can be explained due to the signals weren't acquired at the same location in CCA and/or were acquired close to the carotid bifurcations. The supine position is recommended in the signals acquisition in patients.

The mean LPWV determined by maximum and minimum AD algorithms for each volunteer during the four weeks, see table 12, are closer to typical values for healthy young people. However the standard derivation is greater for both.

The clinical validation is important to characterize the probe. Therefore the analyses in other groups of patients healthy and with cardiovascular disease should be made with a doctor as operator.

CHAPTER VII

FINAL REMARKS

7.3 CONCLUSIONS

The main purpose of this work is to characterize a new double probe based on PZ sensors able to assess LPWV in a non-invasive way and that reproduces the ABP waveform. PWV is considered by Expert Consensus document [1] a predictor of AS therefore it's so important assess this hemodynamic parameter. In our research group, it is developed devices that assess the PWV locally in CCA because it brings information about arterial wall's properties and consequently is a direct measure of AS.

The test bench systems allowed characterize the new PZ probe by the reproduction of some hemodynamic properties of the cardiovascular system. This probe has new features, compared to the previous developed double probe, mainly its new design, ergonomy and ability to measure the pressure waveform called in section 5.1 through the electronic integration of the PZ signal. In waveform analysis was shown that the integrated PZ signal could reproduce the original waveform and the RMSE between both increased after the systolic peak (the RMSE doesn't exceed the 9%). It was also possible to recover the pressure waveform by deconvolution method through IR of two sensors.

The repeatability and cross-talk are other important features of the PZ probe. In the test bench I and in clinical trials was analyzed the repeatability of the probe but it wasn't obtained good results. In relation to the cross-talk analysis was shown that the PZ sensors didn't suffer crosstalk effect.

In the test bench II, the study of the PWV in the latex tube was a new challenge. The behaviour of the tube with DC pressure required an additional study about the D , showing that due to elastic properties of latex the D should be measured to assess the PWV of a Gaussian waveform into the tube. The time resolution was 1.5 ms being the mean of the LPWV was 12.89 ± 6.07 m/s when determined by minimum AD algorithm. The algorithms used showed high relative error, standard derivation and coefficient

variation when to assess LPWV from PZ signals. On the other hand, the algorithms worked well in the signals of pressure sensors.

Despite the difficulty in the signal's acquisition in human CCA, it was obtained LPWV values closed to the reference values of the literature and obtained by other methods as Doppler and ultrasound [1, 66-67]. The LPWV ranged from 2.03 ± 0.74 m/s to 4.71 ± 3.53 m/s by maximum AD algorithm and 2.14 ± 1.33 m/s to 7.22 ± 6.17 m/s by minimum AD algorithm, table 12.

7.4 FUTURE WORK

The previous works showed the feasibility of the PZ sensors in the hemodynamic parameters assessment. The characterization of the new double PZ probe showed some interesting results in the assessment of LPWV. However, there is a long work to do in order to show the feasibility of the probe.

Signal processing

Optimization of the algorithms to assess LPWV is necessary. Five algorithms were implemented in PZ and pressure signals to determine PWV values and the results showed a great discrepancy between them. In clinical trials, the LPWV assessed in the same volunteer showed also different results with different algorithms. It shows the importance to identify the accurate time-reference point of the wave to determine the pulse TT.

In the future, from ABP recorded by PZ probe can assess the LPWV with the algorithms: maximum upstroke of second derivate; time-point at 20% of the upslope of ABP wave and intersecting tangents as well as identify the characteristic parameters like: systolic peak, inflection point and dicrotic notch allowing to assess the Alx.

Double probe

In the test bench I was recognized the importance of an appropriated interface on PZ probe. The study of an interface on PZ sensor is essential to improve the results, it would allow to have a point of contact.

The distance between PZ sensors is another question that can influence the time resolution and to facilitate the acquisition signals in human CCA.

Test bench

During the experiments in test bench II the latex membrane broke. A new structure to replace the latex membrane due to the risk to break and damage the ACT. As mentioned in previous works, it would be important to characterize the probe in a tube filled with a fluid with different density, for example a mixture of glycerine and water that is easy to do in laboratory.

Clinical trials

The clinical trials are the most important part of probe's characterization. In collaboration with the doctors the probe would be characterized in terms of reproducibility and test its performance in healthy patients as well as in patients with CVD.

A large number of signals acquired in human CCA would help to detect problems in acquisition system and improve the probe and the algorithms.

CHAPTER VIII

REFERENCES

- [1] Laurent S., Cockcroft J., Bortel L. *et al.* 2006 Expert consensus document on arterial stiffness: methodological issues and clinical applications *European Heart Journal* **27** 2588-2605
- [2] Cheung Y, 2010 Review - Arterial Stiffness in the Young: Assessment, Determinants, and Implications *Korean Society of Circulation* **40** 153-162
- [3] 'WHO/Europe| Cardiovascular diseases', WHO-World Health Organization, accessed on 27th April 2011:<http://www.euro.who.int/en/what-we-do/health-topics/noncommunicable-diseases/cardiovascular-diseases>
- [4] Arnett D., Evans A. And Riley W. 1994 Arterial Stiffness: A new Cardiovascular risk factor? *American Journal of Epidemiology* **140(8)** 669-682
- [5] 'Coordenação Nacional para as Doenças Cardiovasculares', accessed on 27th April 2011: <http://www.acs.min-saude.pt/cndcv/2009/12/23/campanhaeamavc-2/>
- [6] 'WHO| Cardiovascular diseases', accessed on 27th April 2011: <http://www.who.int/mediacentre/factsheets/fs317/en/index.html>
- [7] 'WHO| Strategic priorities of the WHO Cardiovascular Disease programme', accessed on 27th April 2011. http://www.who.int/cardiovascular_diseases/priorities/en/
- [8] Jatoi N., Mahmud A., Bennett K. and Feely J. 2009 Assesment of arterial stiffness in hypertension: comparison of oscillometric (Arteriograph), piezoelectronic (Complior) and tonometric (SphygmoCor) techniques *Journal of Hypertension* **27** 2189-2191
- [9] Sugawara J., Hayashi K., Yokoi T. et al 2005 Brachial–ankle pulse wave velocity: an index of central arterial stiffness? *Journal of Human Hypertension* **19** 401-406
- [10] Pereira H. 2007 Cardioaccelerometry The assessment of Pulse Wave Velocity using Accelerometers. Project Report 5th year Graduation in Biomedical Engineering – Universidade de Coimbra.
- [11] Ferreira E., 2008 Assessment of Hemodynamic Parameters New approach to the use of Piezoelectric Sensors. Dissertation of 5th year Graduation in Biomedical Engineering - Universidade de Coimbra.
- [12] Almeida V. 2009 Hemodynamic Parameters Assessment An Improvement of Methodologies. Dissertation of 5th year Graduation in Biomedical Engineering – Universidade de Coimbra.
- [13] Pereira T. 2009 Methodologies for Hemodynamic Parameters Assessment. Dissertation of 5th year Graduation in Biomedical Engineering – Universidade de Coimbra.
- [14] Book chapter: Solà, J.; Rimoldi, S. & Allemann, Y. 2010, *Ambulatory monitoring of the cardiovascular system: the role of Pulse Wave Velocity*, in New Developments in Biomedical Engineering, I-Tech Education and Publishing, Vienna, Austria.
- [15] Hermeling E., Hoeks A., Winkens H., Waltenberg L., Reneman R., Kroon A. and

Reesink K. 2010 Noninvasive Assessment of Arterial Stiffness Should, Discriminate Between Systolic and Diastolic Pressure Ranges *Hypertension* **55** 124-130.

[16] Blacher J, Asmar R, Djane S, London G and Safar M 1999 Aortic Pulse Wave Velocity as a Marker of Cardiovascular Risk in Hypertensive Patients *Hypertension* **33** 1111-1117.

[17] Cheung Y. 2010 Arterial Stiffness in the Young: Assessment, Determinants, and Implications. The Korean Society of Cardiology.

[18] Hermeling E., Reesink K., Reneman R., and Hoeks A. 2007 Measurement of local pulse wave velocity: effects of signal processing on precision *Ultrasound in Medicine & Biology* Vol **33** No. 5 774-781.

[19] Avolio A., Butlin M. and Walsh A. 2010 Arterial blood pressure measurement and pulse wave analysis –their role in enhancing cardiovascular assessment *Physiological Measurement* **31** R1-R47.

[20] Meinders J., Hoeks A., 2004 Simultaneous assessment of diameter and pressure waveforms in the carotid artery *Ultrasound in Med. & Biol.* **30** 147-154.

[21] 'Chapter 30: Arterial Pressure Waveforms':
http://web.sgu.edu/medLib/MED_CD/E_CDs/anesthesia/site/content/v03/030267r00.htm, accessed on 10th August 2011.

[22] Medscape Education – 'Arterial Aging: Hemodynamic Changes and Therapeutic Options: Changes in Wave Reflections',
http://www.medscape.org/viewarticle/725326_5, accessed on 10th August 2011.

[23] Bortel L., Vermeersch S. and Segers P. 2010 Arterial waveform and central blood pressure: the complex links between large and small arteries *Artery Research* **4** 118-121.

[24] Wilkinson I., MacCallum H., Flint L., Cockcroft J., Newby D. and Webb D. 2000 The influence of heart rate on augmentation index and central arterial pressure in humans *Journal of Physiology* **525** 263-270.

[25] Murgu JP, et al. 1980 Aortic input impedance in normal man: relationship to pressure wave forms *Circulation* **62** 105-116.

[26] Segers P., Kips J., Trachet B., Swillens A., Vermeersch S., Mahieu D., Rietzschel E., Buyzere M. and Bortel L. 2009 Limitations and pitfalls of non-invasive measurement of arterial pressure wave reflections and pulse wave velocity *Artery Research* **3** 79-88.

[27] <http://www.utexas.edu/features/2005/teragrid/graphics/teragrid1.gif> accessed on 10th August 2011.

- [28] <http://www.clinsci.org/cs/116/0273/cs1160273f02.gif> accessed on 10th August 2011.
- [29] Yasmin and Brown M. 1999 Similarities and differences between augmentation index and pulse wave velocity in the assessment of arterial stiffness *QJ Med* **92** 595-600.
- [30] Nu"rnberger J., Saez A., Dammer S., Mitchell A., Wenzel R., Philipp T. and Schafers R. 2003 Left ventricular ejection time: a potential determinant of pulse wave velocity in young, healthy males *Journal of Hypertension* **21** 2125-2132.
- [31] Boutouyrie P, Briet M, Collin C, Vermeersch S and Pannier B 2009 How to assessment of pulse wave velocity *Artery Research* **3** 3-8
- [32] Hirata K, Kawakami M and O'Rourke M 2006 Pulse Wave Analysis and Pulse Wave Velocity - A Review of Blood Pressure Interpretation 100 Years After Korotkov *Circulation Journal* **70** 1231:1239.
- [33] Callaghan F, Geddes L, Babbs C and Bourland J 1986 Relationship between pulse-wave and arterial elasticity *Medical & Biological Engineering & Computing* **24** 248-254
- [34] Hansen T, Staessen J, Torp-Pedersen C, Rasmussen S, Thijs L, Ibsen H and Jeppesen J 2005 Prognostic Value of Aortic Pulse Wave Velocity as Index of Arterial Stiffness in the General Population *Circulation* **113** 664-670.
- [35] Sugawara J, Hayashi K, Yokoi T and Tanaka H 2010 Carotid-femoral pulse wave velocity: Impact of different arterial path length measurements Elsevier 4 27-31;
- [36] Hermeling E., 2009 Local pulse wave velocity determination: the arterial distension waveform from foot to crest
- [37] Rajzer M, Wojciechowska W, Klocek M, Palka I, Brzozowska-Kiszka M and Kawecka-Jaszcz K. 2008 Comparison of aortic pulse wave velocity measured by three techniques: Complior, SphygmoCor and Arteriograph *Journal of Hypertension* **26** 2001-2007
- [38] Jatoi N, Mahmud A, Bennett K and Feely J 2009 Assessment of arterial stiffness in hypertension: comparison of oscillometric (Arteriograph), piezoelectronic (Complior) and tonometric (SphygmoCor) techniques *Journal of Hypertension* **27** 2186-2191.
- [39] Khir A., O'Brien A., Gibbs J.S.R. and Parker K. 2001 Determination of wave speed and wave separation in the arteries *Journal of Biomechanics* **34** 1145-1155.
- [40] Hermeling E., Reesink K., Reneman R. and Hoeks A. 2008 Confluence of incident and reflected waves interferes with systolic foot detection of the carotid artery distension waveform *Journal of Hypertension* **26** 2374-2380.

- [41] Raben S., Stergiopoulos N., Hellevik L., Smiseth O., Urheim S. and Angelsen B. 2004 An ultrasound-based method for determining pulse wave velocity in superficial arteries *Journal of Biomechanics* **37** 1615-1622. 7
- [42] Brands J., Willigers M., Ledoux A., Reneman S., Hoeks A. 1998 A noninvasive method to estimate pulse wave velocity in arteries locally by means of ultrasound. *Ultrasound Med Biol* **24** 1325–1335.
- [43] Meinders J., Kornet L., Brands P., Hoeks A. 2001 Assessment of local pulse wave velocity in arteries using 2D distension waveforms *Ultrason Imaging* **23** 199–215
- [44] Tarnawski M. 1994 Noninvasive determination of local wave speed and distensibility of the femoral artery by comb-excited Fourier velocity-encoded magnetic resonance imaging: measurements on athletic and nonathletic human subjects *Heart Vessels* **9** 194-201
- [45] Gautschi G. Google Book Search. 'Piezoelectric Sensorics'; [Online] http://books.google.com/books?id=nYFSLcmccC&printsec=frontcover&source=gbs_summary_r&cad=0#PPP1,M1. Assessed on 7 July 2011
- [46] 'Piezoelectric sensor' http://en.wikipedia.org/wiki/Piezoelectric_sensor. Assessed on 7 July 2011
- [47] James Karki, 'Signal Conditioning Piezoelectric Sensors', Texas Instruments, September 2000, <http://focus.ti.com/lit/an/sloa033a/sloa033a.pdf>
- [48] 'Introduction to Piezoelectric Sensors' http://www.piezocryst.com/piezoelectric_sensors.php
- [49] 'Sensors' <https://ccrma.stanford.edu/wiki/Sensors>, accessed on 7 July 2011
- [50] McLaughlin J, McNeill M, Braun B and McCormack P 2003 Piezoelectric sensor determination of arterial pulse wave velocity *Physiol Meas.* **24** 693-702
- [51] Clemente F, Arpaia P and Cimmino P 2010 A piezo-film-based measurement system for global haemodynamic assessment *Physiol Meas.* **31** 697-714
- [52] Katsuda S., Miyashota H., Hasegawa M. Machida N. et al 2004 Characteristic Change in Local Pulse Wave Velocity in Different Segments of the Atherosclerotic Aorta in KHC Rabbits *American Journal of Hypertension* **17** 181-187
- [53] Khir A., Zambanini A. and Parker K. 2004 Local and regional wave speed in the aorta: effects of arterial occlusion *Medical Engineering & Physics* **26** 23-29.
- [54] Hermeling E., Reesink K., Kornmann L., Reneman R. and Hoeks A. 2009 The dicrotic notch as alternative time-reference point to measure local pulse wave velocity

in the carotid artery by means of ultrasonography. *Journal of Hypertension* 27 2028-2035.

[55] Data sheet NI-USB 6009: <http://www.ni.com/pdf/manuals/371303l.pdf>

[56] Zong W, Heldt T, Moody G and Mark R 2003 An open source algorithm to detect onset of arterial blood pressure pulses *Computers in Cardiology* **30** 259-262

[57] Pan J. and Tompkins W. 1985 A real-time QRS detection algorithm *Transactions on Biomedical Engineering* 3 230-236

[58] Pereira H., Pereira T., Almeida V., Borges E., Figueiras E., Simões J. B., Malaquias J. L., Cardoso J. M. R. and Correia C. M. B. 2010 Characterization of a double probe for local pulse wave velocity assessment *Physiol. Meas.* **31** 1449-1465

[59] POCOCK, Gillian and RICHARDS, Christopher, *Fisiologia Humana: A Base da Medicina*, 2nd ed. Guanabara Koogan S.A, 2006, pp. 294.

[60] http://www.engineeredsoftware.com/papers/msa_rr.pdf accessed on 7th June 2011

[61] Pereira H.C., Cardoso J. M., Almeida V., Pereira T., Borges E., Figueiras E., Ferreira L.R., Simoes J.B., Correia C. 2009 Programmable test bench for hemodynamic studies *IFMBE Proc.* **25** 1460ff

[62] Alastruey J., Parker K.m Peiró J., Sherwin S., A One-Dimensional Model of the Cardiovascular System

[63] Papageorgiou G., Jones N.B., 1987 Physical modelling of the arterial wall. Part 1: Testing of tubes of various materials *Journal of Biomedical Engineering* **9** 153-156.

[64] Stamler J., Stamler R., Neaton J., 1993 Blood Pressure, Systolic and Diastolic, and Cardiovascular Risks *Archives of Internal Medicine* 153(5) 598-615.

[65] 'Basic Statistics' <http://www.statsoft.com/textbook/basic-statistics/>. Accessed on 27th July

[66] Dizaji M.m Maerefat M. and Rahgozar S. 2008 Estimation of carotid artery pulse wave velocity by Doppler ultrasonography *J Tehran Univ Heart Center* **2** 91-96

[67] Sorensen G., Jensen J., Udesen J., Holford I. and Jensen J. 2008 Pulse wave velocity in the Carotid Artery *IEEE International Ultrasonics Symposium* 1386-1389